

FACIES ANALYSIS AND PALEODISCHARGE OF RIVERS WITHIN A
COMPOUND INCISED VALLEY, CRETACEOUS FERRON
SANDSTONE, UTAH

By STEPHANIE KIMMERLE, B.Sc.

A Thesis Submitted to the School of Geography and Earth Sciences, and the
School Graduate Studies in Partial Fulfilment of the Requirements for the

Degree Master of Science

McMaster University © Copyright by Stephanie Kimmerle, June 2016

McMaster University MASTER OF SCIENCE (2016) Hamilton, Ontario (Science)

TITLE: Facies Analysis and Paleodischarge of rivers within a Compound Incised Valley, Cretaceous Ferron Sandstone, Utah AUTHOR: Stephanie Kimmerle, B.Sc. (McMaster University) SUPERVISOR: Professor J.P. Bhattacharya NUMBER OF PAGES: 111 (including 2 additional pages, Fig. 36, 37)

ABSTRACT

Classification of river systems based on dimension and lithology of architectural elements is critical in determining their scale and role in ancient drainages as tributaries, distributaries, or trunk river systems. Facies boundaries associated with the zonation of the fluvio-estuarine system can be difficult to predict using standard facies and sequence stratigraphic models, particularly within broad, long-lived compound incised valley fills. These questions are addressed in an outcrop study of incised valleys in the Turonian Ferron Sandstone Member of the Western Interior Seaway, southern Utah. Field data includes 8 measured sections containing detailed lithological, ichnological, paleocurrent, and architectural data, and 3 high resolution gigapan photomosaics of opposing outcrop faces oriented oblique to depositional dip. The compound valley records multiple episodes of cut and fill, with three nested valleys, each containing multiple channel stories. An upward progression from single thread meandering fluvial style, indicated by large scale laterally accreting point bar deposits, to more freely avulsing rivers in upper stories is documented. Lithological analysis of the oldest valley shows grain size distributions ranging from medium lower sandstone at the valley base to fine lower sandstone towards the top, and is characterized by amalgamated macroform deposits with dune scale crossbedding and abundant mud rip up clasts throughout. The second shows variable estuarine laterally accreting point bars, which coarsen away from the valley margin. The youngest valley is dominated by fining upward successions passing from medium lower dune scale cross bedded sandstone at the base with few mud clasts, to rippled very fine upper sandstone and interfingered floodplain shale deposits. Tidal influence is documented; suggesting that rivers were positioned basinward of the paleo backwater length, and estuarine facies seen in V2 suggests they are within the bayline. These rivers are among the largest documented in the Ferron and show that fluvial style and scale changes regionally within this large valley system.

ACKNOWLEDGEMENTS

This research would not be possible without the unending support, guidance, and patience of my advisor Dr. Janok Bhattacharya. I am very thankful for the many opportunities he has provided me with to further myself academically and as a young professional. He has been a constant encouragement to strive to produce the best work possible, and an excellent example of an engaged and contributing member within the geoscience community.

I am hugely grateful to my parents, David and Diane, who have always encouraged me to work hard and define my own meaning of success - without them I would not have the means or drive to even begin this project.

I would like to thank Sandeep Sharma, Wen Lin, Cristina Genovese, Logan Jung-Ritchie, George Pemberton, and Mohammed Ullah who provided assistance with technical aspects of the project. Without the positive attitude and resourcefulness of David Kynaston, Harrison Martin, Natasha Cycles and Matthew Leung, certain field challenges in the summers of 2014 and 2015 would have surely been insurmountable. I would like to thank my committee members Dr. Carolyn Eyles and Dr. Joe Boyce for their guidance and review of my research.

Finally, I would like to acknowledge NSERC and our consortium sponsors: BP, EcoPetrol, and Inpex, who provided funding for this project. Thank you for your generous support.

TABLE OF CONTENTS

LIST OF FIGURES 6

LIST OF TABLES 8

1. INTRODUCTION 9

 1.1. Geologic Setting 12

 1.2. Previous Studies 13

 1.3. Study Area 15

 1.4. Data and Methodology 16

2. FACIES DESCRIPTIONS AND INTERPRETATIONS 19

 2.1. Overview 19

 2.2. Facies 1 – Coarse Grained Fluvial Sandstone (CFS) 19

 2.3. Facies 2 – Medium to Fine Grained Fluvial Sandstone (MFFS) 20

 2.4. Facies 3 – Tide-Affected Fluvial Sandstone (TFS) 21

 2.5. Facies 4 – Tide-Influenced Inclined Heterolithic Strata (TIHS) 22

 2.6. Facies 5 – Abandoned Fluvial Channel Fill (AC) 23

 2.7. Facies 6 – Fluvial Floodplain Mudstone (MF) 24

 2.8. Facies 7 – Marine Middle to Upper Shoreface Sandstone (MU) 24

 2.9. Facies 8 – Marine Lower Shoreface Heterolithics (ML) 25

3. VALLEY FILL AND ARCHITECTURE 26

 3.1. Evidence for a Compound Incised Valley 26

 3.2. Valley 3 26

 3.3. Valley 2 28

 3.4. Point bars vs Counter Point bars in V2 30

 3.5. Valley 1 31

 3.6. General Fluvial Style 31

4. PALEOHYRAULIC ANALYSIS 34

 4.1. Overview 34

 4.2. Estimation of Sequence 1 Paleoslope 35

 4.3. Paleohydraulics for V3 36

 4.4. Paleohydraulics for V2 38

 4.5. Paleohydraulics for V1 39

5. DISCUSSION 40

 5.1. Backwaters and Baylines 40

5.2. Wheeler Analysis	41
5.3. A Stepped Forced Regressive CIV	43
5.4. High Frequency Allocyclic Eustacy	45
5.5. Fluvio-estuarine Facies Models	45
5.6. Value as an Outcrop Analog.....	47
6. CONCLUSIONS	47
7. REFERENCES	50

LIST OF FIGURES

- Figure 1. W/T plot for incised valleys in modern and ancient systems
- Figure 2. Valley fill versus sea level rise
- Figure 3. Ferron regional cross section
- Figure 4. Paleogeography of the Cretaceous Western Interior Seaway
- Figure 5. Ferron stratigraphic framework, dip and strike sections
- Figure 6. Ferron outcrop belt
- Figure 7. Study area map
- Figure 8. Mud rip up clast rich zone near the base of a valley.
- Figure 9. Bank collapse, slumped and deformed blocks
- Figure 10. Log impression and associated *Teredolites clavatus* burrows.
- Figure 11. Dense mat of *Teredolites longissimus* at underside of bed
- Figure 12. *Teredolites clavatus* and *Paleophycus* burrows
- Figure 13. *Pelecypodichnus (Lockeia)* burrows and a preserved log impression
- Figure 14. Undulating erosional scour surface
- Figure 15. Stacked dune-scale cross-sets
- Figure 16. Bar-scale lateral accretion beds
- Figure 17. Rose diagrams showing paleocurrent and accretion directions for V1, V2, and V3
- Figure 18. Current ripples
- Figure 19. Rib and furrows
- Figure 20. Double mud draped quasi-planar stratification
- Figure 21. Tidal bundles within dune-scale cross bedding
- Figure 22. IHS in estuarine muddy upper point bar deposits
- Figure 23. Normal fault in mud-dominated IHS
- Figure 24. Estuarine and marine trace fossils
- Figure 25. *Lockeia* bivalve burrows

Figure 26. Rhythmic interlaminated mud and sandstones with *Lockeia*

Figure 27. Sand beds pinching out towards the valley margin

Figure 28. Organic-rich floodplain shale

Figure 29. Root casts

Figure 30. *Ophiomorpha* burrows

Figure 31. *Rhizocorallium* and *Thalassinoides* traces

Figure 32. Dune-scale cross-bedded upper shoreface sandstone

Figure 33. Flooding surface at top of parasequence 5a upper shoreface sandstone

Figure 34. Current ripple cross-lamination

Figure 35. Correlated North Cliff face with measured sections (T1, S0 – S4)

Figure 36. East Cliff exposure; gigapan, bedding architecture, grain size distribution

Figure 37. North Cliff exposure; gigapan, bedding architecture, grain size distribution

Figure 38. South Cliff exposure; gigapan, bedding architecture, grain size distribution

Figure 39. Schematic diagram of counter point bars in a meandering river

Figure 40. Diagram of meander inflection point in a counter point bar

Figure 41. Schematic diagram of point bars in a meandering river

Figure 42. Paleogeographic reconstruction of V3

Figure 43. Paleogeographic reconstruction of V2

Figure 44. Paleogeographic reconstruction of V1

Figure 45. Paleoslope estimation based on onlap distance

Figure 46. V3 cross set thickness vs frequency

Figure 47. V3 cross set thickness histogram

Figure 48. Cumulative grain size for V3

Figure 49. Cumulative grain size for V2

Figure 50. V2 cross set thickness vs frequency

Figure 51. V2 cross set thickness histogram

Figure 52. Cumulative grain size for V1

Figure 53. V1 histogram showing cross set thickness vs frequency

Figure 54. Backwater limit model

Figure 55. Wheeler diagram of the East Cliff exposure

Figure 56. Wheeler diagram of the North Cliff exposure

Figure 57. Wheeler diagram of the South Cliff exposure

LIST OF TABLES

Table 1. Order of bounding surfaces

Table 2. Facies descriptions

Table 3. Paleohydraulic analysis

Table 4. D_{50} , D_{90} , and slope for channels in V3, V2, V1

Table 5. Measured Channel Widths from Outcrop

Table 6. Backwater and Bayline limits

1.0 INTRODUCTION

Compound incised valleys (CIV's) represent multiple episodes of cut and fill by rivers as a response to changing base level over geologic time (Shanley & McCabe 1994; Wright & Marriott 1993). Episodes of incision correspond to times of falling sea level (regression) and delta building, and filling occurs during regional sea level lowstand as a response to changing accommodation (Van Wagoner et al. 1990; Posamentier & Vail 1988; Allen & Posamentier 1993; Willis 1997). Incised valleys are defined as elongate, fluvially derived topographic lows with a regionally unconformable erosional scour surface across which a seaward shift in facies has occurred (Zaitlin et al. 1994). Stratigraphic and topographic valleys are typically much larger in width and depth than the rivers that form them, and contain multiple stacked or amalgamated channel stories (Strong & Paola 2010). Examples from the modern and ancient record indicate that incised valleys can range in scale from tens of kilometers to less than a kilometer in width, and in depth from a few meters to hundreds of metres (Posamentier & Vail 1988; Blum et al. 2013). Ancient systems are divided into coastal-plain valleys, and bedrock valleys (Blum et al. 2013). The valleys in the present study incise into shallow marine strata and are classified as coastal-plain incised valleys, as opposed to those which incise into bedrock (Blum et al. 2013). Examples of coastal plain valleys from the ancient record tend to range widely in thickness and width; 2 – 210 m in thickness, and up to 100 km in width, with a W/T of 5 – 3500 (Gibling 2006). Valleys which incise into bedrock are narrower, and have W/T ratios that consistently fall between 400 – 800 (Blum et al. 2013). Figure 1 describes the scale of valley fills by plotting W/T ratios for modern and ancient valleys. These trends indicate scaling relationships for channel body geometry that are valuable for estimating channel belt and stratigraphic valley width in

areas where outcrop exposure is limited in lateral extent, but vertical thickness is well preserved (Gibling 2006).

Stratigraphic analysis of incised valley systems can reveal information about climate cyclicity, tectonic activity, and eustatic sea level fluctuations for the region in question (Blum & Tornqvist 2000; Mitchum et al. 1991). Simple valley fills tend to preserve coarse-grained material at their base and fine upwards into transgressive estuarine facies, eventually filling the valley and passing into interfingering fluvial channel and floodplain facies (Shanley & McCabe 1994). Generally, valleys have been hypothesized to be cut and initially filled by braided or low-sinuosity meandering systems (Shanley & McCabe 1994). As sea level rises, the system tends to show an increase in preservation of tide-influenced facies and rivers become more sinuous with preserved laterally accreting point bars. Eventually, as the valley is filled, channels become unconfined and isolated, and the system is dominated by overbank floodplain facies (Fig. 2) (Shanley & McCabe 1994).

As proposed by Willis (1997), cut and fill mechanisms record changes in the ratio between relative sediment supply and accommodation, as a function of base level change and subsidence. The Willis model can be used as a predictive tool for ancient systems to account for the preservation of estuarine facies, prevalence of aggradation, and erosional capacity of the valley base across the proximal to distal valley profile. For example, those valleys that experience high sedimentation rate and low accommodation are likely to comprise dominantly fluvial fill that pass upward into marine or transgressive facies forming “flood-topped” valley fill. The reverse scenario for valleys with a high rate of accommodation increase relative to sediment supply, fill primarily with transgressive or estuarine facies and have been termed “flood-based” (Willis 1997; Li et al. 2010).

Channel slope and sediment caliber control fluvial style; an increase in one or both of these variables may cause a shift in style from meandering, to braided, and vice versa (Church 2006). Slope has a first order control on the length of the backwater and bayline limit, and corresponding facies changes along the channel profile (Bhattacharya et al. 2015).

Recognition of lateral and vertical facies variation is critical for optimizing hydrocarbon extraction from fluvial reservoirs, and for this reason, further study of facies architecture for predicting fluvio-estuarine behavior as a response to controlling factors is valuable (Van Wagoner et al. 1990; Miall 1988; Allen & Posamentier 1993). Traditional outcrop studies of ancient incised valley fills emphasize the use of vertical measured sections compared with bedding architecture analysis to reconstruct fluvial style and grain size variability across channels and from proximal to distal reaches of a valley (Miall 1985). These methods are particularly useful in capturing subtle changes in grain size distribution within bar and channel forms, facies variability, range in paleocurrent flow direction, and general accretion and fluvial styles (Allen 1964; Bridge & Tye 2000; Miall 1988; Miall 1985). This study addresses questions about the formation of Ferron incised valleys and their chronostratigraphic significance within the previously existing regional Ferron stratigraphic framework, and the factors controlling their internal architectural and facies organization. In doing so, a detailed facies analysis and architectural study including paleohydraulic reconstruction of formative Ferron rivers within sequence 1 along the Fremont River Canyon, has been conducted.

The Ferron is a commonly used analog for fluvio-deltaic hydrocarbon reservoirs, however the scale of the Ferron system calls into question its value as an appropriate analog for continental-scale drainage systems (Bhattacharya et al. 2015; Deveugle et al. 2014; Bhattacharya & Tye 2004). Numerous exposures of the Ferron Notom Delta CIV show significant tide-

influence and estuarine facies, posing concerns for lateral continuity of reservoir compartments and potential barriers and baffles to subsurface fluid flow. Identifying controls on inclined heterolithic strata (IHS) and the spatial trends of this facies within this valley is important for comparisons to other tide-influenced fluvio-estuarine examples.

This study documents the architectural and facies heterogeneity within CIV deposits, and may have implications for reservoir engineering modeling in mapping these complex deposits and constraining the dimensions of key architectural elements. This work can be applied to reservoir characterization studies of meandering fluvio-estuarine deposits within CIVs, to increase recovery efficiency from these types of hydrocarbon reservoirs. Facies similarities of formative Ferron rivers reveal that they likely represent appropriate analogs to other Cretaceous CIV fills, such as and the heavy-oil reservoirs of the McMurray Formation, and the Morrow Formation, eastern Colorado and western Kansas (Deveugle et al. 2014; Bowen & Weimer, 2003), although scale differences must be accounted for.

1.1 Geologic Setting

The Ferron Sandstone Member is a Turonian age regressive fluvio-deltaic sandstone tongue within the Mancos Shale Formation, and is bounded by the transgressive marine shales of the Blue Gate Shale Member above, and the Tununk Member below (Garrison & Van Den Bergh 2006; Peterson et al. 1980). Figure 3 shows the Ferron fluvio-deltaic wedge was deposited from the Sevier orogenic belt northeastward into the Western Interior foreland basin, which was experiencing increasing accommodation through rapid subsidence and sea level rise (Ryer & Anderson 2004; Armstrong 1968). North America during the Cretaceous was experiencing greenhouse climate conditions with high global sea level, wherein much of the

continent was flooded. This formed the Western Interior Seaway, which extended from the Gulf of Mexico north across the continent into the Boreal Sea (Ryer & Anderson 2004).

Paleogeographic reconstructions of North America place Utah at approximately 45° north of the equator during the Turonian, at the interface between the continental landscape and the interior seaway, suggesting a subtropical depositional environment (Ryer & Anderson 2004; Bhattacharya & MacEachern 2009).

The Ferron Sandstone was deposited in three delta lobes; the northernmost Vernal Delta, the Last Chance Delta, and the Notom Delta (Fig. 4) (Hale 1946; Hale & Van De Graaff 1964; Gardner 1995a; Gardner 1995b). The present study is located within the Notom Delta, which progrades to the northeast and contains a record of 7 sequences, or 4th order eustatic cycles (Famubode & Bhattacharya 2016). Figure 5 shows the regional stratigraphic framework in dip and strike view and the approximate location of this study, including the datum surface for all measured sections (parasequence 5a) (Li 2009; Zhu et al. 2012). The Notom delta has been informally divided into upper and lower lithologic units by Hill (1982), where lower units are dominated by marine delta-front to prodelta deposits showing various shoreline trajectories. However, these units show interfingering where upper units locally incise into shoreface sandstones of the lower Ferron units. Incised valley fills pass upward into unconfined floodplain and localized channel deposits towards the Blue Gate Shale contact (Li et al. 2010; Famubode & Bhattacharya 2016).

1.2 Previous Studies

Zhu et al. (2012) identified “one forced regressive sequence set, five depositional sequences, 18 parasequence sets, and 43 parasequences” within the Ferron Notom Delta. Further

work by Li et al., (2010) has determined there are 6 depositional sequences, of which the present study area is located within the youngest, sequence 1 (Fig. 5). Regional correlation of the Ferron Notom Delta by several workers (Li et al. 2010; Li & Bhattacharya 2013; Ullah et al. 2015; Zhu et al. 2012) has documented a series of incised valley terraces representing at least 3 episodes of cut and fill. The composite base of these valleys marks sequence boundary 1. This composite surface has been mapped across an area approximately 30 km wide and 40-50 km from proximal to distal areas. These valleys have been designated as V3 (oldest valley terrace), V2, and V1 (youngest valley terrace) (Li et al. 2010; Li & Bhattacharya 2013; Ullah et al. 2015; Zhu et al. 2012). Each valley exhibits a unique paleocurrent, architectural, sedimentological, and tidal signature, and these criteria have been used to correlate these valleys across sequence 1.

Li et al. (2010) conducted facies, architectural, and paleohydraulic analysis on a CIV exposure in the Neilson Wash region, to the northeast of the present study area. Li et al. (2010) mapped the erosional scour surface (SB 1) at the base of this valley system throughout Neilson Wash to the Fremont River and interpreted this as a regionally conformable bypass surface. Li and Bhattacharya (2013) linked this surface to valleys in Coalmine Wash, located approximately 8 km north of Neilson Wash. An upward transition from finer grained and more tide-influenced valley fill in lower valleys (V3 and V2) to more coarse fluvial deposits in the upper valley was documented. Maximum erosional relief is up to 17 m between the two valleys and is estimated to extend up to 10 km in width (Li & Bhattacharya 2013). Elsewhere in sequence 1, up to 20-30 m of erosional relief has been documented (Ullah et al. 2015).

Recent work by Ullah et al. (2015) from the Neilson Wash area compares fluvial style and tidal signature to upstream exposures in the Caineville region. This study reconstructs paleoslope, paleohydraulics, and channel dimensions for V3, V2, and V1, and estimates

backwater and bayline limits in order to compare to the same parameter estimates in other well documented exposures of this CIV.

Time stratigraphic analysis suggests that the entire CIV system was cut and filled over a 60,000 – 100,000 year period, and that individual cut and fill episodes may represent 20,000 year cycles associated with Milankovitch precessional periods (Zhu et al. 2012; Li et al. 2010; Li & Bhattacharya 2013; Ullah et al. 2015). In this way, each correlative valley basal scour surface represents a successive high frequency sequence boundary. This sequence stratigraphic approach is valuable in determining the relative importance of autogenic and allogenic controlling mechanisms on fluvial sedimentation in the Cretaceous Seaway, and can be used to identify glacio-eustasy as the primary driver in the Ferron system, as opposed to tectonics or changes in sediment supply (Fielding 2011).

1.3 Study Area

The present study is focused on a previously unmapped CIV exposure within sequence 1. It is exposed along vertical cliff faces oriented oblique to depositional dip along the canyon walls of the Fremont River, north of Sweetwater Creek. The site is located approximately 16 km west of Hanksville, and 1 km south of Highway 24 in Wayne County, Utah (see red box in Figure 6). This outcrop map has been modified from Li et al. (2010) to include the present study area and all known surface exposures of the Ferron Notom Complex. The stratigraphic datum used in this study is the flooding surface capping marine shoreface sandstones of parasequence 5a (sequence 2). Figure 7 shows a Google Earth image of the study area and highlights the locations of three well exposed outcrop faces, termed; North Cliffs, South Cliffs, and East Cliffs, with respect to their geographical orientation. Also noted on the map are the locations of measured sections.

Each exposure documents a unique orientation to view architecturally similar fluvial elements and thus presents challenges in correlating sediment bodies across the study site, but is also useful in identifying dramatically varying features across a relatively small area.

The purpose of this study is to identify this CIV's position within the greater Ferron paleovalley stratigraphy and to determine its role as a tributary or trunk river system. Change in channel slope is calculated across simple valley fills in order to ascertain the control on changing sediment caliber and channel morphology as valleys fill over time. This study aims to link rates of incision and valley fill to ~ 20,000 year Milankovitch scale cyclicity as a first order control on accommodation and sedimentation in the Cretaceous Western Interior Seaway. Comparison between all sequence 1 exposures of this large-scale compound valley system, and between proximal and distal fluvial facies allows evaluation and testing of backwater and bayline limits, which have implications for the position of key facies boundaries, such as the gravel-sand transition zone and limits of tidal facies (Bhattacharya et al. 2015).

1.4 Data and Methodology

Field data was collected in the summers of 2014 and 2015 and includes 8 lithostratigraphic measured sections supplemented with high resolution gigapan photomosaics of 3 outcrop faces (Fig. 7). Measured sections record detailed lithological, ichnological, paleocurrent, and architectural data, which have been combined with gigapan images to produce detailed bedding architecture and grain size variability diagrams. Additionally, measured sections record detailed architectural observations, including frequency and thickness of cross-sets, storey thickness, and inclination and accretion direction of dipping beds. Trace fossil identification was conducted to discern marine influence (MacEachern et al. 2009; Maceachern

& Pemberton 1994; Savrda 1991). Technical climbing gear and ropes were required on vertical cliffs as well as hand-held GPS, measuring tape, jacob's staff and abney level, and compass. Grain size diameters were measured in the field using a handlens and grainsize card. In areas where access was impossible, a ground-based laser rangefinder was used to measure the geometry and dimensions of architectural elements. In total, 127 paleocurrent flow direction measurements were taken from dune-scale cross-bedding, current ripples, and rib and furrow structures.

In addition to bedding architecture, grain size variability diagrams have been produced for all exposures and aim to illustrate the lithological heterogeneity between valleys and within discrete channel forms. Warm tones represent coarse grain sizes, which range from pebbles to mU sandstone, yellow to green represent fL to vFL sandstones, and cool hues represent silt to clay.

Fluvial style and channel sinuosity are estimated from bedding architecture, integrated with paleocurrent data from measured sections (Miall 1985). Bridge (2003) provides a method for estimating channel sinuosity based on the range in measured paleocurrent directions, where a large range in values represents a high sinuosity channel, and a narrow range represents a low-sinuosity to straight channel.

Paleohydraulic analysis, using empirical scaling relationships, was conducted based on measured maximum point bar height and mean preserved cross-set thickness (Mackey & Bridge 1995; Leclair & Bridge 2001; Bridge & Tye 2000; Bhattacharya & Tye 2004; Holbrook & Wanas 2014).

D_{50} and D_{90} grain diameters were calculated by plotting cumulative frequency for grain sizes within the lowermost cross-stratified portion of a channel, representing the coarsest material transported as bedload. D_{50} and bankfull channel depth were used to estimate channel slope, as per the method described by Holbrook and Wanas (2014). Channel slope and depth was then used to estimate backwater and bayline limits for each valley within this CIV (Blum et al. 2013; Paola & Mohrig 1996).

Facies analysis was conducted according to the classification scheme of Miall (1996), and was used to categorize sediments within and above incised valleys according to lithology, biota, sedimentary structures, and to group deposits into depositional facies. Tide-affected deposits were identified based on the observation of double mud drapes and tidal reworking, and marine-influenced deposits were identified based on the presence of marine to estuarine biota.

Correlation of sediment bodies was done by walking out of beds and identifying key surfaces in photomosaic cross sections according to the surface hierarchy of Miall (1988; 1985) (Table 1). Relative valley ages were determined by analyzing cross-cutting relationships and downlap and onlap patterns from detailed gigapan photomosaics and bedding architecture (Wheeler 1958). Each cross section intersects at least one measured section to provide some measure of control on lithology and accretion direction. Key surfaces are highlighted in which valley basal erosional scour surfaces (sequence boundaries) are in bold red, and channel basal surfaces are in bold blue. According to Miall (1988; 1991) (Table 1), red lines correspond to 6th-7th order surfaces where in most localities the base of V3 represents a 7th order surface, and the base of V2 and V1 represent 6th order surfaces. Channel basal or concave-up features are bounded by blue lines and represent 5th order surfaces. Accretion surfaces, representing primarily macroform (bar-scale) accretion and occasionally dune-scale features, are 3rd-4th order surfaces

and are identified by fine black lines. These include laterally accreting point bars, accretion foresets, sand beds which pinch out toward valley margins, and dune-scale cross sets.

2.0 FACIES AND INTERPRETATIONS

2.1 Overview

Six individual facies have been identified with this compound incised valley including unconfined fluvial deposits above the stratigraphic valley. Two additional facies characterize the marine strata of parasequence 4 below the valley. Table 2 summarizes facies found in this study, and includes a brief description of observed lithology, biota, and sedimentary structures.

2.2 Facies 1 – Coarse Grained Fluvial Sandstone (CFS)

Description – Facies 1 (CFS) represents the coarsest material found within the CIV and generally does not exceed 2 m in overall thickness. Lithology ranges in size from pebbles to medium lower sandstone, where pebble-sized material represents a small percentage of total grain size distribution, and are only found along valley basal surfaces. Mud rip-up clasts are abundant and often form mud clast rich beds (~1 m thick) along valley and channel bases (Fig. 8). Coarse sediment is often massive to poorly stratified, however occasionally dune-scale cross-stratification and planar stratification can be seen. Beds are normally graded and fine upwards into fine sandstone where dune-scale cross bedding is dominant. Soft sediment deformation and slumping of previously deposited fluvial sediment is common (Fig. 9). Log impressions can be found along valley basal surfaces and may contain *Teredolites clavatus* (Fig. 10), *Teredolites longissimus* (Fig. 11), and *Paleophycus* (Fig. 12), and *Pelecypodichnus* (*Lockeia*) (Fig. 13).

Interpretation – Fluvially derived medium to coarse grained sandstone with minor pebble size material and abundant mud rip-up clasts, characterize channel basal lag deposits, and are typical of deposits which directly overlie sequence boundary 1 (Fig. 14). Coarse grained sandstone with vague stratification and imbricated clast horizons indicate upper flow regime bedload transport, and were likely deposited during channel basal scouring (Holbrook & Bhattacharya 2012). This facies is often used to mark the base of fining upward channel storeys, and when paired with a significant increase in grain size from underlying units, can be used to identify valley basal surfaces, and regional composite scour surfaces (Holbrook & Bhattacharya 2012). *Paleophycus* associated with *Teredolites clavatus* and *Teredolites longissimus* suggest a brief moment of marine incursion (Fig. 10, 11, 12), however *Pelecypodichnus (Lockeia)* burrows and fossilized log impressions (Fig. 13) indicate a freshwater environment.

2.3 Facies 2 – Medium to Fine Grained Fluvial Sandstone (MFFS)

Description – Lithologies range from fine lower to medium lower sandstone with minor mudstone interbeds. Mud rip-up clasts are common along cross-stratified accretion surfaces. Plant material and coal is common, including wood and log impressions, however no burrowing is observed. Dune-scale crossbedding (Fig. 15) and bar-scale accretion bedding (Fig. 16) are most common, and paleoflow direction is 90° to the accretion direction. Paleocurrent and accretion directions are given in Figure 17. Though less common, planar stratification and current ripple cross lamination are also found (Fig. 18). Towards upper valley fills, where plan-view channels are exposed, dune-scale cross bedding shows rib and furrow structures (Fig. 19). Soft sediment deformation within this facies is relatively common. Sandstones generally lack significant volumes of mud, and show amalgamated fining upward successions that overlie 5th order concave-up channel basal surfaces.

Interpretation – Large, uniformly dipping foresets represent bar-scale accretion forming unit bars, and dune-scale cross-stratified accretion sets amalgamate to form laterally accreting point bars or compound bars. All bar-scale accretion was found to dip at approximately 90° to paleocurrent flow, as measured from dune-scale cross bedding within the same channel storey (Fig. 17). This indicates that lateral accretion is the primary fluvial depositional style within this reach of the CIV system. Large scale soft sediment deformation is indicative of erosion induced channel bank collapse as a result of rapid channel avulsion and entrainment of preexisting sediment. Small scale soft sediment deformation represents high sedimentation rate and rapid dewatering, or possible seismites associated with local earthquakes (Li et al. 2010).

2.4 Facies 3 - Tide-Affected Fluvial Sandstone (TFS)

Description – Dominant grain size is fine lower to medium lower sandstone with coupled mud laminations. Double mud drapes are rare, but found within quasi-planar stratification within fine lower sandstone (Fig. 20), and cross-sets within fine upper sandstone (Fig. 21). Occurrences do not exceed 30 cm in thickness. Alternating mudstone and fine sand interlaminations are common in upper valley fills and show repetitive cyclicality, and possible brackish to fresh water ichnogenera. These include *Planolites* and *Paleophycus* concentrated within mud-dominated strata. Minor plant material and coal fragments are present. TFS is architecturally similar to MFFS in that it occurs in stacked fining upward successions that overlie 5th order concave-up channel basal surfaces.

Interpretation – Double mud drapes and brackish traces are evidence for diurnal tidal processes and indicates an fresh to estuarine depositional environment (Visser 1980). Tide-affected facies are more prevalent near the base of valley fills (V3, V1). Cyclical mudstone and

fine sand interlamination likely represent tidal cycles preserved in low flow velocity conditions within a valley marginal setting within the tidal backwater limit. *Planolites* and *Paleophycus*, are not definitive evidence for an estuarine environment, and may represent deposition within either the bayline or within the tidal backwater limit only.

2.5 Facies 4 – Tide-Influenced Inclined Heterolithic Strata (TIHS)

Description – Facies 4 is characterized by uniformly dipping beds (5 -16°) at 90° to paleoflow direction (Fig. 17) with grain sizes ranging from silt and mudstone beds to very fine upper sand. IHS are present in 3-15 cm thick beds, which alternate between silt to mudstone and very fine lower to very fine upper sand (Fig. 22). IHS are up to 5.3 m in vertical thickness and up to 30 m in lateral width. The proportion of sandstone ranges from 30 – 50%. Small-scale soft sediment deformation is pervasive throughout and includes slumping, dewatering and loading structures, normal faulting (throw < 3 cm) (Fig. 23), deformed current cross lamination, and dewatering cracks. Marine traces are abundant within mud-rich beds in the upper 1.5 m. Ichnogenera include *Chondrites*, *Planolites*, *Paleophycus*, *Rhizocorallium*, and simple *Teichichnus* showing no more than 3 spreite (Fig. 24).

Interpretation – These IHS are interpreted to represent large-scale laterally accreting point bars or counter point bars, which become more fine grained and preserve greater marine influence upward. Marine traces, specifically *Chondrites*, indicate incursion of marine water and a fully marine to brackish setting (Gingras et al. 2009). *Teichichnus* with 2-3 spreite, and together with other marine associated traces, such as *Rhizocorallium* and *Paleophycus*, are typical of an estuarine or brackish water environment (Gingras et al. 2009). Heavy soft sediment

deformation, including normal faults, slumping, small-scale ball and pillows, cracking and convolute laminations, suggest rapid sedimentation and frequent dewatering or earthquakes.

2.6 Facies 5 – Abandoned Fluvial Channel Fill (AC)

Description - AC comprises very fine lower to fine upper sandstone with interbedded and interlaminated mudstones and coaly mudstones. Plant material, shale beds with slickensides, root casts, and coal are common. Bivalve burrows (*Lockeia*), are frequently found in abundance along sand and mudstone bed contacts (Fig. 25, 26). Beds are generally uniformly dipping (3-8°) and pinch out towards or onlap the valley margin (Fig. 27), with *Fugichnia* escape structures found within several sandstone beds in V1. Low angle bar-scale accretion, current ripple cross lamination, and planar lamination are the dominant sedimentary structures, with some occurrences of small-scale soft sediment deformation. Abandoned channel sand bodies and crevasse splays fine upward and are generally no greater than 1 m in thickness.

Interpretation – This facies is characteristic of upper fluvial channel fill, crevasse splay, or overbank levee deposits. Overall, these deposits signify a decrease in flow energy and typically represent the onset of channel abandonment and mud-plug formation. Where *Lockeia* are found in dense mats of uniform shape and high abundance (Fig. 25), a freshwater environment is interpreted. Rhythmically interlaminated mudstones and sandstones may represent tide-affected sedimentation within the backwater limit (Fig. 26). This facies is similar to TIHS, except that it shows a lack of marine traces and double mud drapes, and elements are smaller in scale where sandstone and mudstone packages generally do not exceed 1-2 m in thickness. Root casts indicate prolonged subaerial exposure, and are further evidence for a freshwater setting. *Fugichnia* escape structures seen in valley marginal sandstone beds, and soft

sediment deformation suggest locally high sedimentation rates, perhaps during periodic flood events.

2.7 Facies 6 - Fluvial Floodplain Mudstone (FM)

Description – Floodplain mudstones are dominated by finely laminated fissile siltstones, mudstones, and coaly mudstones with infrequent minor very fine grained sand beds (Fig. 28). Slickensides, cracks, plant material, and coal are abundant, and some sand beds preserve current ripples and root casts (Fig. 29). Minor bivalve burrowing is seen along sand bed contacts, however no marine trace fossils were observed. Floodplain facies range in thickness from a few cm, up to 0.8 m.

Interpretation – Deposition of > 0.5 m thick freshwater mud packages indicate prolonged overbank deposition within the floodplain outside of the confined valley. Small < 10 cm sand beds represent flood event deposition of overbank fines when water levels rise high enough to transport suspended load sand over channel levees and into the floodplain area adjacent to the active channel. Normally graded sand beds may represent flood-associated crevasse splays. Slickensides indicate repeated wet-dry cycles under low sedimentation rate and flow conditions, and root casts indicate long term subaerial exposure with adequate dry periods to allow plant growth.

2.8 Facies 7 – Marine Shoreface Sandstone (MS)

Description – This facies contains relatively homogeneous fine lower to fine upper well sorted sandstones with some carbonaceous material and moderate to heavy bioturbation throughout. Common ichnogenera include *Skolithos*, *Ophiomorpha*, *Thalassinoides* and *Rhizocorallium* (Fig. 30, 31). Generally, these deposits exhibit a massive appearance, however

they tend to show greater preservation of hummocky and swaley cross stratification upwards. The top of this facies shows dune-scale cross stratification (Fig. 32) and planar stratification. Individual coarsening upward successions achieve a maximum preserved thickness of 7.5 m.

Interpretation – MS facies is characteristic of shoaling upward prograding shoreface deposits and represent a proximal marine environment (Plint 2010).

2.9 Facies 8 – Marine Heterolithics (MH)

Description – Parasequence 4 contains 4 – 5.5 m of Heterolithics represented by alternating siltstone and very fine upper to fine lower sandstone beds (Fig. 33). Sand beds thicken and coarsen upwards and are hummocky or swaley cross-stratified, with some beds bearing oscillatory wave ripples and combined flow ripples, planar cross stratification, or in beds with high bioturbation index, a more massive appearance. Siltstone beds are generally bioturbated and show current ripple cross lamination (Fig. 34), planar cross stratification, and normal grading. Bioturbation in siltstone beds is dominated by *Chondrites*, *Planolites*, and *Paleophycus* traces, and sand beds show more common *Skolithos*, *Ophiomorpha*, *Thalassinoides*, and *Paleophycus*.

Interpretation – These more mud dominated strata represent toe of shoreface transitional heterolithics. Sandstone beds represent high energy storm events, which cause rapid sedimentation and preserve storm-associated structures (HSC, SCS) better than the lower energy siltstone beds, which are often more stable and more bioturbated (Gani et al. 2008). Low to moderate bioturbation paired with the prevalence of wave and combined flow ripples supports a wave-dominated offshore marine environment, with a possible deltaic (i.e. fluvial) influence (MacEachern et al. 2005).

3.0 VALLEY FILL AND ARCHITECTURE

3.1 Evidence for a Compound Incised Valley

Figure 35 shows a schematic correlation of measured sections (T1, S0 – S4) taken along the North Cliff exposure. Fining upward fluvial successions, representing individual channel stories, coarsening upward marine parasequences, and facies types are shown. A basinward shift in depositional facies is shown by the truncation of MS and onlap of CFS units across the lowermost valley basal erosional surface. Three episodes of cut and fill are identified within the compound valley, each exhibiting a regionally correlative basal erosional surface, truncation of underlying units, onlap of significantly coarser fluvial units, and multi-storey channel fill.

A series of bedding architecture and grain size variability diagrams have been produced for the East, North, and South Cliff exposures, and are given in Figures 36, 37, and 38 respectively. Measured sections show up to 17 m of erosional relief and indicate a compound valley fill. Total relief on the CIV is estimated based on 677 GPS elevation points of the variably preserved top parasequence 4 surface across a 1.5 km² area within the study site (Kynaston, *in prep*). Depth of valley incision subtracted from the maximum preserved elevation of this surface indicates the upper limit for total CIV erosional relief is approximately 28 m.

3.2 Valley 3

Evidence of the earliest episode of cut and fill within this compound incised valley is indicated by V3 and identified within all three cliff exposures. Generally speaking, V3 represents the thinnest preserved valley fill, but is removed in areas where V1, V2, and V3 are stacked and V2 deepens. Along the South Cliff exposure (Fig. 38), V3 ranges in preserved thickness from 3.5 m to a maximum of 5.5 m. The North and East Cliffs (Fig. 36 - 37) show less

preservation. Across the area, V3 shows a maximum of 5 vertically amalgamated channel stories and a maximum of 9 discrete channel bodies within the same exposure (East Cliffs, Fig. 36), where channels appear to accrete and dip towards the north to northwest. This can be seen clearly in Figure 36, which shows broad channel-fill complexes formed by lateral channel migration and avulsion (Miall 1985). The South Cliff exposure (Fig. 38) shows vertically stacked channel forms where the valley fill is more aggradational.

The base of V3 represents sequence boundary 1 where CFS valley basal facies shows clear truncation of underlying MS facies across an undulating composite U-shaped valley floor, seen in diagrams of the North and South Cliff exposures (Fig. 37 - 38). The lowermost 1 m of V3 displays CFS which fines into MFFS within the first 1-2 m from the base and typically shows amalgamated macroform deposits. Double mud drapes, indicating TFS, are found locally near the base of V3 (Fig. 20). Logs with *Teredolites clavatus* (Fig. 10) and *Paleophycus* (Fig. 12) are also found along the base, indicating a transgressive surface. With the exception of valley basal traces, V3 shows relatively sparse evidence for tide-influence, with only a few occurrences of double mud drapes and no other estuarine biota.

Figure 17 shows rose diagrams, which indicate paleocurrent and accretion directions for V3. Flow directions generally fall within a range of 0° - 35° , with a mean value of 19.8° . These flow directions agree with data from Ullah et al., (2015) who shows a paleocurrent range between 0° - 25° for V3 at Neilson Wash. Deformed fluvial deposits and limited 3D exposures of dune-scale cross beds, taken from rope-access measured sections, account for the limited paleocurrent and accretion data for this valley system in the present study area. A secondary paleocurrent signature, flowing to the south to southwest, may represent reworking by tidal

processes. This supports the interpretation that V3 lies within the tidal backwater limit (Blum et al. 2013).

Amalgamated channel deposits within V3 are typically made up of dune-scale cross sets, which range in thickness from 5 to 40 cm. Grain size distributions are biased towards coarse basal lag facies (CFS), since these deposits are preferentially preserved as younger overlying medium to fine grained sandstones have often been removed by overlying V2 deposits.

Fluvial style in V3 is interpreted as low-sinuosity single-thread meandering, as indicated by laterally accreting point bar deposits that show a narrow range in paleocurrent flow directions (Fig. 17) (Bridge 2003). These point bars are 2.1 – 3.0 m in vertical thickness and are seen on the East Cliff exposure at an oblique to right-angle view to accretion direction (Fig. 36). Since the East Cliffs are oriented approximately north-south, and flow direction is north-east, and accretion direction is northwest, these point bars are easily identified.

3.3 Valley 2

V2 represents the second episode of cut and fill, truncating and locally removing underlying V3 deposits. V2 and V3 basal surfaces combine to form a regional composite scour surface (RCS) (Holbrook & Bhattacharya, 2012). V2 is present in all three exposures and is the most extensively preserved valley within the CIV. Maximum preserved thickness of V2 is 9.1 m and maximum preserved single storey height is 5.3 m measured by hand at the South Cliff exposure from a large-scale laterally accreting point bar (Fig. 22, 38). Maximum preserved lateral point bar width is approximately 30 m. At the South Cliff exposure (Fig. 38), V2 shows a maximum of 2 preserved channel stories, however up to 7 vertically stacked channel stories are observed along the North Cliff exposure (Fig. 37), and up to 5 along the East Cliff (Fig. 36).

Bedding architecture diagrams indicate the dominant fluvial style in V2 is relatively high sinuosity single-thread meandering channels. Laterally accreting point bar deposits, which are dominated by mud and silt at the valley margin, coarsen towards the centre of the channel belt. Point bar accretion surfaces dip between $5 - 16^\circ$ to the north and are generally between 10 – 30 cm in thickness, alternating between mud-dominated and sand-dominated strata. At the valley margin, these IHS have an estimated 30-50% net to gross. The system transitions to MFFS with approximately 60-80% net to gross over a distance of only 100 m toward the interior of the channel. This dramatic change in grain size across a limited lateral extent indicates a high degree of lithological complexity and heterogeneity.

Basal V2 fill is generally finer than V3, where CFS facies fines into amalgamated MFFS channel stories. The East Cliff exposure shows north-accreting channels, which aggrade vertically and show a generally homogenous fine upper to medium lower grain size distribution (Fig. 36). This is also seen in the North Cliff exposures of V2 (Fig. 37). A shift from laterally accreting channels in V3 to more vertically aggradational channel stacking in V2 is evidence for a more basin distal position. Significant tide-influence indicates that this system was positioned basinward of the bayline and was connected to the main trunk channel (Blum et al. 2013), as opposed to a restricted meander cutoff.

Measured sections include 66 paleocurrent measurements for deposits within V2 (Fig. 16). The mean value is 148.8° , which corresponds to a southeast flow direction. Values range from northeast to south and are based on 3D views of cross-sets, and are oriented 90° to the direction of laterally accreting point bars (Fig. 17). These data agree with Ullah et al., (2015) who found V2 paleocurrent measurements to fall within a range of $110 - 150^\circ$, with a mean value of 120° .

3.4 Point bar vs Counter Point bar Models for Valley 2

A study by Donselaar and Overeem (2008) addresses the lithological complexity and connectivity of a mixed-load, low gradient single-thread meandering river from the Miocene Ebro Basin. They suggest two alternative models for the formation of abandoned channel mud-plugs, (1) where the plug fills the entire channel depth to bank full and compartmentalizes the meander belt, and (2) where 1-2 m of trough cross bedded sandstone, as an extension of a sandy point bar, floors the channel basal zone before the plug is deposited. This sandy channel floor serves to connect coarse-grained meander scrolls and has implications for reservoir development from these types of reservoirs.

The mud-dominated strata in V2, upon first glance, may be interpreted as an abandoned channel mud-plug under the first model suggested by Donselaar and Overeem (2008). However closer examination reveals that these deposits formed under active flow conditions within a trunk channel. Mud-rich strata are present towards the base of the channel floor and show no connection to, nor the presence of sand-dominated trough cross bedded sandstone, as suggested by the second model (Donselaar & Overeem 2008).

V2 IHS are thus more likely to represent counter point bars within an estuarine regime. Counter point bars can form in meandering river systems as the channel approaches and contacts an obstacle, in this case, the valley margin. Lateral channel migration occurs until flow is impeded by the harder valley marginal substrate, and the meander channel must adjust to downstream accretion (Smith et al. 2009). This produces a concave shaped scroll bar (Fig. 39, 40), as opposed to convex shaped scroll bar, which is typical of classic laterally accreting point

bars formed on the inside of meander loops (Fig. 41). Counter point bars are typically much finer grained than their associated point bars. For instance a study of the modern Peace River, Alberta, showed that counter point bars had a net to gross of 10-20% where their adjacent point bars had a net to gross of > 95-100% (Smith et al. 2009). This is also seen in the ancient counter point bar IHS deposits of the McMurray Formation, Alberta (Smith et al. 2009).

The mud-dominated IHS in V2, as seen in Figure 37 and 38, show fining towards the valley margin as well as fining in the downstream direction. Since paleoflow direction for V2 is to the southeast, this is seen when the slightly more proximal North Cliff exposure (Fig. 37) is compared to the more distal South Cliff exposure (Fig. 38). These exposures are oriented roughly parallel to each other with respect to depositional dip, and record a fining in grain size as the valley marginal accretion style transitions from lateral with a downstream component, to fully downstream. As the counter point bars extend away from the valley margin, a higher fraction of very fine to fine sand is deposited (Fig. 37, 38).

3.5 Valley 1

The youngest valley within the CIV is termed V1 and erosionally removes the top V2 strata and passes from valley fill within the U-shaped CIV feature, to more freely avulsing unconfined fluvial sandstone and floodplain shales. Total valley relief is up to 11 m. CFS facies is only variably present, and is represented by a thin, locally present basal pebble lag which fines quickly into MFFS facies. Paleohydraulic analysis indicates a relatively high-sinuosity single-thread meandering fluvial style (Fig. 17). Large-scale point bar features seen in the East Cliff exposure (Fig. 36), are between 3.0 – 3.3 m in vertical thickness. The base of V1 shows local mud draped cross-sets, suggesting TFS facies. Along the basal scour surface of V1, CFS facies

with *Pelecypodichnus (Lockeia)* is identified, along with preserved wood logs; this is evidence for a freshwater system. Within 30 lateral meters of this exposure, *Teredolites longissimus* is seen within 1 m above the valley basal surface overlying a variably exposed, < 10 cm thick coal deposit (Fig. 11). This indicates full ingress of marine water, and therefore a transgressive surface, which can be observed locally for approximately 10 m in lateral extent (Maceachern & Pemberton 1994). No other marine traces have been identified within V1 or within the unconfined fluvial deposits above. As V1 fills and exits the confines of the valley feature, AC facies is observed, particularly prevalent towards valley marginal settings. Sandstone beds fine and pinch out toward valley margins and become increasingly interbedded with floodplain shale and organic rich zones. This facies shows abundant mats of *Lockeia* concentrated within sand and mud interlaminated units. In such vast numbers (Fig. 25, 26), this likely represents a freshwater environment with slow sedimentation rate. Interbedded very fine sand and mudstones (Fig. 26, 27) show rhythmic deposition, which may represent tidal effects. This places V1 within the tidal backwater limit, but outside of the bayline limit (Blum et al. 2013). FM facies becomes common in thick > 50 cm packages towards the upper part of V1 and outside the confined valley, and rooted paleosols indicate subaerial exposure (Fig. 28, 29).

Based on a total of 32 measurements, paleocurrent analysis for V1 shows a flow direction to the east, southeast with a mean value of 118.1° , and a range between $50 - 170^\circ$ (Fig. 17). These results broadly concur with Ullah et al. (2015) who present a range in paleocurrents from $40 - 110^\circ$ with a mean value of 61° from the Neilson Wash area. Opposing paleocurrents to the west and southwest may represent tidal effects, which would place V1 within the tidal backwater limit.

3.6 General Fluvial Style

Paleogeographic reconstructions based on channel dimensions and paleocurrent data have been produced for all three valleys and can be seen in figure 42, 43, and 44. This CIV is initially filled by low-sinuosity single thread meandering rivers, which deposit in high velocity, high discharge fluvial systems; velocity and discharge estimates for formative rivers are given in Table 3. Successive episodes of incision exhibit different fill features, for instance V2 shows relatively high preservation of tide-influenced and estuarine facies, large-scale mud-dominated IHS, and a suite of marine ichnogenera. Side-attached point bars with a wide range in paleocurrent directions are evidence for high-sinuosity single-thread meandering fluvial style (Fig. 17, 38) (Bridge 2003; Miall 1985). V2 style is dominated by laterally accreting point bars, however some channel stories show amalgamated fluvial channels with dune-scale cross bedding and bar-scale accretion. In V1, channels become unconfined and greater overbank floodplain shale and coal deposition is preserved (Shanley & McCabe 1994).

Detailed work in the Neilson Wash area by Li et al., (2010) has identified two cut and fill episodes (V1, V2) which form a CIV which can be traced for 7 km and records up to 17 m of erosional relief. Li et al. (2010) showed that both valley fills document an upward transition from fluvial facies to tide-influenced facies and back to fluvial facies. V1 shows a change in fluvial style from braided at the valley base, indicated by bi-directional downlap of fluvial units, to single-thread meandering, to low-sinuosity fluvial style towards the top. Rivers in V2 are consistently single-thread meandering and are more fine-grained and tide-influenced than those deposits of V1. Ullah et al. (2015) from Neilson Wash shows significant braided style in all three valleys.

These results differ from the Fremont Canyon site where V2 deposits were formed by generally fine-grained single-thread meandering rivers and tend to show minor tide-influence

towards either the base or top of valley fill. This is inconsistent with results from Li et al. (2010), where greater tide-influence and several distinct style changes are observed. V1 preserves the coarsest material in the CIV at the Fremont Canyon, where grain size at the valley base are typically coarse lower with sparse pebbles. V1 at this site does not however record any evidence for braided rivers, with no observable occurrence of bi-directional downlap of braid bars. V1 fluvial style passes from amalgamated fluvial channels and point bars, which are evidence for single-thread meandering fluvial style (seen on East Cliff exposure in Figure 36) to more mud-prone floodplain shale facies.

Comparison between these sites, which are interpreted to record the same stratigraphic valleys, shows that across a broad, long-lived CIV, exceptional heterogeneity is observed. Fluvial style and facies changes are documented within individual valleys as they fill (Li et al., 2010), and do not necessarily correspond to consistent changes in other areas of the greater CIV. Wide incised valley (> 15 km) typically represent a greater range of depositional settings with greater tidal reworking, and can exhibit far more heterogeneity than narrow valley examples (Krystinik & Leckie 1992). These findings highlight the importance of identifying reach-specific and temporal controls on fluvial style and facies within CIVs, such as valley slope, channel slope, discharge, and amplitude of glacio-eustatic cycles.

4.0 PALEOHYDRAULIC ANALYSIS

4.1 Overview

A detailed paleohydraulic analysis has been conducted for formative rivers within this compound incised valley system. Methods for calculating paleo flow depths from cross-set thickness have been adopted from LeClair and Bridge (2001), and point bar height scaling

relationships are from Bridge and Mackey (1993), Bridge (1993), Hajek and Heller (2012), and Holbrook and Wanas (2014). Based on flow depth, a suite of paleohydrological parameters can be estimated, including channel width, channel belt width, flow velocity, and water discharge. According to the method of Bridge and Tye (2000), numerous cross-set thickness measurements can be used to estimate the height of their formative dunes, which then scale to the mean flow depth of the channel. The mean of these cross-set values (S_m), and the standard deviation (S_{sd}) of the data set are calculated, and if S_{sd}/S_m is equal to 0.88 ± 0.3 , the data is suitable for use in calculating mean dune height (h_m). Maximum bankfull flow depth (D) scales to 6 to 10 times mean dune height (h_m) and can be used to estimate the active channel water depths (Bridge & Tye 2000). Channel widths were estimated using empirical equations width from outcrop (Bridge & Mackey 1993), and are compared to estimates based on point bar widths observed directly from outcrop (Ethridge & Schumm 1977). These width estimates are significantly smaller than those calculated by empirical methods, and since they have been derived using a more reliable method, can be used in comparison to test the validity of standard fluvial scaling relationships. These results are given in Table 5. Mean flow velocity is calculated using the Chezy Standard Coefficient, hydraulic radius (geometric factor of 0.65 multiplied by channel area, divided by wetted perimeter), and slope (Parker 2004). Discharge is calculated by multiplying channel cross sectional by mean flow velocity (Bhattacharya & Tye 2004). Complete results are given in Tables 3 and 4.

4.2 Estimation of Paleoslope

Paleoslope for sequence 1, as calculated by Bhattacharya et al. (2015), is 0.0014 or 0.08° . This agrees with typical slope values for other sequences in the Ferron, which generally range from $0.00076 - 0.0026$ (Bhattacharya et al. 2015). These slope estimates are based on long-

profile erosional relief of incised valleys as mapped on the Ferron dip cross section (Fig. 45) (Zhu et al. 2012). Slopes on this order indicate Ferron trunk rivers were steep and sediment rich rivers.

An alternative method for calculating slope has been outlined by Holbrook and Wanas (2014) and Lynds et al. (2014) and uses shear stress, submerged dimensionless density, D_{50} , and mean bankfull flow depth. A suite of D_{50} values have been generated for each valley and independent channel slopes have been calculated for formative rivers in valley-basal, mid-valley, and upper-valley positions; these have been termed CH3, CH2, and CH1 respectively (Table 3).

Given the order of magnitude range in numerically possible paleoslope values for sequence 1, multiple velocity and discharge estimates reflect both methods. Table 3 shows the complete paleohydraulic analysis; low-end velocity and discharge estimates correspond to slopes based on calculated D_{50} , and high-end estimates correspond to the stratigraphically derived slope of 0.0014 for all of sequence 1. Greater control on channel paleoslope would greatly improve this paleohydraulic analysis and would constrain minimum and maximum values to within one order of magnitude.

4.3 Paleohydraulics for V3

Figures 46 and 47 graphically represent cross-set thickness measurements versus frequency. The distribution resembles a right skewed curve, with the highest frequency falling between 9 – 17 cm in thickness. Cross-sets greater in thickness than 50 cm were excluded from this data set, as those beds likely represent bar-scale accretion foresets, rather than dunes, and should not be used for estimation of paleoflow depth using the Bridge and Tye (2000) method. Cumulative frequency curves have been produced for representative channels within V3; an upper-valley

channel (CH1), and mid-valley channel (CH2), and a basal-valley channel (CH3) (Fig. 48). This was done to determine changes in channel morphology and flow characteristics as the valley fills over time. Results are shown in Table 3, and provide the calculated D_{50} and D_{90} values for these channels as well as corresponding channel slope estimates, which for CH3, CH2, and CH1, are 0.00040, 0.00024, and 0.00013 respectively. As successive channels fill V3, D_{50} , or sediment caliber decreases. This may be attributed to a decrease in channel slope as filling occurs.

Using the above techniques, mean dune height is calculated to be 0.46 m, which is used to calculate a maximum bankfull flow depth of 6.1 m (Bridge & Tye 2000). Maximum channel width is 237 m and channel belt width is 1.5 – 2.2 km (Bhattacharya & Tye 2004; Bridge & Tye 2000; Bridge & Mackey 1993). Mean flow velocity using a slope of 0.0004, using the method of Holbrook and Wanas (2014), yields a water flow velocity of 1.2 m/s. This is multiplied by cross-sectional channel area to estimate a water discharge of 1707 m³/s. Paleohydraulic estimates are lower when based on point bar dimensions, where channel width is 30-45 m. This may in part be due to incomplete preservation of point bars, and therefore underestimation of bankfull channel depth and width. Maximum preserved point bar height is 3.0 m, maximum bankfull flow depth is 3.3 m, empirically derived channel width is 78.7 m, maximum channel belt width is 523 m, velocity is 1.1 m/s, and discharge is 284 m³/s. This agrees with data from Ullah et al. (2015) in Neilson Wash, who give a velocity range of 0.7 – 1.2 m/s and a discharge range of 70 – 639 m³/s.

When channel slope of 0.0014 is used, paleohydraulic estimates are much higher. Velocity and discharge based on cross-set thickness increases to a maximum of 3.1 m/s and 4506 m³/s respectively. These numbers, when based on point bar height increase to 2.0 m/s for velocity, and 2829 m³/s for discharge, and are outside the range of values presented by Ullah et al. (2015).

4.4 Paleohydraulics for V2

Cumulative grain sizes of representative channels for V2 are shown in Figure 49, slope values for representative channels, CH3, CH2, and CH1 are 0.00030, 0.00015, and 0.00019 respectively. These data suggest that a decrease in slope occurred as V2 was filled, and is supported by a general decrease in sediment caliber upwards (Table 4).

Channel deposits in the interior of the valley system, seen on the East Cliff exposures (Fig. 36) are made up largely of dune-scale cross sets, which range in thickness from 3 – 30 cm with the greatest frequency occurring between 5 – 10 cm (Fig. 50, 51). Mean dune height for V2 is calculated to be 0.18 cm, which yields a mean flow depth of 2.7 m. Channel width is 56.2 m, and maximum channel belt width is 774 m (Bhattacharya & Tye 2004; Bridge & Tye 2000). Based on the channel slope of 0.0003, flow velocity is 0.8 m/s and water discharge between 127 m³/s. These values are generally consistent with Li et al., (2010) data for V2 from Neilson Wash.

Measured section and laser rangefinder data provide excellent control on the maximum preserved point bar height seen in the South Cliff exposures in V2, which have been measured between 5.0 – 5.3 m and maximum bar width is 30 m (Bridge & Tye 2000). These large-scale point bars show bar-top rollovers, which indicates near full preservation of bar height. Point bar height scales to approximately 90% of flow depth (Hajek & Heller 2012). Maximum bankfull flow depth is 5.89 m, which yields a maximum channel width of 222 m, and a maximum channel belt width of 2.2 km. Point bar width scales to 2/3 active channel width, indicating V2 formative channels were up to 90 m wide as measured from the East Cliff exposure, and 53 m wide based on the South Cliff point bars (Ethridge & Schumm 1977). When a slope of 0.0003 is used,

velocity is 0.7 m/s and discharge is 880 m³/s. This velocity estimate also aligns with Li et al. (2010), and Ullah et al. (2015) for both Caineville and Neilson Wash.

When a slope of 0.0014 is used in conjunction with cross-set thickness data, velocity and discharge estimates are 1.8 m/s, and 279 m³/s respectively. When point bar height data is used, these values increase to 2.2 m/s and 2829 m³/s. These results describe the range in size and scale of formative rivers within this valley, and highlight the value in constraining fluvial hydraulic estimates. See Table 3 and 4 for complete results.

4.5 Paleohydraulics for V1

Generally speaking, V1 was formed by the shallowest rivers within this CIV, and this may be in part due to a sampling bias towards the more freely avulsing fluvial deposits nearing the unconfined area above the true incised valley. Cumulative frequency curves for representative channels for V1, as seen in Figure 52, provide D₅₀ estimates, which are used to calculate channel slope (Table 4). Slope decreases as valley filling progresses upward, where CH3 slope is 0.00057, CH2 is 0.00042, and CH1 is 0.00028. This may be attributed to decreasing sediment caliber upwards, or may represent the transition from confined and amalgamated fluvial style to unconfined floodplain and localized fluvial channel deposition. This would also account for the shallower channels, as seen in Table 3, when compared with V2 and V3 paleohydraulics.

The majority of cross-sets fall within the range of 2-6 cm in thickness, with a maximum preserved thickness of 12 cm (Fig. 53). Average dune height based on mean cross-set thickness is 0.08 m, which yields an average flow depth of 1.4 m, channel width of 16.4 m, and channel belt width of 111 m. Velocity estimates, based on a slope of 0.00057, is 0.8 m/s, and discharge is

19 m³/s. Maximum point bar height, measured at 3.3 m yields a bankfull flow depth of 3.67 m, channel width of 93.6 m, and a maximum channel belt width of 1.1 km, velocity of 0.9 m/s, and discharge of 1126 m³/s. Outcrop derived channel widths indicate V1 formative rivers were up to 38 m wide as measured from the South Cliffs, and up to 75 m wide based North architecture (Ethridge & Schumm 1977). This discrepancy between calculation methods can be accounted for based on where these architectural elements are located within the valley. Point bars in V1 are typically located in a valley-central position, however the majority of cross-set thickness measurements were made in a valley-marginal setting, where rivers may have been less constricted and generally more shallow. The majority of these results align with Ullah et al. (2015) from Neilson Wash and Caineville, however are low for the range of values calculated by Li et al. (2010).

When a slope of 0.0014 is used, velocity and discharge values increase dramatically. For the cross-set thickness method, velocity is 1.3 m/s and discharge is 30 m³/s. When point bar height is used, these numbers are 2.9 m/s and 2855 m³/s respectively. These results are generally high when compared with other studies of sequence 1 valleys (Li et al. 2010; Ullah et al. 2015).

5.0 DISCUSSION

5.1 Backwaters and Baylines

The backwater length refers to the landward limit within a fluvial system that marine and tidal effects can propagate upstream (Blum et al. 2013; Paola & Mohrig 1996). Figure 54 show the conceptual diagram depicting the relationship between the backwater length and the fluvial-deltaic system (Blum et al. 2013). This model is able to predict the decline in rate of erosion, degree of channel aggradation, and preservation of tide-influenced facies with respect to valley

position. This limit is given by channel depth/slope, and in the case of V2, sequence 1 of the Ferron, the backwater limit has been calculated to lie between 3 – 9 km from the Ferron paleoshoreline by Ullah et al., (2015). Both backwater and bayline calculations hinge upon estimation of channel slope, which for this study have been calculated: 0.00040 for V3, 0.00030 for V2, and 0.00057 for V1 (Paola & Mohrig 1996; Holbrook & Wanas 2014; Ullah et al. 2015). Based on these slope estimates, the backwater limit is calculated to be 2.5 – 7.2 km for V1, 9 – 22.0 km for V2, and 9.5 – 15.2 km for V3. If a slope of 0.0014 is used, backwater limits are 1.0 – 2.9 km, 1.9 – 4.7 km, and 1.6 – 4.3 km respectively (Table 6).

The bayline represents the landward limit of marine ingress, or the landward most position where marine or brackish water may be present, and is expressed as tidal range/slope (Blum et al. 2013; Bhattacharya et al. 2015). Tidal range for the Ferron was probably low meso-tidal or micro-tidal, suggesting maximum tidal range was less than 2 m (Ryer & Anderson 2004). Using the range in slope values provided by Ullah et al. (2015), the bayline limit for V2 is estimated to fall between 0.6 – 2.8 km from the Ferron paleoshoreline. Slope for V2 from this study yields a maximum bayline limit of 6.6 km from the paleoshoreline. V2 shows abundant estuarine facies and must be in direct communication with the marine system and is therefore interpreted to lie within the bayline limit. Bayline limits for V1 and V3 of this study are 3.5 km and 5.0 km respectively (Table 6).

5.2 Wheeler Analysis

CIVs are hypothesized to form a composite erosional discontinuity that is produced over multiple base-level cycles, and since this surface does not represent any individual geomorphic feature, it represents a stratigraphic and not a topographic valley (Strong and Paola 2008).

Wheeler diagrams, which include facies information, have been produced for all cliff exposures to show the interpreted time stratigraphy of the valley fills (Figs. 55, 56, 57) (Wheeler 1985). Special attention has been paid to categorize channel bodies as fluvial-dominated, tide-affected, or marine-influenced, depending on abundance of tidal and marine features. The valley composite erosional surface, sequence boundary 1, is shown by the red line separating the valley fill units above, from parasequence 4 sandstones beneath. This surface, as illustrated by these diagrams, does not represent a single episode of incision, but is a diachronous composite scour surface. The red lines between valley deposits are interpreted as high frequency sequence boundaries and since each cut and fill episode is interpreted to represent a single 20,000 year Milankovitch cycle, valley incision likely represents no more than 10,000 years of hiatus.

This is seen on the East Cliff Wheeler diagram, which shows both V2 and V3 deposits occupying the space which directly overlies sequence boundary 1 (Fig. 55). The orientation of channel forms in all valleys show laterally amalgamated channel stories and a general south to north channel migration direction. The North Cliff Wheeler diagram juxtaposes deposits from all three valleys upon sequence boundary 1 (Fig. 56). As opposed to those of the East Cliffs, channel stories in the North Cliff section tend to show vertical amalgamation. The South Cliff Wheeler diagram (Fig. 57) also places all three valleys upon the sequence boundary 1 surface and shows vertically amalgamated channel stories within V1 and V3, and lateral accretion in V2, which migrates from west to east as the channel develops. Wheeler analysis for these exposures show that the CIV basal erosional surface, sequence boundary 1, is diachronous, and fluvial deposits within valleys are also diachronous.

5.3 A Stepped Forced Regressive CIV

The Fremont Canyon study shows a general decrease in tide-influence as the CIV fills. V3 is tide-affected within 2 m of the valley base and becomes fluvial-dominated upwards. V3 is thereby interpreted as “flood-based” according to the Willis (1997) model. V2 shows the greatest abundance of marine features, where estuarine biota increase in abundance towards the top 1.5 m of valley fill, and is generally categorized as marine-influenced. V2 is thus “flood-topped”, where the valley contains increasing estuarine and tide-influenced facies upwards. It is critical to note the change in facies within V2 from marine-influenced to fluvial-dominated across the valley. This change highlights the need for greater understanding of the controls on extent and preservation of tidal and marine influenced facies. V1 in the present study shows local *Teredolites*, *Paleophycus*, and double mud draped cross-sets near the valley base, suggesting a tide-affected regime. This likely indicates that V1 is “flood-based”, and experienced marine flooding during an early lowstand minor transgressive phase as the valley began to fill (Willis 1997). As V1 filling progressed, deposition out-paced sea-level rise, and deposits transitioned into fluvial facies. Data from this study agrees that V1 was the most proximal since it exhibits the coarsest sediment in the CIV. This is congruent with observations from Coalmine Wash and Neilson Wash, which determine V1 as the coarsest fill (Li & Bhattacharya 2013; Li et al., 2010). A possible explanation for the fluvial-dominated nature of V1 in Coalmine Wash is that it was located in a more proximal location relative to V1 deposits of the Fremont Canyon, and therefore did not experience flooding during its initial filling stage (Li & Bhattacharya 2013). According to the criteria by Li and Bhattacharya (2013), this CIV is identified as having undergone stepped forced regression. This is based on an observed transition from “flood-based” to “flood-topped”, and back to “flood-based” valley fill and a general decrease in tide-influence across successive

fills. Degree of transgression, or relative sea level is shown on Wheeler diagrams (Fig. 55 - 57) for all cliff exposures. Each exposure documents three episodes of incision and three successive fill cycles of decreasing amplitude. A general increase in basal grain size, indicating increasing distance from the paleoshoreline across successive fills, and identification of multiple valley terraces, each documenting multiple channel stories, supports this interpretation.

Li and Bhattacharya (2013) identified high-frequency stepped forced regression as the primary driver for CIV cut and fill in the Coalmine Wash area. As in the present study, three episodes of cut and fill were identified with a total erosional relief of up to 17 m. V3 was found to contain mostly tide-influenced fluvial deposits, with bimodal paleocurrent flow directions indicating tidal reworking. V2 contains 90% fluvial sandstone, with tide-influenced deposits confined to the upper 10%. V2 shows large-scale lateral accretion which suggests single-thread meandering fluvial style (Miall 1985; Li & Bhattacharya 2013). V1 was filled with fluvial deposits and shows no evidence for tide-influence. It is the only valley to contain extraformational pebbles at the base, and is thus interpreted to represent the farthest valley from the paleoshoreline. The Willis (1997) model categorizes V3 in Coalmine Wash as “flood-based”, where tide-influence is only observed within the basal part of the valley, indicating marine transgression early in valley filling. V2 is categorized as “flood-topped”, where the valley was filled with fluvial deposits and capped with tide-influenced deposits as the system was transgressed towards the end stage of valley filling. This CIV represents an overall basinward shift in facies and less tidal influence with each successive valley fill. Increased erosional down-cutting, and decreased tide-influenced deposits record a long-term stepped forced regression, separated by three transgressive phases which decreased in amplitude as the CIV developed (Li and Bhattacharya 2013).

5.4 High Frequency Allocyclic Eustasy

Sufficient evidence has been put forward to present this system as a CIV with multiple episodes of cut and fill in direct response to sea level change within the Cretaceous Seaway. V3, V2, and V1 exhibit erosional scour surfaces at their base, marking a regionally disconformable regressive surface. These surfaces regionally truncate underlying deposits, and are filled with amalgamated multi-storey fluvial and estuarine deposits. Several locations within the valley exhibit unequivocal evidence for ingress of marine water and thereby record phases of marine transgression.

Chronostratigraphic analysis of the Ferron Notom Delta has been conducted using $^{40}\text{Ar}/^{39}\text{Ar}$ dating of sanidine crystals from several regionally extensive bentonite ash beds. The entire delta complex was deposited between 91.25 Ma and 90.63 Ma, over a period of approximately 620,000 years (Zhu, 2010). There are 7 sequences in the Ferron, thereby each sequence is estimated to have been deposited in less than 100,000 years (Famubode & Bhattacharya 2016). As seen in the regional dip cross section (Fig. 5), the oldest half of sequence 1 is dominated by incised valley fill whereas the younger deposits, which make up the second half of sequence 1, are characterized by unconfined floodplain shales and isolated fluvial channels. Therefore, since three episodes of incision and fill have been recorded within the lower deposits of sequence 1, each valley likely represents ~20,000 year cut and fill cycles, which is congruent with timescales associated with < 20,000 year Milankovitch glacio-eustatic cycles.

5.5 Fluvio-estuarine Facies Models

Many studies have shown that incised valleys deposits can be exceedingly complex and traditional facies models may fail to capture the subtleties of wide compound valley fills. The

tripartite model for wave-dominated estuaries has been used to categorize incised valley fills and predict key facies boundaries. The Fremont Canyon study is interpreted to represent a regressive tide-influenced incised valley complex, which falls within segment 2 of this model, where decreasing tide and marine influence is recorded landward. Dalrymple and Choi (2007) discuss the transgressive nature of estuarine incised valley deposits, where the bayline is represented by the inner end of segment 2. For this model to hold true for the Fremont Canyon study, far more tidal evidence should be observed across all valley fills. For instance, MacEachern and Pemberton (1994) present a litholog (refer to Fig. 23) from a fluvio-estuarine CIV channel-fill complex from the Crystal Field, Viking Formation, Alberta Canada. The log shows multiple incisions and fills with abundant tidal facies including a vast suite of ichnogenera, capped by pebble conglomerates and a flooding surface. In even the most proximal lithologs, facies associations appear to show distinct tide-influence over all stages of valley formation. This is not so for the Ferron CIV, which appears to be far more fluvial in nature. Measured sections from the Fremont Canyon study do not document a *Glossifungites* surface along the basal sequence boundary or across subsequent sequence boundaries. Tide-influence is rare, and estuarine ichnogenera appear only near upper valley fill in V2 and local *Teredolites* surfaces elsewhere in V3 and V1. These valleys are nevertheless interpreted to fall within the backwater limit (Blum et al. 2013). Ferron examples are not capped by pebble conglomerates or flooding surfaces, but grade upward into unconfined fluvial channels and floodplain mudstones, indicating an overall regressive regime, as opposed to the transgressive nature of the Viking Formation. This exemplifies the need for a regressive valley fill facies model which addresses systems where sedimentation out-paces sea level rise. Such a model would be better applied to the present

study, than the more traditional transgressive-estuarine models referred to by MacEachern and Pemberton (1994), and Dalrymple and Choi (2007).

5.6 Value as an Outcrop Analog

Incised valley deposits make up an important class of reservoir, and host a significant portion of global petroleum reserves. Understanding and predicting the internal complexities within CIV fills helps to solve recovery problems often faced with these types of reservoirs. The Morrow Formation of eastern Colorado and western Kansas contains a compound incised valley which shows a total of five preserved sequences. Valley fill transitions from fluvial-dominated, to fluvial with interfingering estuarine facies, to tidal inlet channels and estuarine mudstone facies. Each of these facies represents significant changes in reservoir performance in producing Morrow fields (Bowen & Weimer, 2003). Bowen and Weimer identify the primary valley-fill facies as fluvial-dominated, however estuarine components presents significant reservoir performance challenges. Terraces, which preserve the deepest lowstand deposits, all the way through to transgressive and highstand deposits are more likely to show all segments of the tripartite estuarine facies model. Incised valleys of the Morrow Formation present an interesting comparison to the greater Ferron Notom Delta Complex, where multiple workers have identified various systems tracts and a greater variety of tide-dominated facies than what has been observed in the present study alone.

6.0 CONCLUSIONS

1. Fremont Canyon exposures show a compound incised valley with 3 individual episodes of cut and fill forming a regional composite scour surface, which can be linked to other incised valley exposures across sequence 1 of the Ferron. The Ferron Notom outcrop belt is more

extensive than earlier workers have previously presented, and has been modified to include all known Ferron exposures in the Wayne County area, Utah.

2. Wheeler analysis indicates the composite valley basal erosional surface; sequence boundary 1, is diachronous across the study area.
3. The nature and frequency of cut and fills documented in this study supports Li et al. (2010), and Zhu et al. (2012), which state that Milankovitch-scale sea level fluctuations in the Cretaceous Western Interior Seaway exert a first order control on episodes of incision and fill within this CIV. Chronostratigraphic analysis suggests the CIV was cut and filled in a 60,000 year period; therefore each episode may represent ~20,000 year Milankovitch-scale cyclicity.
4. This study shows that CIV fill passes upwards from “flood-based”, to “flood-topped”, to “flood-based” with each successive valley fill, punctuated by three regressive and then transgressive episodes of decreasing amplitude, thus forming a stepped forced regressive tide-influenced incised valley complex.
5. Tidal facies, including estuarine ichnogenera and double mud drapes, suggests that these exposures lie within the backwater limit, and V2 lies within the bayline limit. Backwater and bayline limit analysis places V1 within 7.2 km, V2 within 6.6 km, and V3 within 15.2 km of the Ferron paleoshoreline.
6. Formative rivers were capable of delivering water discharges on the order of 2855 m³/s for V1, up to 2829 m³/s for V2, and 4506 m³/s for V3, and are interpreted as trunk rivers.
7. All valleys document a decrease in sediment caliber (D₅₀ grain size) upwards, which may be

attributed to decreasing channel slope as the valleys filled over time.

8. Traditional facies models for fluvio-estuarine systems over-simplify lithologic distributions within compound incised valley fills. The Fremont Canyon CIV is far more fluvial in nature than other fluvio-estuarine CIVs and does not correspond well with traditional transgressive estuarine incised valley models, despite evidence that valley segments are within the tidal backwater limit (and within the bayline for V2).
9. This CIV is part of a broad, long lived paleovalley system and is thus extremely heterogeneous with regard to architectural fill, tidal facies, and grain size distribution across simple valley fills and across its entirety. The Ferron CIV may be an appropriate analog for other large-scale Cretaceous CIVs such as the fluvio-estuarine McMurray Formation, and Morrow Formation.

7.0 REFERENCES

- Allen, G.P. & Posamentier, H.W., 1993, Sequence stratigraphy and facies model of an incised valley fill: The Gironde Estuary, France. *Journal of Sedimentary Petrology*, v. 63 no. 3, p. 378–391.
- Allen, J.R.L., 1964, A review of the origin and characteristics of recent alluvial sediments. *Sedimentology*, v. 5, p. 89–191.
- Armstrong, R.L., 1968, Sevier Orogenic belt in Nevada and Utah. *Geological Sciences of America Bulletin*, v. 79, p. 429–258.
- Bhattacharya, J.P., Copeland, P., Lawton, T.F., Holbrook, J., 2015, Estimation of source area , river paleo-discharge , paleoslope , and sediment budgets of linked deep-time depositional systems and implications for hydrocarbon potential. *Earth Science Reviews*, p. 1–34.
- Bhattacharya, J.P. & MacEachern, J.A., 2009, Hyperpynal rivers and prodeltaic shelves in the Cretaceous Seaway of North America. *Journal of Sedimentary Research*, v. 79, p. 184–209.
- Bhattacharya, J.P. & Tye, R.S., 2004, Searching for Modern Ferron Analogs and Application to Subsurface Interpretation. *AAPG Studies in Geology*, 50, p. 39–57.
- Bowen, D., Weimer, P., 2003, Regional sequence stratigraphic setting and reservoir geology of Morrow incised-valley sandstones (lower Pennsylvanian), eastern Colorado and western Kansas. *AAPG*. v. 5, no. 5, p. 781 – 815.
- Blum, M. Martin, J., Milliken, K., Garvin, M., 2013, Paleovalley systems : Insights from Quaternary analogs and experiments. *Earth Science Reviews*, v. 116, p. 128–169.
- Blum, M.D. & Tornqvist, T.E., 2000, Fluvial responses to climate and sea-level change : a review and look forward. *Sedimentology*. v. 47, p. 2–48.
- Bridge, J.S., 2003, Rivers and Floodplains. Blackwell.
- Bridge, J.S. & Tye, R.S., 2000, Interpreting the dimensions of ancient fluvial channel bars, channels, and channel belts from wireline-logs and cores. *AAPG Bulletin*, v. 84, no.8, p. 1205–1228.
- Church, M., 2006, Bed Material Transport and the Morphology of Alluvial River Channels. *Annual Review of Earth and Planetary Sciences*, v. 34, p. 325–356.
- Dalrymple, R., Choi, K, 2007, Morphologic and facies trends through the fluvial-marine transition in tide-dominated depositional systems: A schematic framework for environmental and sequence-stratigraphic interpretation. *Earth Science Reviews*, v. 81, p. 135 – 174.
- Dalrymple, R., Zaitlin, B., Boyd, R, 1992, Estuarine Facies Models: Conceptual Basis and Stratigraphic Implications: Perspective. *Journal of Sedimentary Research*, v. 62, no. 6, p. 1130-1146.

- Deveugle, P.E.K., Jackson, M.D., Hampson, G.J., Stewart, J., Clough, M.D., Ehighebo, T., Farrell, M.E., Calvert, C.S., Miller, J.K., 2014, A comparative study of reservoir modeling techniques and their impact on predicted performance of fluvial-dominated deltaic reservoirs. *AAPG Bulletin*, v. 98, no. 4, p. 729–763.
- Donselaar, M.E., Overeem, I., 2008, Connectivity of fluvial point-bar deposits: An example from the Miocene Huesca fluvial fan, Ebro Basin, Spain. *AAPG Bulletin*, v. 9, no. 9, p. 1109 – 1129.
- Ethridge F.G., Schumm, S.A., 1977, Reconstructing Paleochannel Morphologic and Flow Characteristics: Methodology, Limitations, and Assessment. *Fluvial Sedimentology*, v. 5, p. 705–721.
- Famubode, O. & Bhattacharya, J.P., 2016, Sequence Stratigraphic Analysis of the youngest non-marine sequence in the Cretaceous Ferron-Notom Delta, South Central Utah, USA. *Journal of Sedimentary Research*, v. 86, p. 168-198.
- Fielding, C.R., 2011, Foreland basin structural growth recorded in the Turonian Ferron Sandstone of the Western Interior Seaway Basin , USA. *Geology*, v. 39, no. 12, p. 1107–1110.
- Gani, R.M., Bhattacharya, J.P. & MacEachern, J.A., 2008, Using Ichnology to determine relative influence of waves, storms, tides, and rivers in deltaic deposits: examples from Cretaceous western interior seaway, U.S.A. *Applied Ichnology*, p.209–225.
- Gardner, M.H., 1995a, Tectonic and eustatic controls on the stratal architecture of mid-Cretaceous stratigraphic sequences, central western interior foreland basin of North America. *Stratigraphic Evolution of Foreland Basins*, v. 52, p. 243–281.
- Gardner, M.H., 1995b, The stratigraphic hierarchy and tectonic history of the mid-Cretaceous foreland basin of central Utah. *Stratigraphic Evolution of Foreland Basins: SEPM, Special Publication*, v. 52, p. 283–303.
- Garrison, J.R. & Van Den Bergh, T.C.V., 2006, Effects of Sedimentation rate, rate of relative rise in sea level and duration of sea-level cycle on the filling of incised valleys: examples of filled and “overfilled” incised valleys from the Upper Ferron Sandstone, Last Chance Delta, East-Central Utah,. *SEPM Special Publication*, v. 85, p. 239–279.
- Gibling, M.R., 2006, Width and Thickness of Fluvial Channel Bodies and Valley Fills in the Geological Record: A Literature Compilation and Classification. *Journal of Sedimentary Research*, v. 76, no. 5, p. 731–770.
- Gingras, M.K., Bann, K.L., MacEachern, J.A., Waldron, J., Pemberton, S.G., 2009, A Conceptual Framework for the application of trace fossils. *Applied Ichnology*, v. 52, p. 1–26.
- Griffin, C.R., 2013. Facies Architecture, Paleo-hydraulics and Fluvial Style of a Falling Stage Terrace Deposit within a Compound Incised Valley System , Ferron Notom Delta , Utah (*unpublished thesis*).

- Hajek, E.A. & Heller, P.L., 2012, Flow-depth scaling in alluvial architecture and nonmarine sequence stratigraphy: example from the Castlegate Sandstone, Central Utah, U.S.A. *Journal of Sedimentary Research*, v. 82, p. 121–130.
- Hale, L.A., 1946. Depositional history of the Ferron formation, central Utah. *Utah Geological Association*, p. 29–40.
- Hale, L.A. & Van De Graaff, F., 1964, Cretaceous Stratigraphy and facies patterns - northeastern Utah and Adjacent areas. *Utah Geological Ass*, p. 115–137.
- Hill, R.B., 1982, Depositional environments of the Upper Cretaceous Ferron Sandstone, south of Notom, Wayne County, Utah, *Brigham Young University, Geology Studies*, v. 29, p. 59-83.
- Holbrook, J. & Wanas, H., 2014, A Fulcrum Approach To Assessing Source-To-Sink Mass Balance Using Channel Paleohydrologic Parameters Derivable From Common Fluvial Data Sets With An Example From the Cretaceous of Egypt. *Journal of Sedimentary Research*, v. 84, no. 5, p.349–372.
- Holbrook, J.M. & Bhattacharya, J.P., 2012, Reappraisal of the sequence boundary in time and space: Case and considerations for an SU (subaerial unconformity) that is not a sediment bypass surface, a time barrier, or an unconformity. *Earth-Science Reviews*, v. 113, no. 3-4, p. 271–302.
- Krystinik, L.F. & Leckie, D.A., 1992, A Tale of Two Valleys: Predicting Facies Architecture and Reservoir Quality in Incised Valley Fills. *AAPG Search and Discovery*, Article #91012.
- Leclair, S.F. & Bridge, J.S., 2001, Quantitative interpretation of sedimentary structures formed by river dunes. *Journal of Sedimentary Research*, v. 71, no. 5, p. 713–716.
- Li, W., 2009. Valleys, facies and sequence stratigraphy of the Ferron Notom Delta, Capital Reef, Utah.
- Li, W., Bhattacharya, J.P., Campbell, C., 2010, Temporal Evolution of Fluvial Style in a Compound Incised-Valley Fill, Ferron “Notom Delta”, Henry Mountains Region, Utah (U.S.A.). *Journal of Sedimentary Research*, v. 80, no. 6, p. 529–549.
- Li, Y., 2012, Facies Architectural Study of Incised Valleys, Distributary Channels and mouth Bars in the Cretaceous Ferron Notom Delta, Southern Central Utah, USA.
- Li, Y. & Bhattacharya, J.P., 2013, Facies-Architecture Study of A Stepped, Forced Regressive Compound Incised Valley In the Ferron Notom Delta, Southern Central Utah, U.S.A. *Journal of Sedimentary Research*, v. 83, no. 3, p. 206–225.
- Lynds, R.M., Mohrig, D., Hajek, E.A., Heller, P.L., 2014, Paleoslope Reconstruction in Sandy Suspended-Load-Dominant Rivers, *Journal of Sedimentary Research*, v. 84, p. 825-836.
- MacEachern, J.A., Bann, K.L., Bhattacharya, J.P., Howell, C.D., 2005. Ichnology of deltas: organism responses to the dynamic interplay of rivers, waves, storms, and tides. *SEPM Special Publication No. 83*, p. 49-85.

- MacEachern, J.A., Gingras, M.K., Bann, K., Dafoe, L.T., Pemberton, S.G., 2009, Applications of ichnology to high-resolution genetic stratigraphic paradigms. In *Applied Ichnology*. p. 95 – 129.
- Maceachern, J.A. & Pemberton, S.G., 1994, Ichnological aspects of incised-valley fill systems from the Viking Formation of the Western Canada Sedimentary Basin, Alberta, Canada. *SEPM Special Publication*, v. 51, p. 129–157.
- Mackey, S.D. & Bridge, J.S., 1995, Three-Dimensional Model of Alluvial Stratigraphy: Theory and Application. *Journal of Sedimentary Research*, v. 65, no. 1, p. 7–31.
- Miall, A.D., 2010, Alluvial deposits, in James, N. P., and Dalrymple, R.W., eds., *Facies Models 4: Geological Association of Canada*, p. 105-137.
- Miall, A.D., 1988, Architectural elements and bounding surfaces in fluvial deposits: anatomy of the Kayenta formation (lower jurassic), Southwest Colorado. *Sedimentary Geology*, v. 55, no. 3-4, p. 233–262.
- Miall, A.D., 1985, Architectural-element analysis: A new method of facies analysis applied to fluvial deposits. *Earth-Science Reviews*, v. 22, p. 261–308.
- Miall, A.D., 1988, Reservoir Heterogeneities in Fluvial Sandstones: Lesson From Outcrop Studies. *The AAPG Bulletin*, v. 72, no. 6, p. 682–697.
- Mitchum, R.M., Van Wagoner, J.C., 1991, High-frequency sequences and their stacking patterns : sequence-stratigraphic evidence of high-frequency eustatic cycles. *Sedimentary Geology*, v. 70, p. 1–2.
- Paola, C. & Mohrig, D., 1996, Palaeohydraulics revisited: paleoslope estimation in coarse-grained braided rivers. *Basin Research*, v. 8, p. 243–254.
- Parker, G., 2004, 1D Sediment Transport Morphodynamics with Applications to Rivers and Turbidity Currents: E book, <http://www.nced.umn.edu/>.
- Peterson, F., Ryder, R.T. & Law, B.E., 1980, Stratigraphy, sedimentology, and regional relationships of the Cretaceous system in the Henry Mountains Region, Utah. *Henry Mountains Symposium*, p.151–170.
- Plint, G.A., 2010, Wave- and Storm-dominated shoreline and shallow marine, in James, N. P., and Dalrymple, R.W., eds., *Facies Models 4: Geological Association of Canada*, p. 165-199.
- Posamentier, H.W. & Vail, P.R., 1988, Sequence Stratigraphy: Sequences and Systems Tract Development. *CSPG Memoir*, v. 15, p. 571–573.
- Richards, B.H., 2014, Fluvial to marine facies succession in a compound incised valley system in the Ferron-Notom Delta, Utah (*unpublished thesis*).
- Ryer, T.A. & Anderson, P.B., 2004, Facies of the Ferron Sandstone, East-Central Utah. *AAPG Studies in Geology*, v. 50, p. 59–78.

- Savrda, C.E., 1991, Teredolites, wood substrates, and sea-level dynamics. *Geology*, v. 19, p. 905–908.
- Shanley, K.W. & McCabe, P.J., 1994, Perspectives on the Sequence Stratigraphy of Continental Strata. *AAPG Bulletin*, v. 78, no. 4, p. 544–568.
- Smith D., Hubbard, S., Leckie, D., Fustic, M., 2009, Counter point bar deposits: lithofacies and reservoir significance in the meandering modern Peace River and ancient McMurray Formation, Alberta, Canada. *Sedimentology*, v. 56, p. 1655 – 1669.
- Strong, N. & Paola, C., 2010, Valleys That Never Were: Time Surfaces Versus Stratigraphic Surfaces. *Journal of Sedimentary Research*, v. 80, no. 1, p. 4–5.
- Ullah, M.S., 2015, Fluvial Architecture and paleohydraulic analysis of ancient river deposits in plan-view and 2-D vertical outcrops of the Turonian Ferron Notom Delta, Utah: From allogenic valleys to autogenic bars.
- Ullah, M.S., Bhattacharya, J.P. & Dupre, W.R., 2015, Confluence scours versus incised valleys: examples from the Cretaceous Ferron Notom Delta, Southeastern Utah, U.S.A. *Journal of Sedimentary Research*, v. 85, p. 445–458.
- Visser, M.J., 1980, Neap-spring cycles reflected in Holocene subtidal large-scale bedform deposits : A preliminary note. *Geology*, v. 8, no. 11, p. 543–546.
- Van Wagoner, J.C., Mitchum, R.M., Campion, K.M., Rahmanian, V.D., 1990, Siliciclastic Sequence Stratigraphy in Well Logs, Cores, and Outcrops: Concepts for High-Resolution Correlation of Time and Facies. *AAPG Methods in Exploration*, v. 7, p. 1–55.
- Wheeler, H.E., 1958, Time Stratigraphy. *AAPG Bulletin*, v. 42, p. 1047 – 1063.
- Willis, B.J., 1997, Architecture of fluvial-dominated valley-fill deposits in the Cretaceous Fall River Formation. *Sedimentology*, v. 44, p. 735–757.
- Wright, V.P. & Marriott, S.B., 1993, The sequence stratigraphy of fluvial depositional systems: the role of floodplain sediment storage. *Sedimentary Geology*, v. 86, p. 203–210.
- Zaitlin, B.A., Dalrymple, R.W. & Boyd, R., 1994, The Stratigraphic Organization of Incised-valley Systems associated with Relative Sea-level Change. *SEPM Special Publication*, v. 51, p. 45-60.
- Zhu, Y., Bhattacharya, J.P., Li, W., Lapen, T.J., Jicha, B.R., Singer, B.S., 2012, Milankovitch-Scale Sequence Stratigraphy and Stepped Forced Regressions of the Turonian Ferron Notom Deltaic Complex, South-Central Utah, U.S.A. *Journal of Sedimentary Research*, v. 82, no. 9, p. 723–746.
- Zhu, Y., 2010. Sequence Stratigraphy and Facies Architecture of the Cretaceous Ferron notom Delta Complex, South Central Utah, USA.

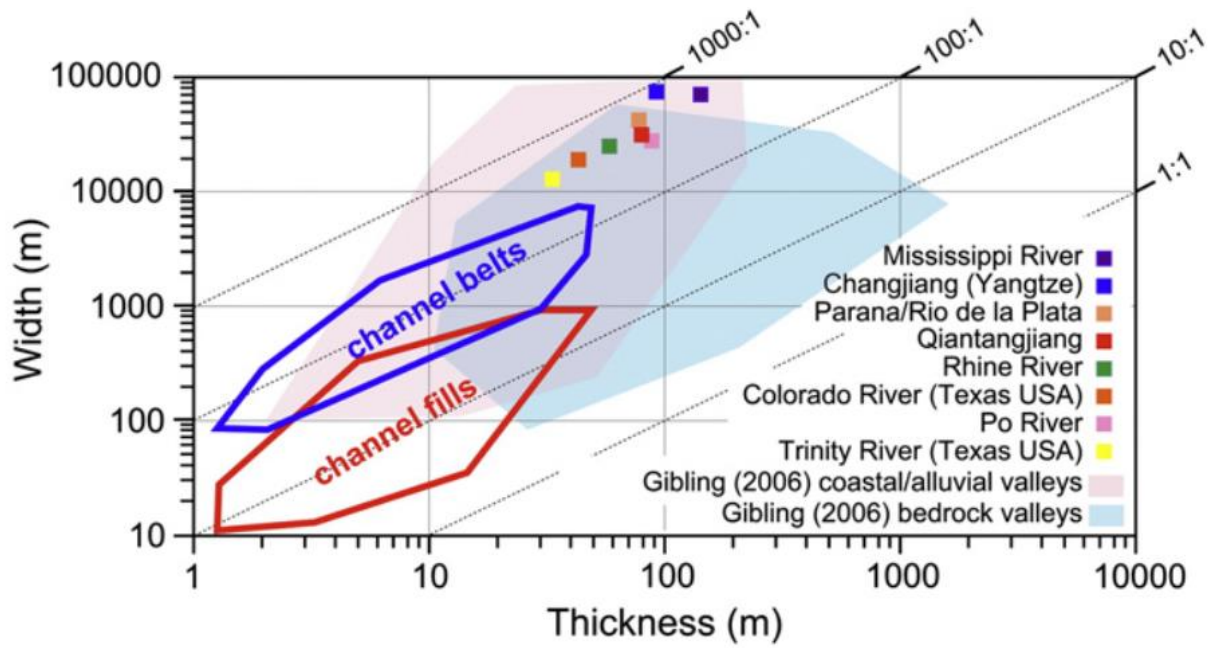


Figure 1. W/T plot for a suite of modern valleys, a selection of 60 ancient coastal-plain examples, and several from the bedrock alluvial realm (Blum et al. 2013).

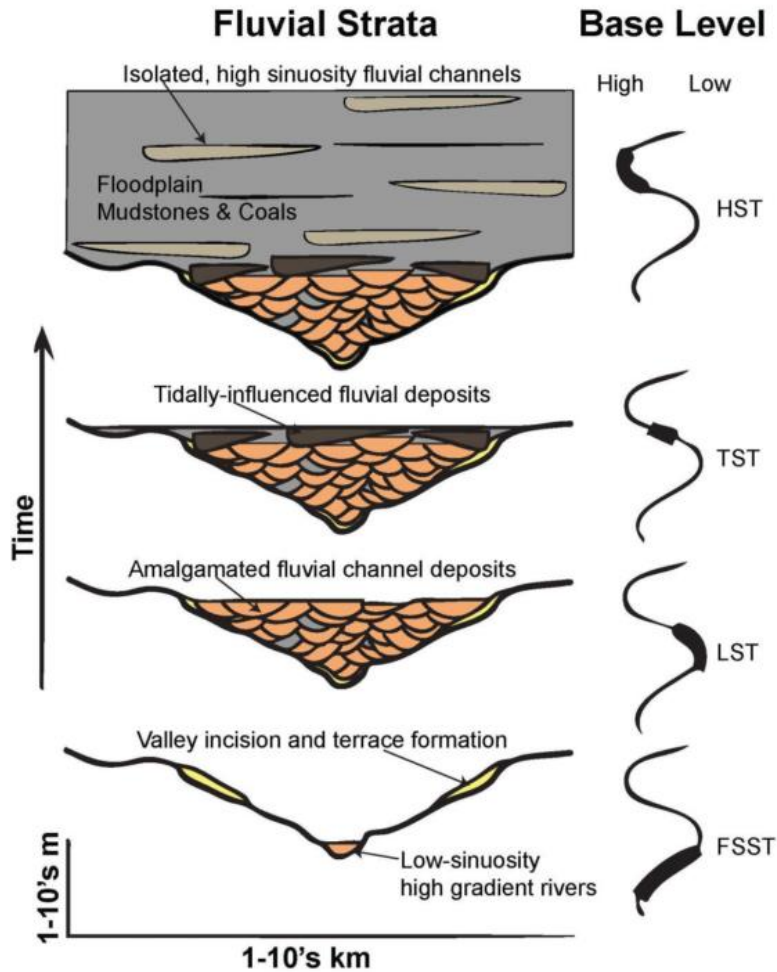


Figure 2. Schematic diagram showing incised valley fill in strike view, and fluvial style and facies evolution as sea-level rises over time. This model by Shanley and McCabe (1994), (modified by Hilton, (2013); Griffin (2013)), predicts that valley fill begins with deposition by low sinuosity single-thread meandering systems forming amalgamated fluvial channels which pass upward into increasingly tide-influenced facies. As the system becomes unconfined, isolated freely avulsing high sinuosity fluvial channels and floodplain shales are deposited.

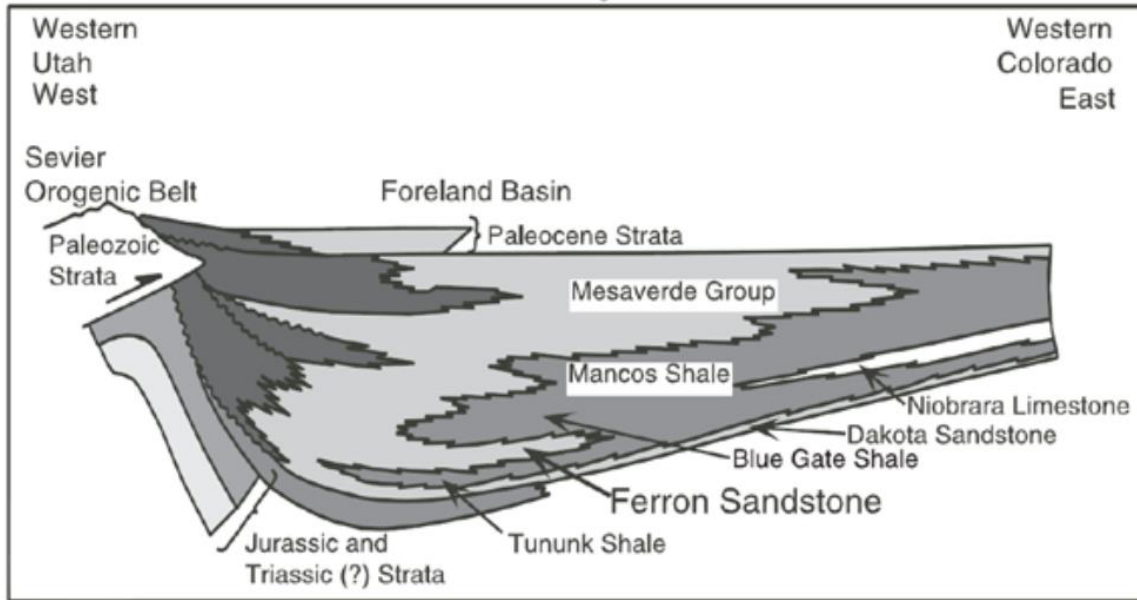


Figure 3. Regional cross section showing the stratigraphy of the Mancos Shale Formation and the Ferron Sandstone Member; a north-eastward thinning clastic wedge that was deposited into the Western Interior Seaway, sourced from the Sevier Orogenic Belt to the west (Armstrong 1968).

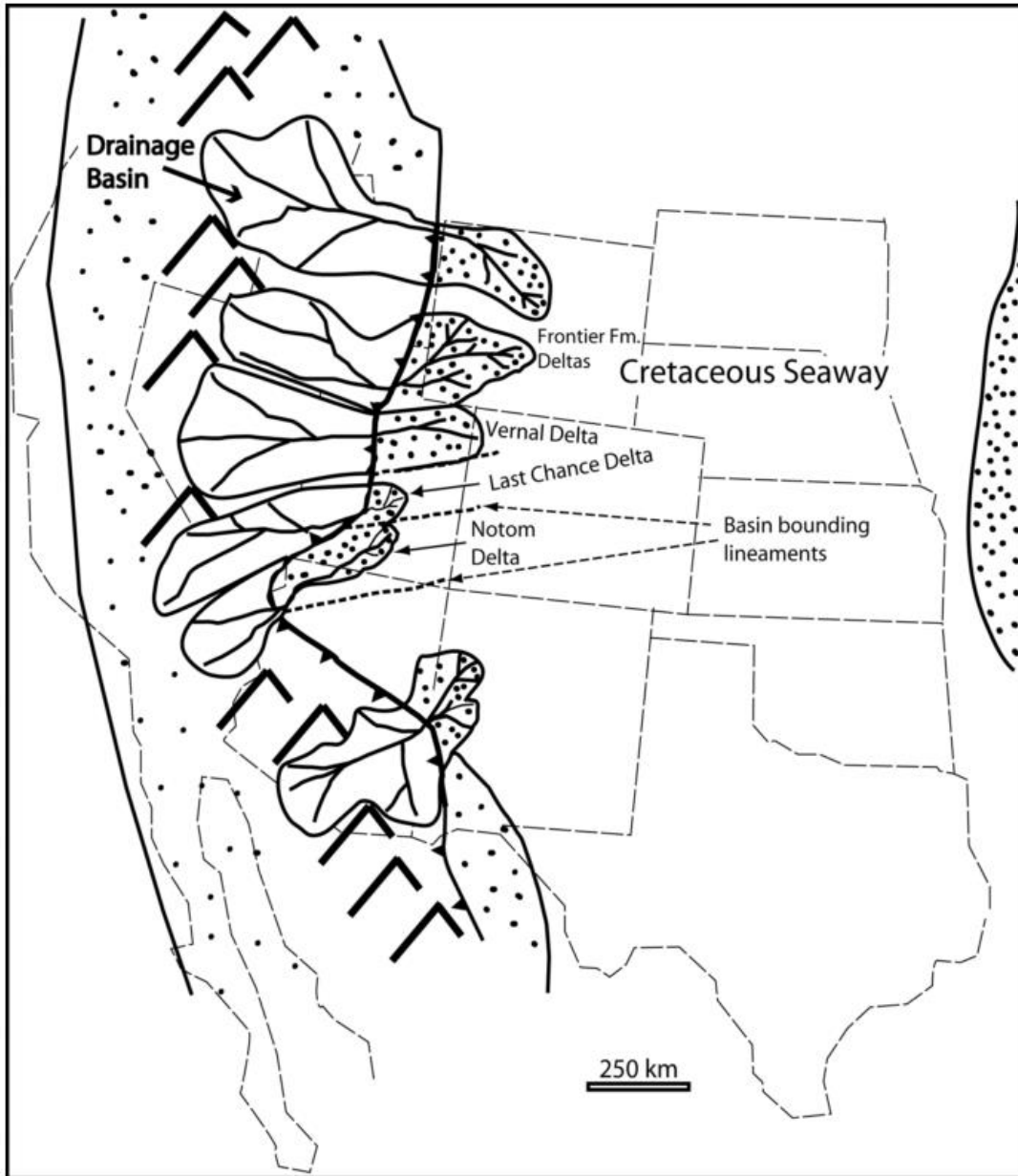


Figure 4. Paleogeographic map showing the Western Interior Seaway occupying much of the continental U.S.A., and Ferron fluvio-deltaic wedges, the Vernal Delta, the Last Chance Delta, and the Notom Delta (Bhattacharya & Tye 2004, modified from Gardner 1995a).

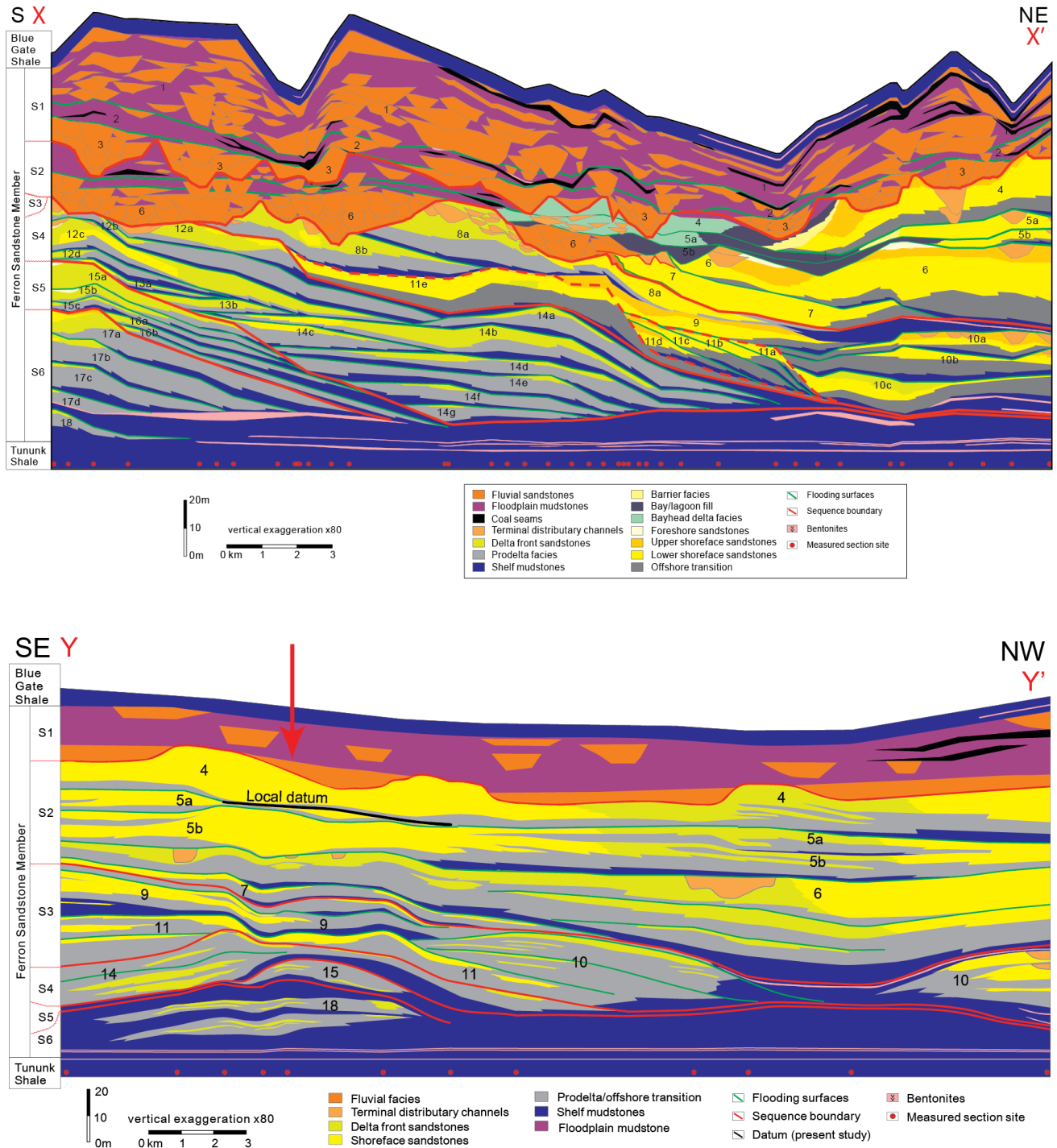


Figure 5. Dip cross section (above) and strike cross section (below) of the Ferron Notom Delta. The black line represents the stratigraphic location of the datum used in the study and the red arrow indicates the approximate location of study area within sequence 1 incised valley fill (Zhu et al., 2012; Li 2009).

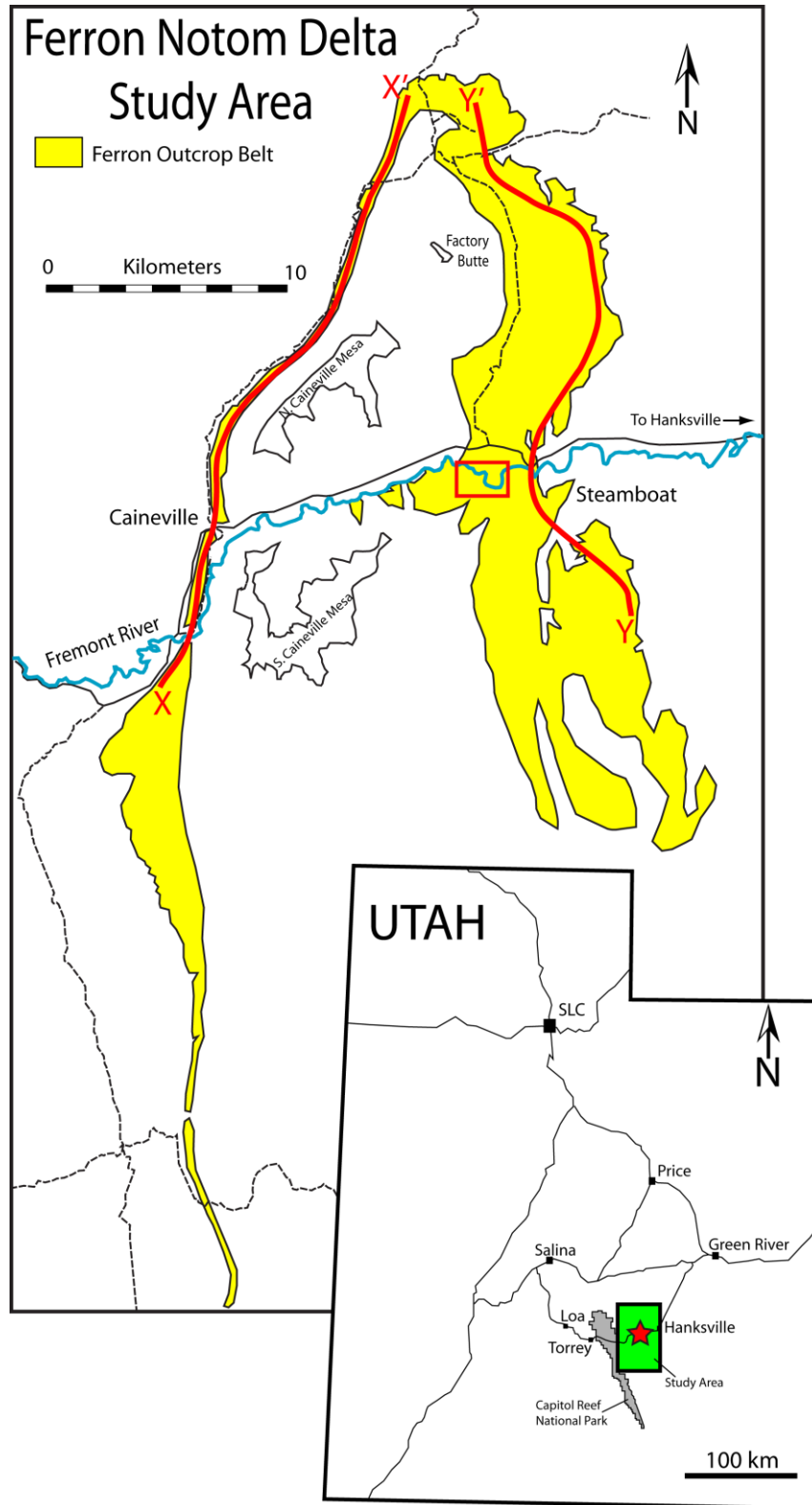


Figure 6. Map of the Ferron Notom Delta outcrop in the Hanksville region, Utah. The present study is located along the banks of the Fremont River and is marked by the red box. Locations of cross-sections in Figure 5 are shown at X – X’ and Y – Y’.

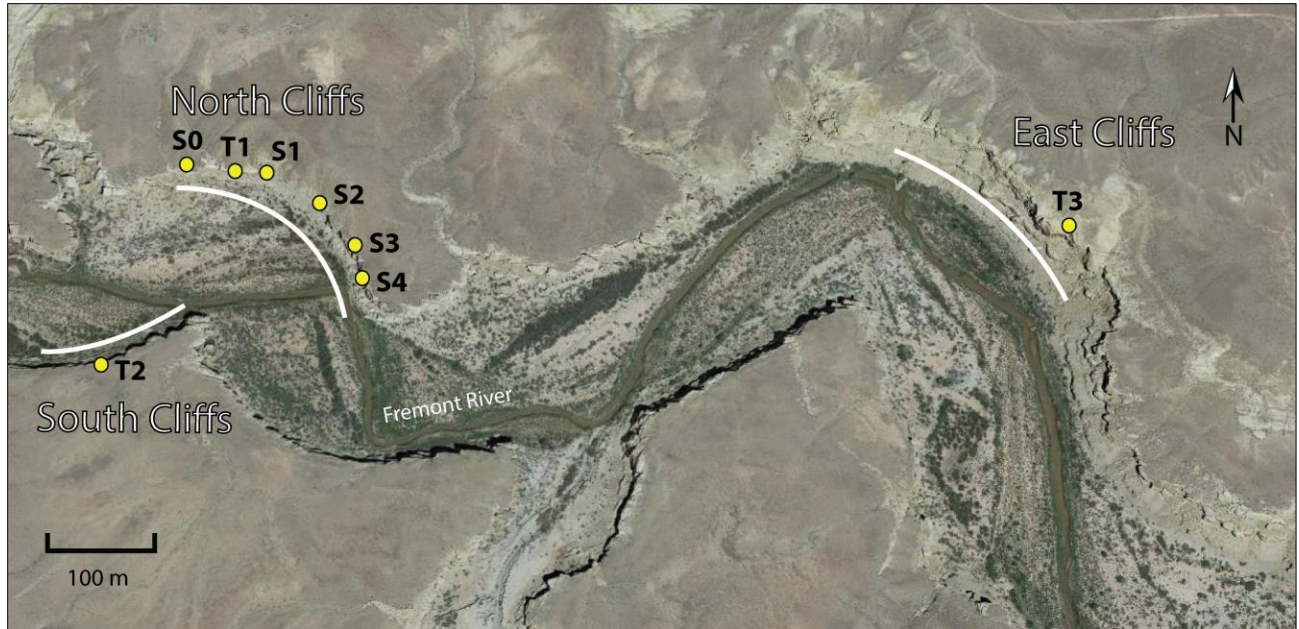


Figure 7. Google Earth image of the study area with incised valleys exposed on cliffs along the Fremont River near Sweetwater Creek, Utah. Cross sections indicate the locations of gigapan photomosaics, interpreted bedding architecture diagrams, and grain size distribution diagrams for the North, South, and East Cliff exposures. Yellow dots show the locations of measured sections.



Figure 8. Mud rip up clast rich zone near the base of a valley.



Figure 9. Vertical cliff face showing slumped and deformed block with preserved internal laminations from bank collapse of previously deposited channel fill.



Figure 10. Underside view of base of V3, with log impression and associated *Teredolites clavatus* burrows.



Figure 11. Dense mat of *Teredolites longissimus* at underside of bed in contact with underlying coal, marking a transgressive surface, indicating full incursion of marine water within 1 m of base of V1.

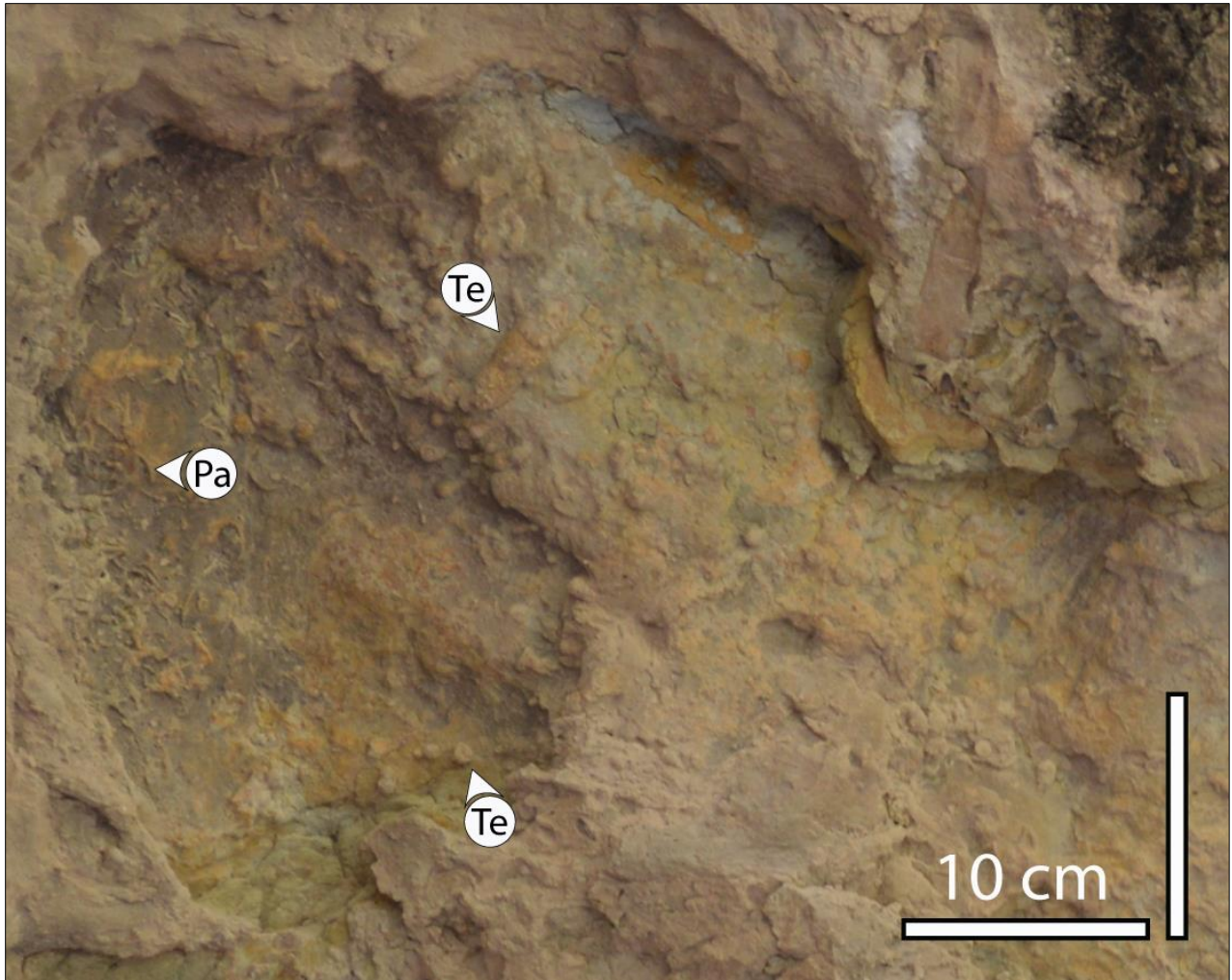


Figure 12. *Teredolites clavatus* and *Paleophycus* burrows at the underside of V3 basal surface; traces are associated with wood log deposition and influx of marine water.

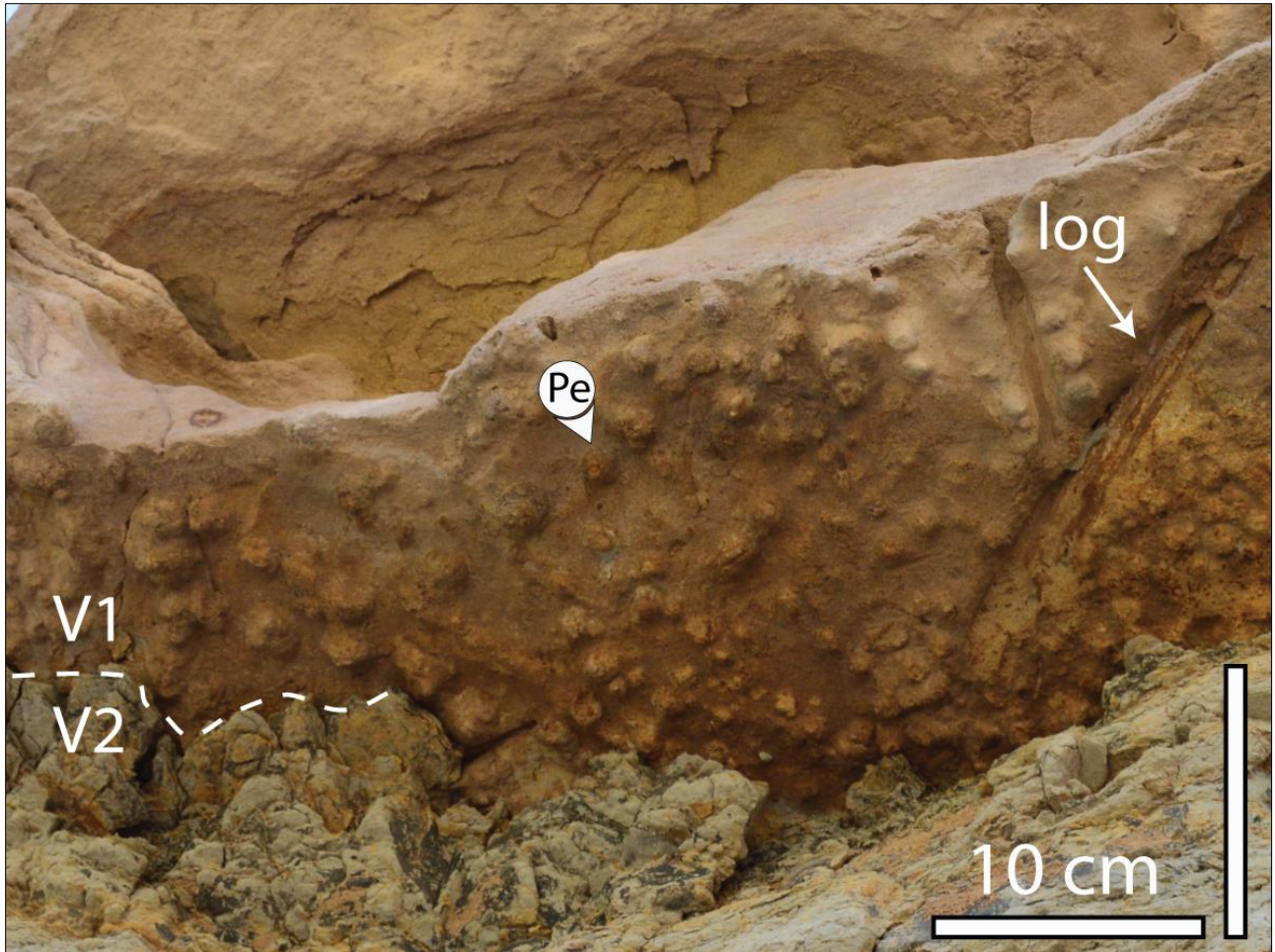


Figure 13. *Pelecypodichnus (Lockeia)* burrows and a preserved log impression on the underside of the valley basal erosional surface of V1, indicating a fresh water environment. Note mud-dominated deposits of underlying V2 IHS.

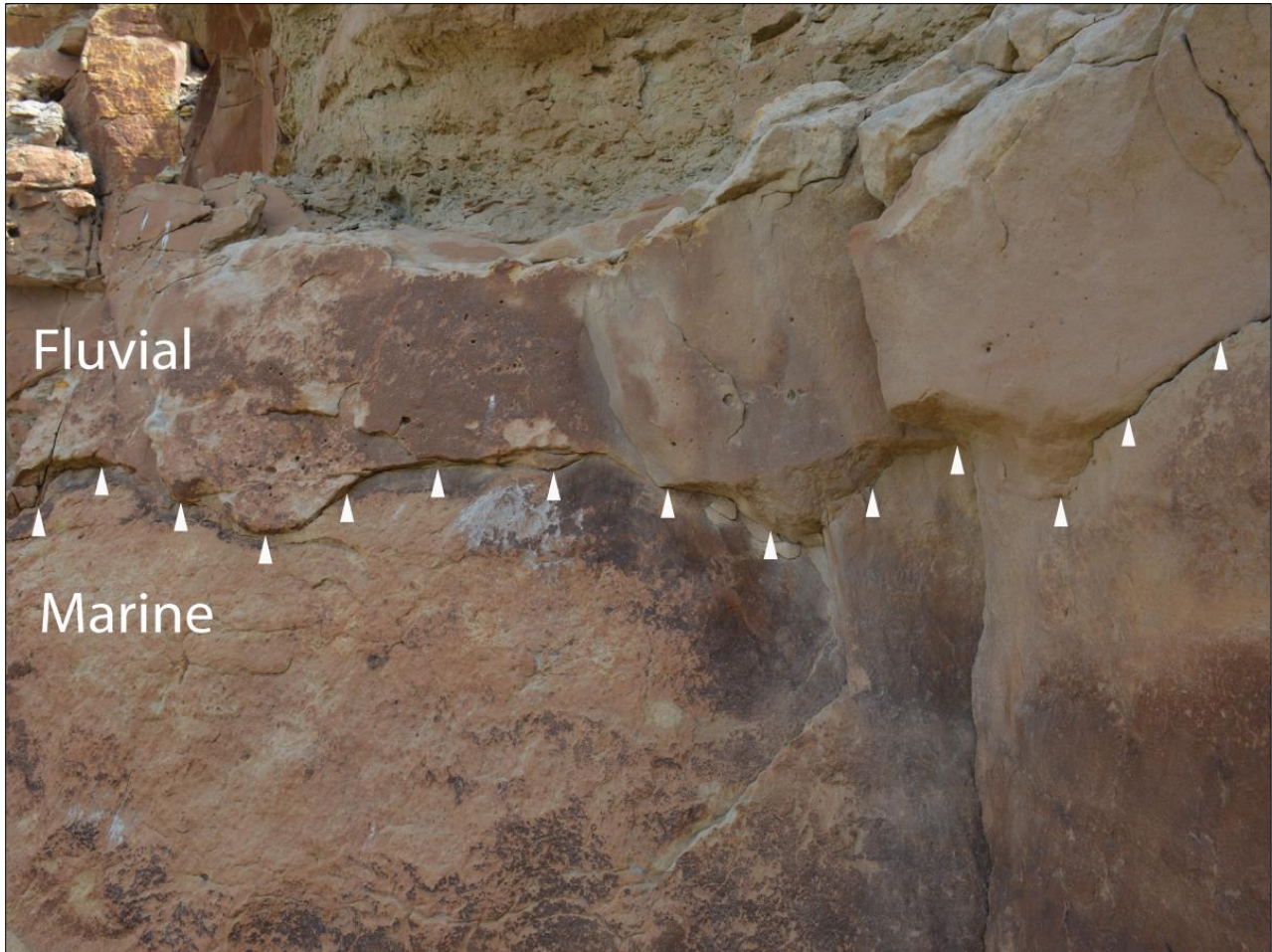


Figure 14. Undulating erosional scour surface marking abrupt transition from underlying marine shoreface (PS 4) to fluvial deposits above (V3). This basinward shift in facies across the erosional surface marked by the white arrows is sequence boundary 1.

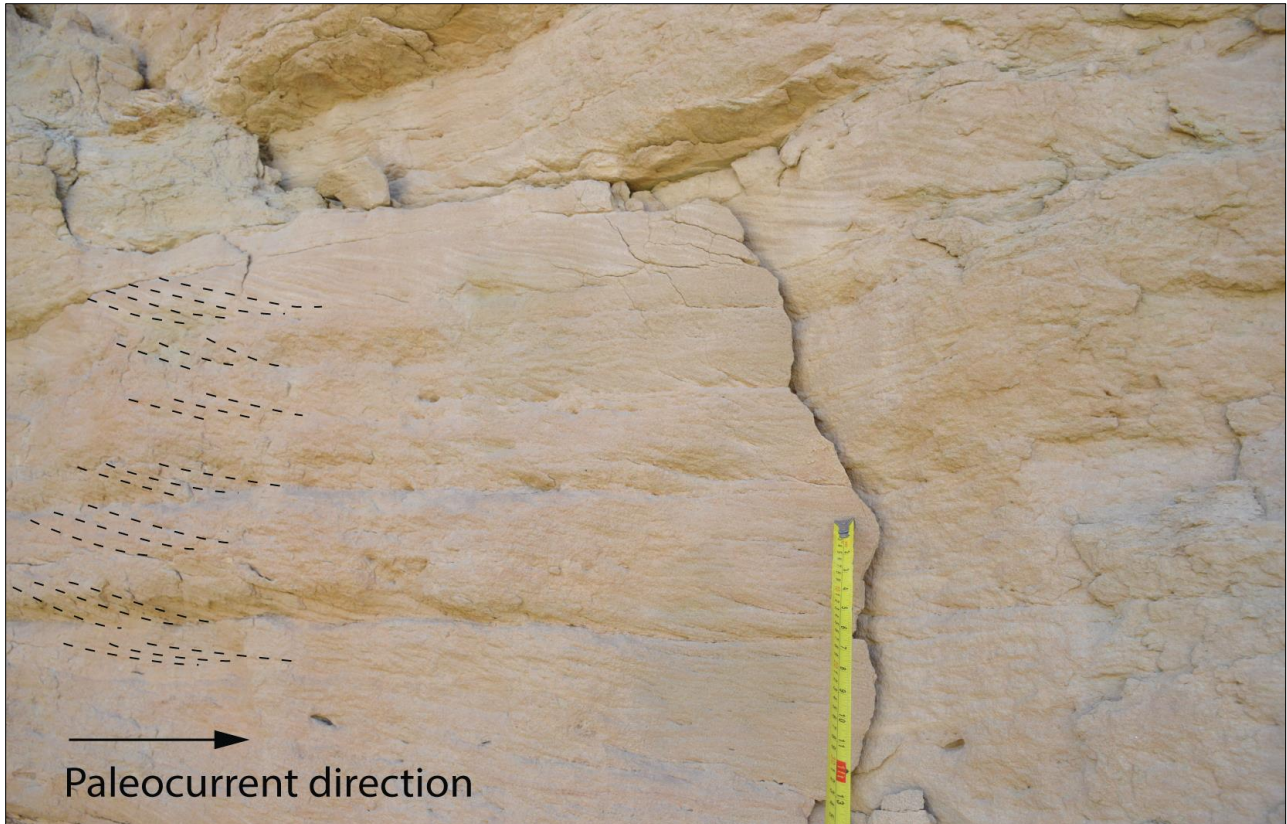


Figure 15. Stacked dune-scale cross-sets in fine upper sandstone.



Figure 16. Bar-scale lateral accretion beds dipping at 18°.

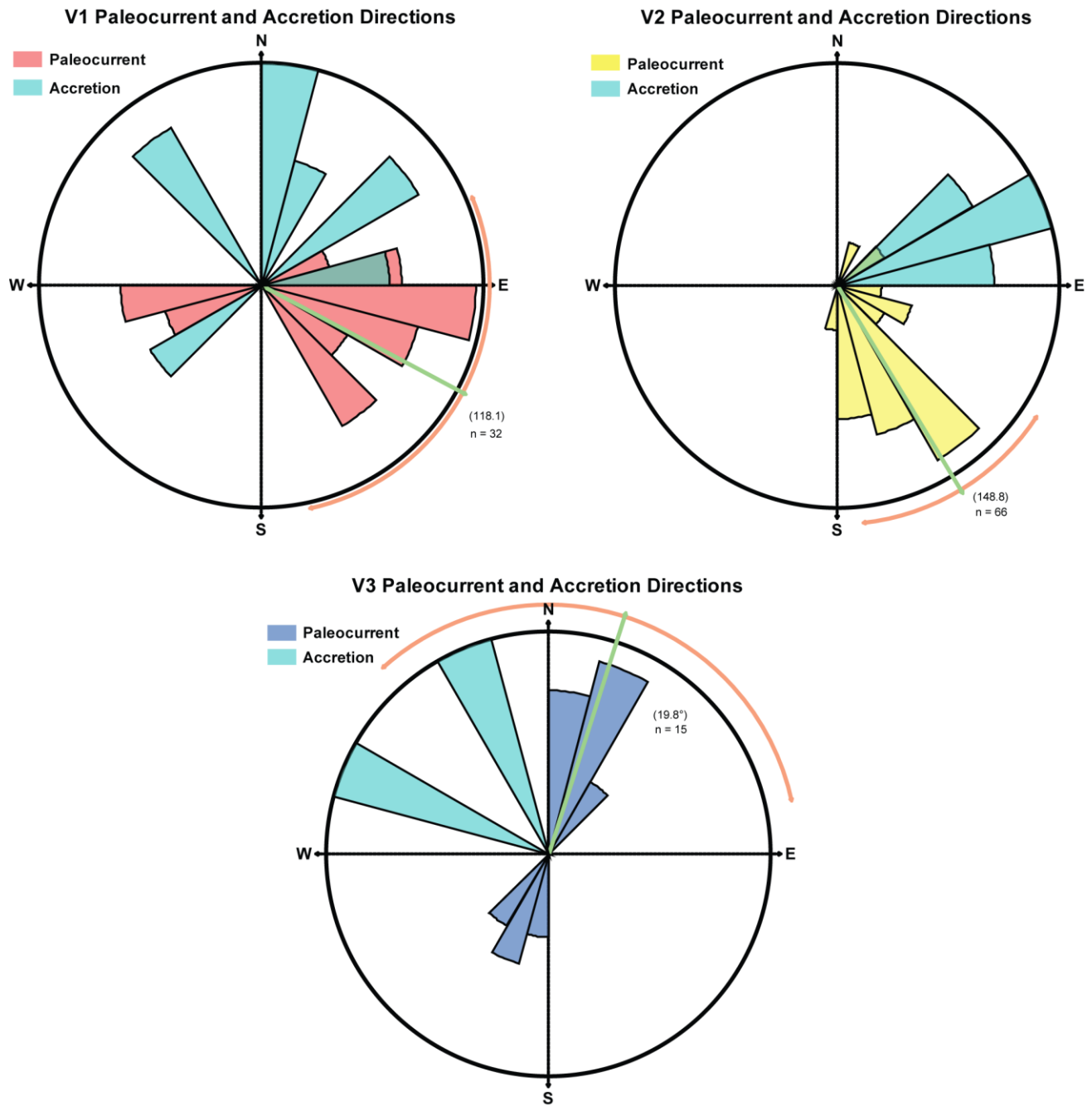


Figure 17. Rose diagrams showing paleocurrent and accretion directions derived from measured sections for V1, V2, and V3. Opposing paleocurrent directions may represent reworking by tidal processes.

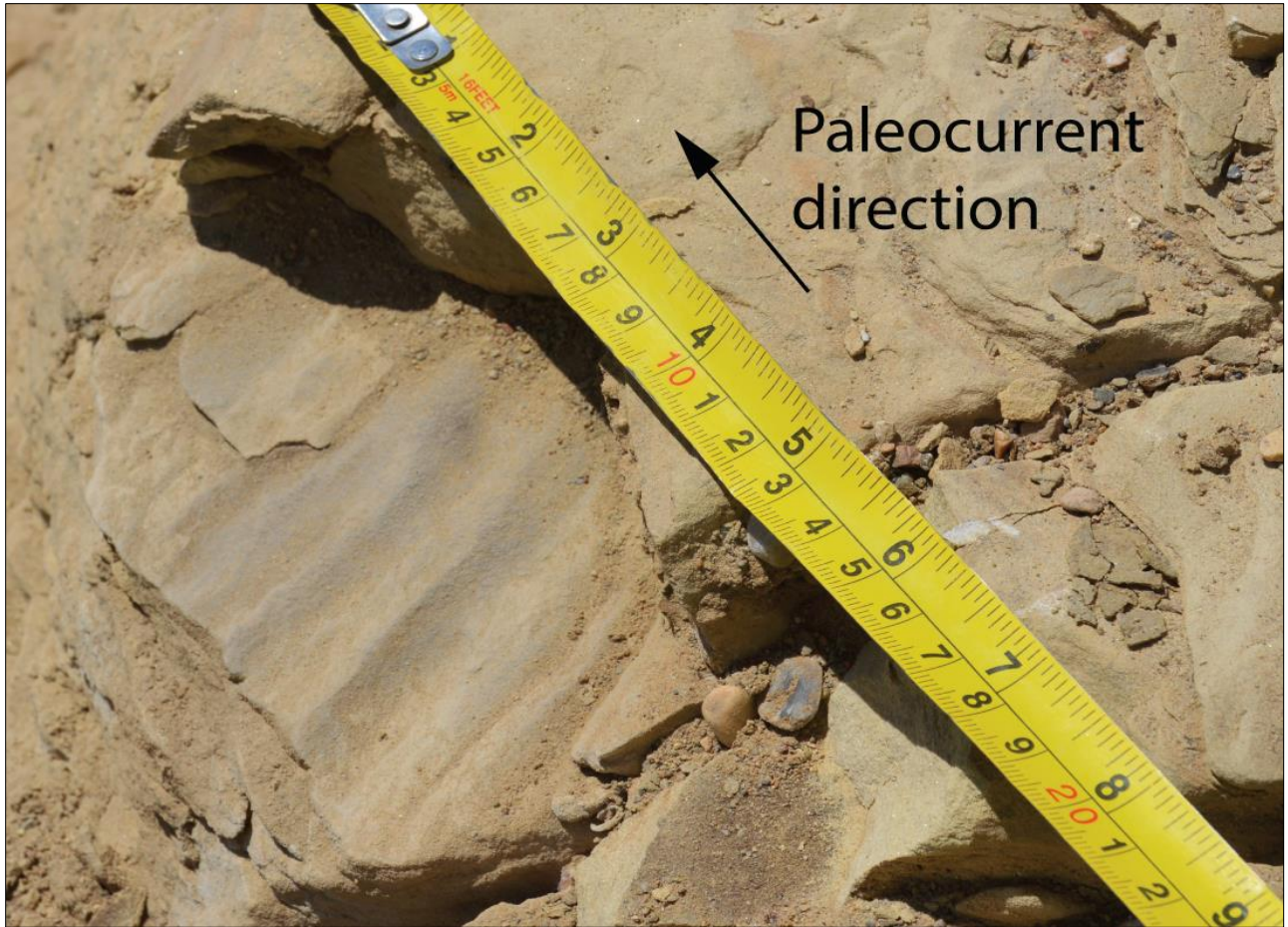


Figure 18. Current ripples in fine lower sandstone indicating paleocurrent flow direction.



Figure 19. Rib and furrows; the planform expression of dune-scale cross bedding. 1.5 m J-staff for scale.



Figure 20. Double mud draped quasi-planar stratification in medium grained sandstone in V3.

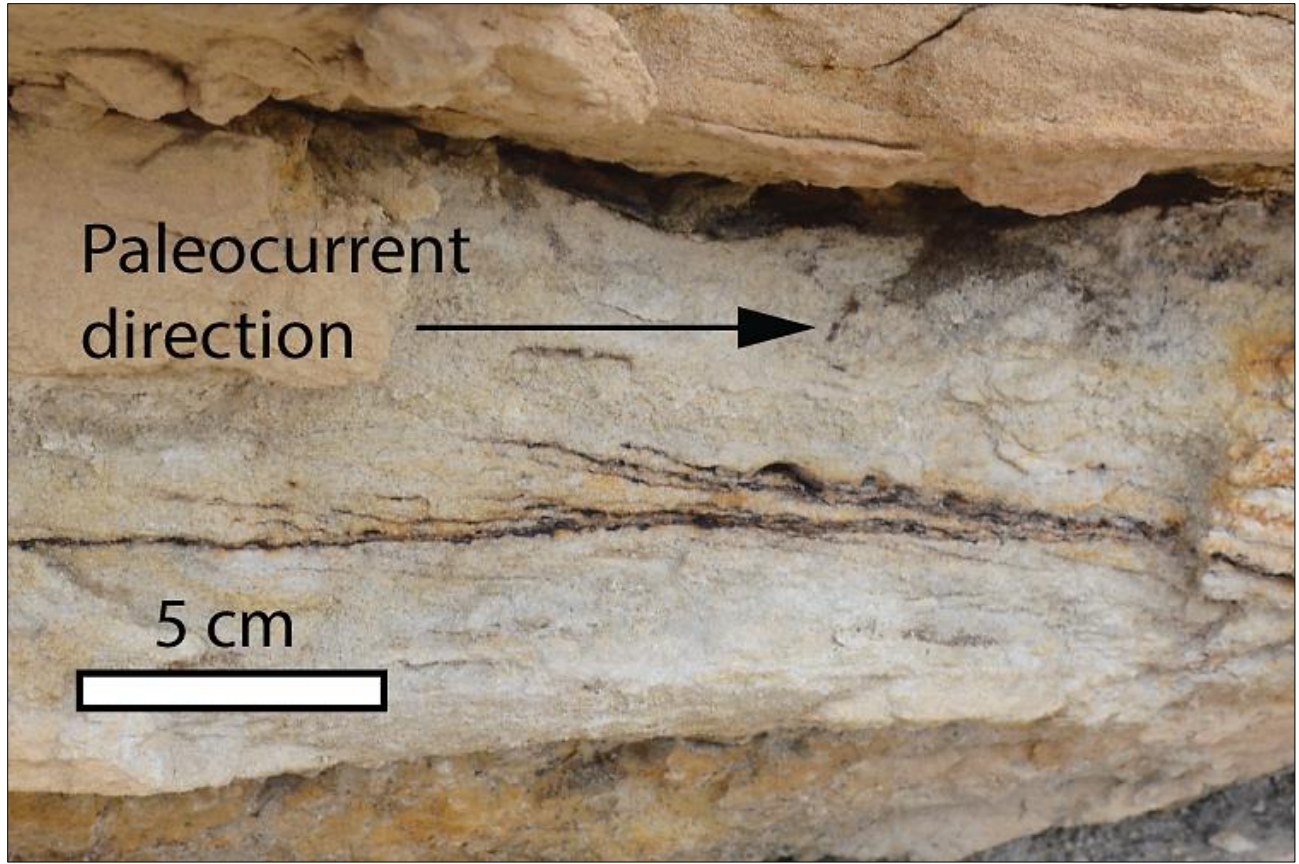


Figure 21. Dune-scale cross bedding with double mud drapes in fine grained sandstone, near the base of V1.

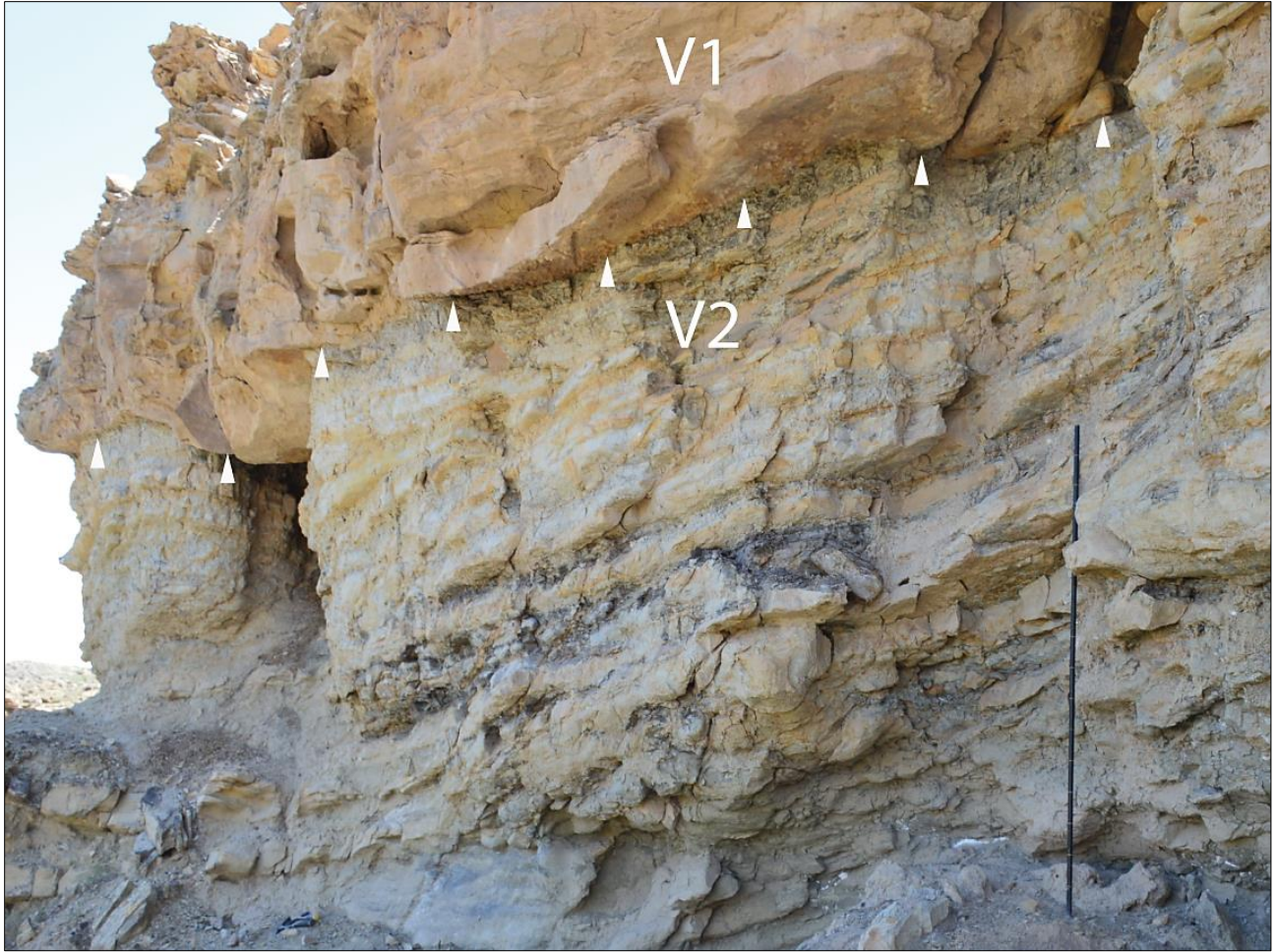


Figure 22. IHS in estuarine muddy upper point bar deposits of V2. Note the undulating erosional base marked by the white arrows and relatively clean and coarse sandstone of overlying V1. Note the 1.5 m J-staff for scale.



Figure 23. Normal fault in mud-dominated IHS of V2.

Figure 24 (following page). Estuarine and marine trace fossils in mud-dominated IHS within V2. Ichnogenera include *Chondrites*, *Rhizocorallium*, *Planolites*, *Paleophycus*, and simple *Teichichnus*.

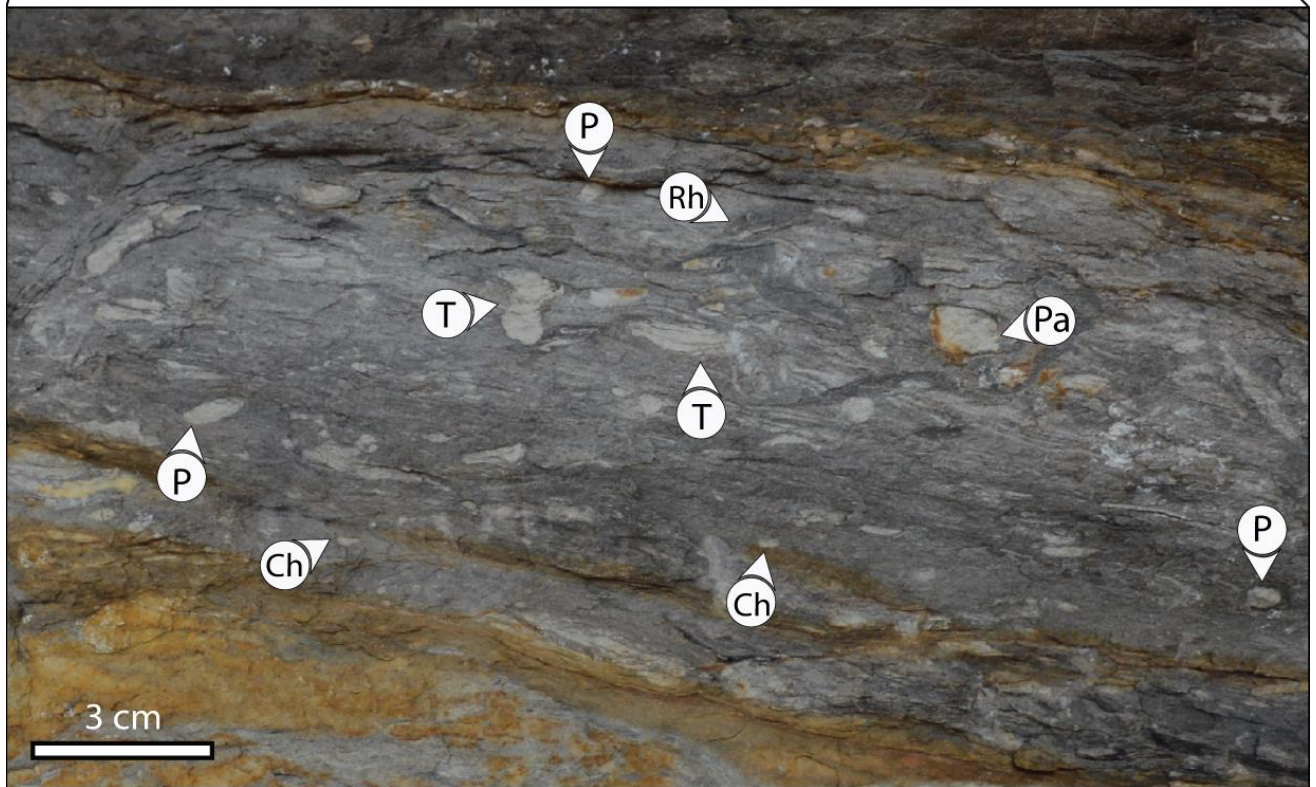
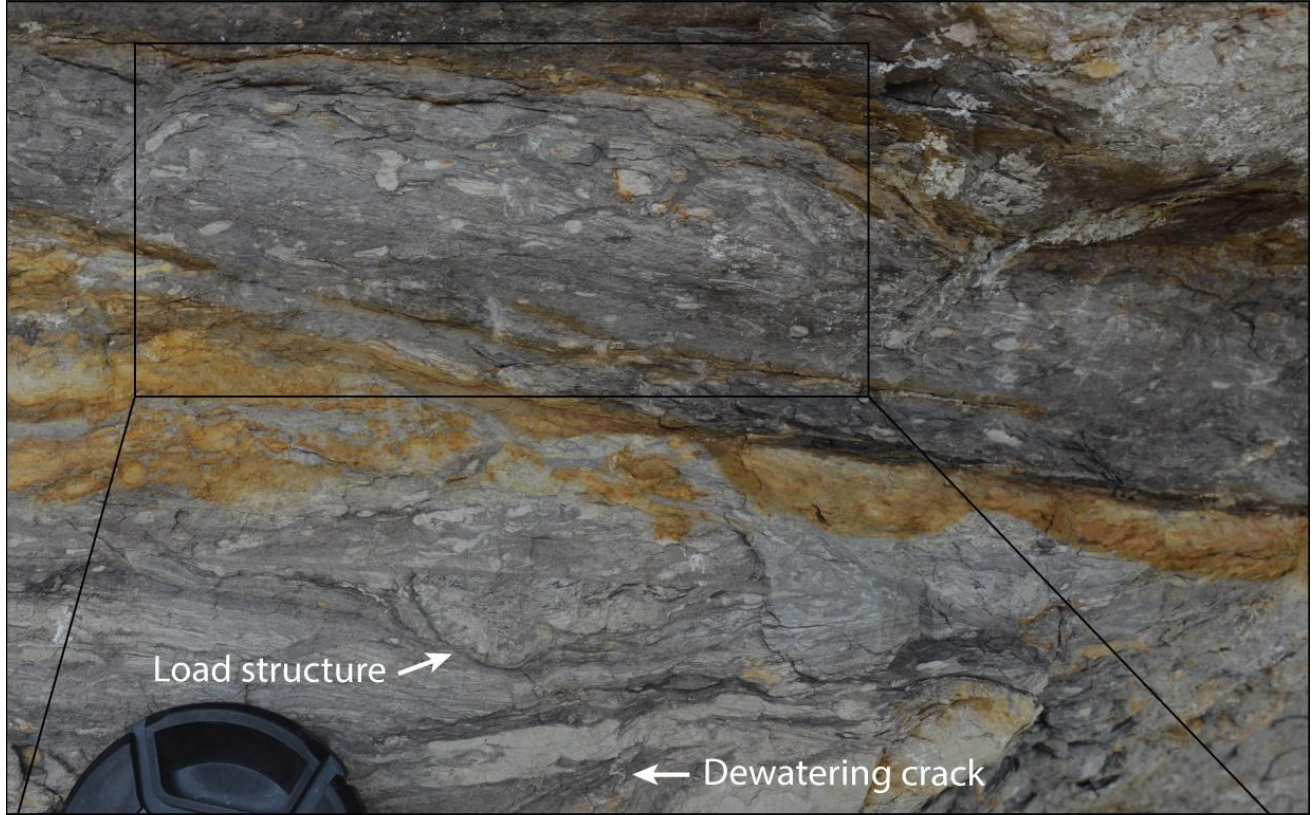




Figure 25. *Lockeia* bivalve burrows at underside of sand beds in V1.

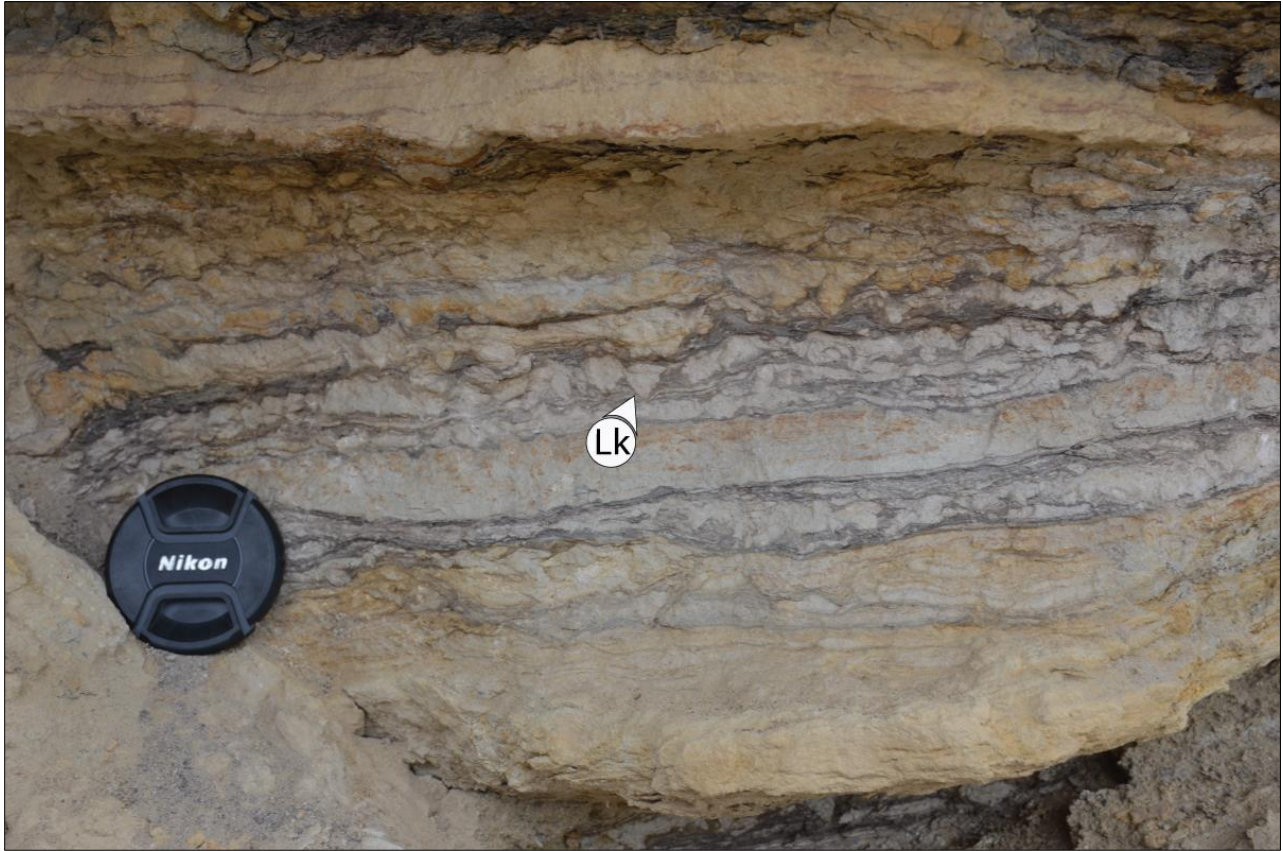


Figure 26. Rhythmic interlaminated mudstone and sandstone with *Lockeia* bivalve burrows in V1.



Figure 27. Sand beds pinching out to the left towards the valley margin (V1).



Figure 28. Organic-rich floodplain shale from V1.

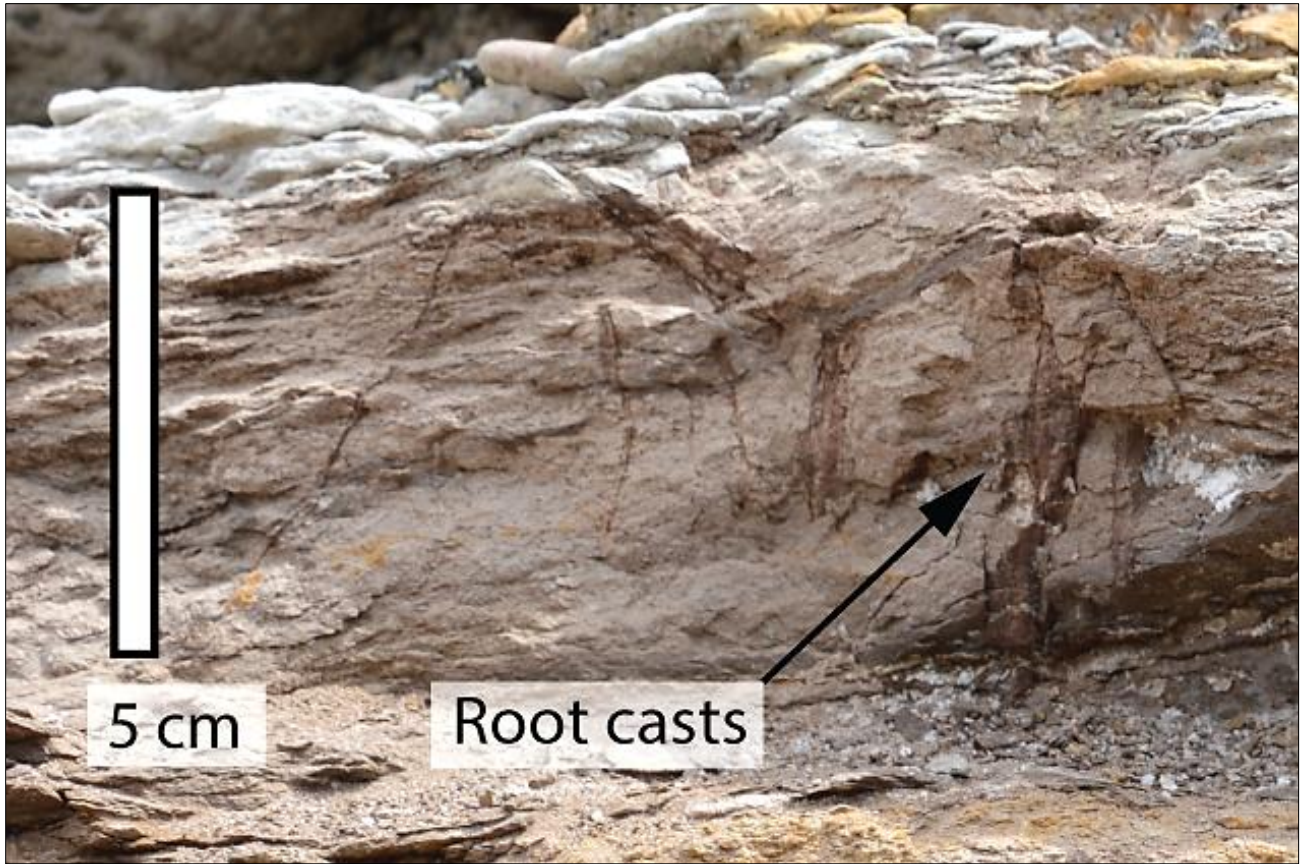


Figure 29. Root casts in very fine sand and shale in V1.

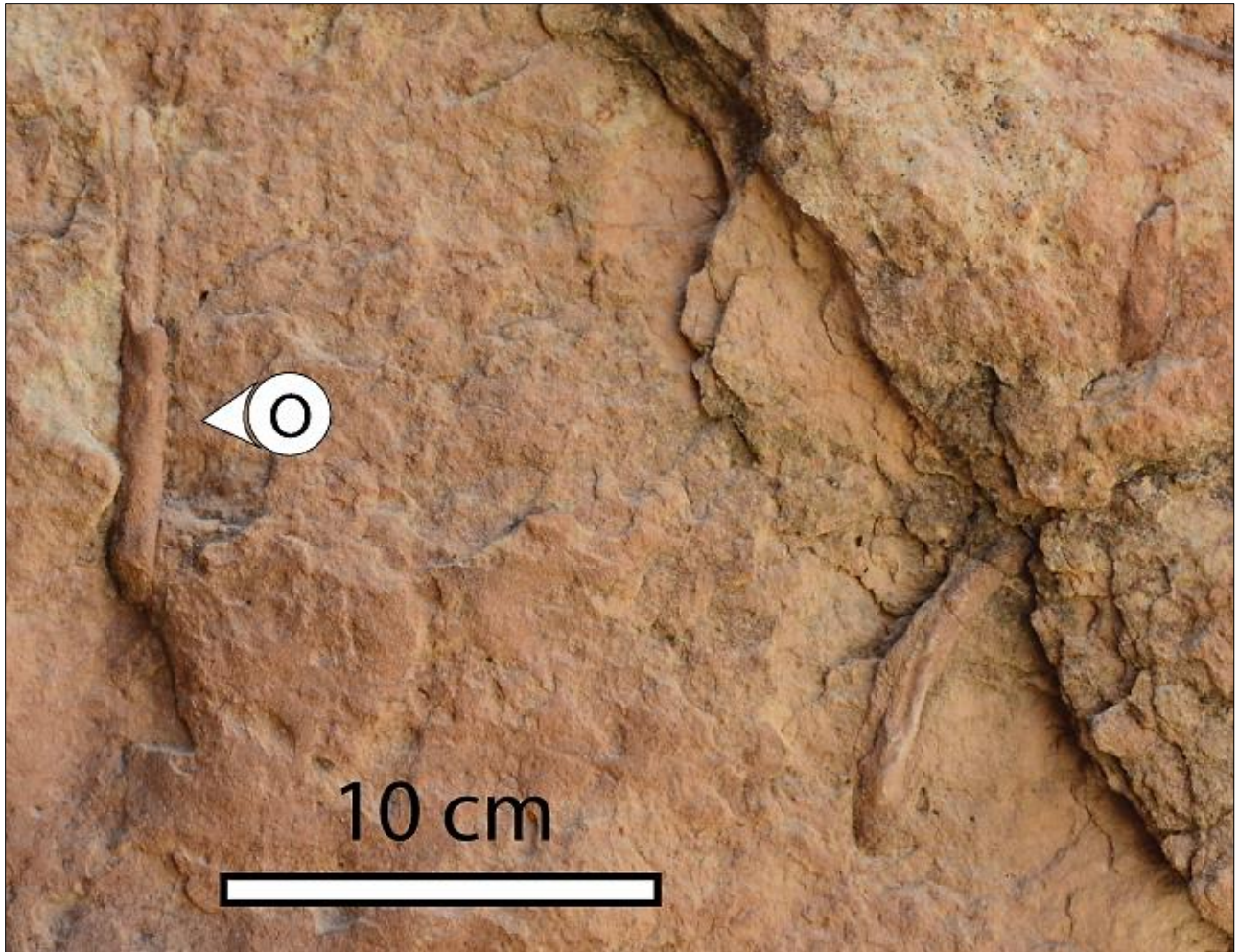


Figure 30. *Ophiomorpha* burrows in heavily bioturbated middle shoreface sandstones of parasequence 4.

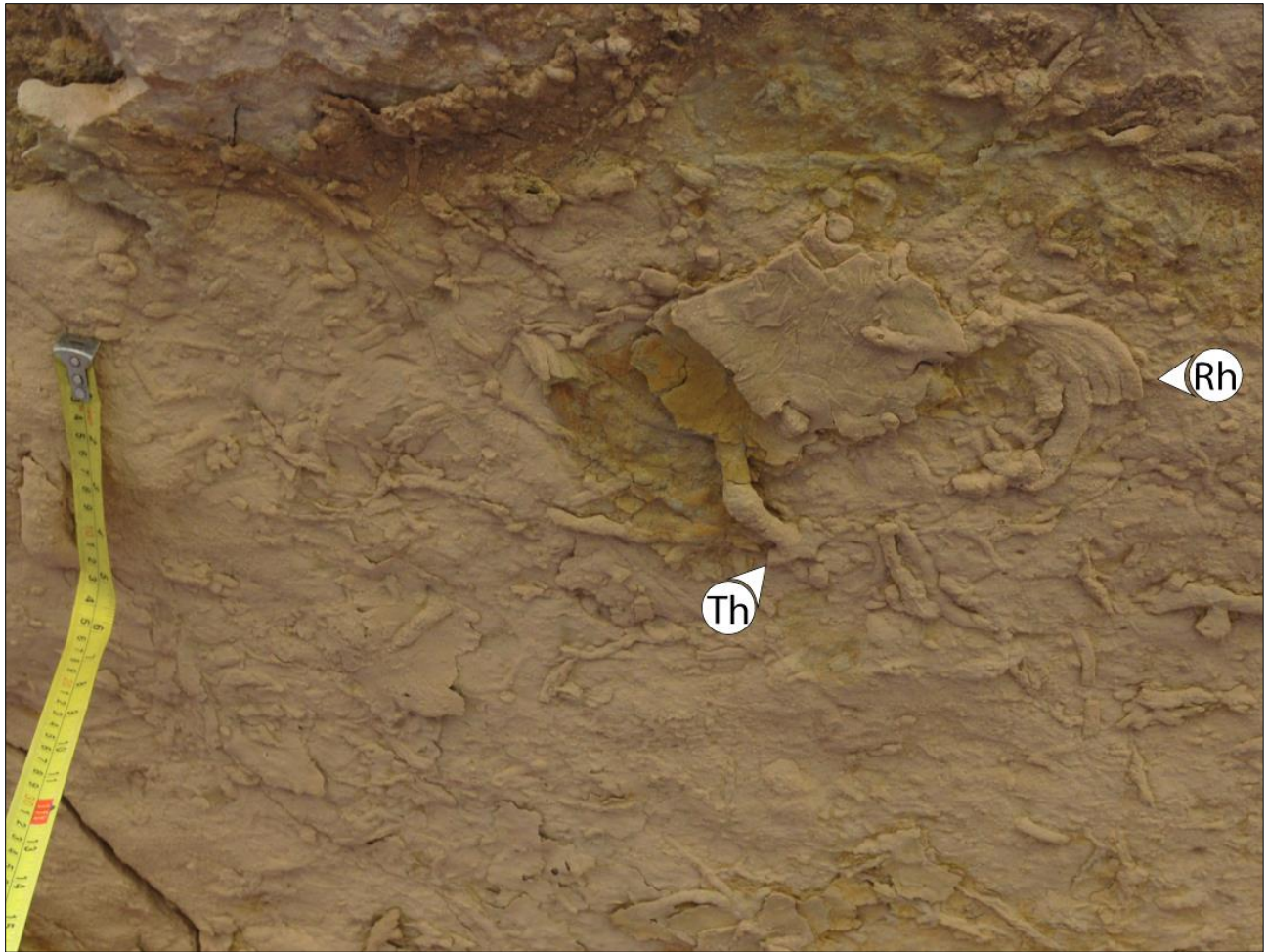


Figure 31. The underside of a sandstone bed in middle shoreface sandstones of parasequence 4, showing *Rhizocorallium* and *Thalassinoides* traces.



Figure 32. Dune-scale cross-bedded upper shoreface sandstone.

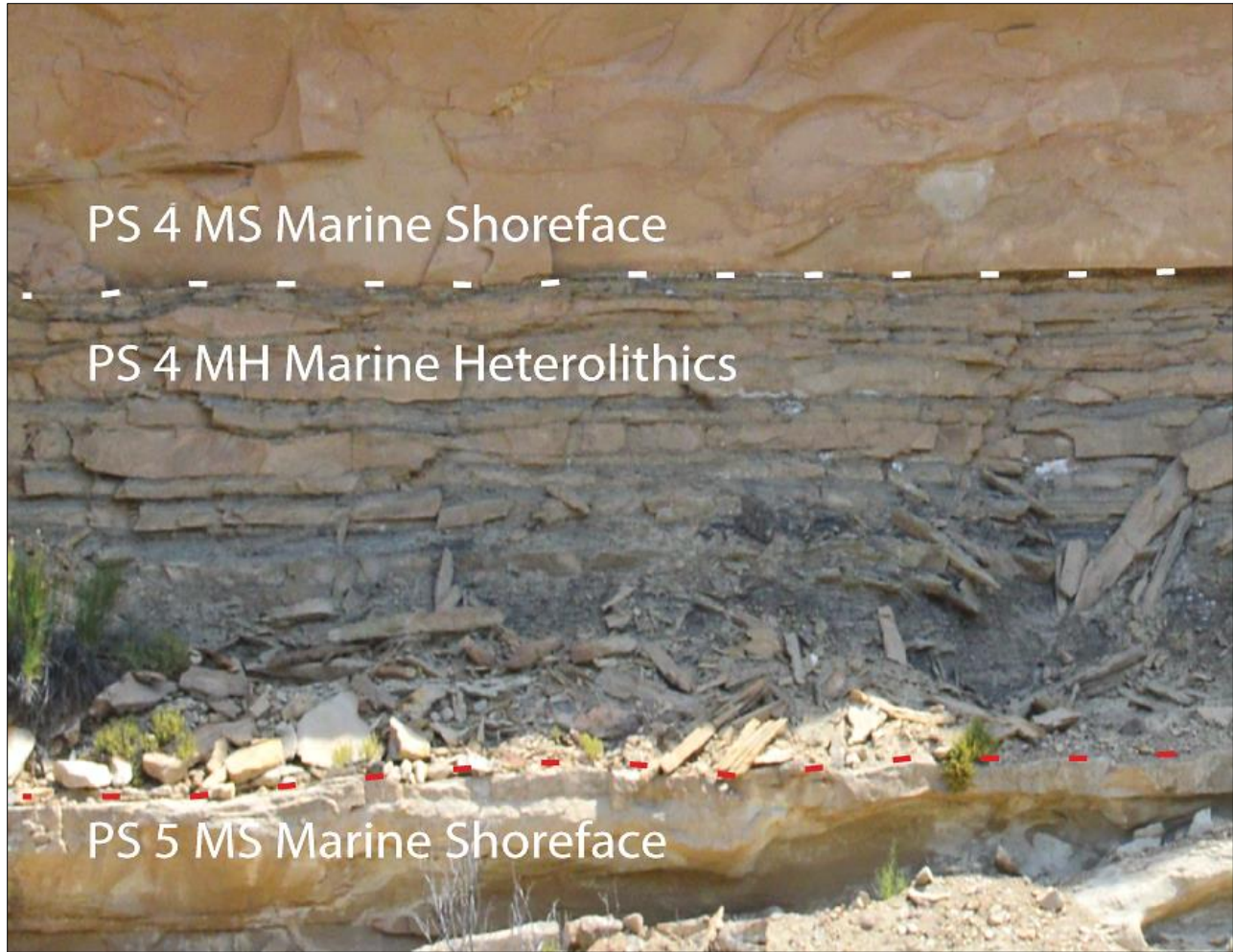


Figure 33. Flooding surface at red dashed line between parasequence 5a MS marine shoreface sandstones and MH marine heterolithics of parasequence 4. This passes upward into MS marine shoreface sandstones parasequence 4 and represents a classic shoaling upward deltaic parasequence (Plint 2010).



Figure 34. Current ripple cross-lamination in very fine sandstones of MH marine heterolithics.

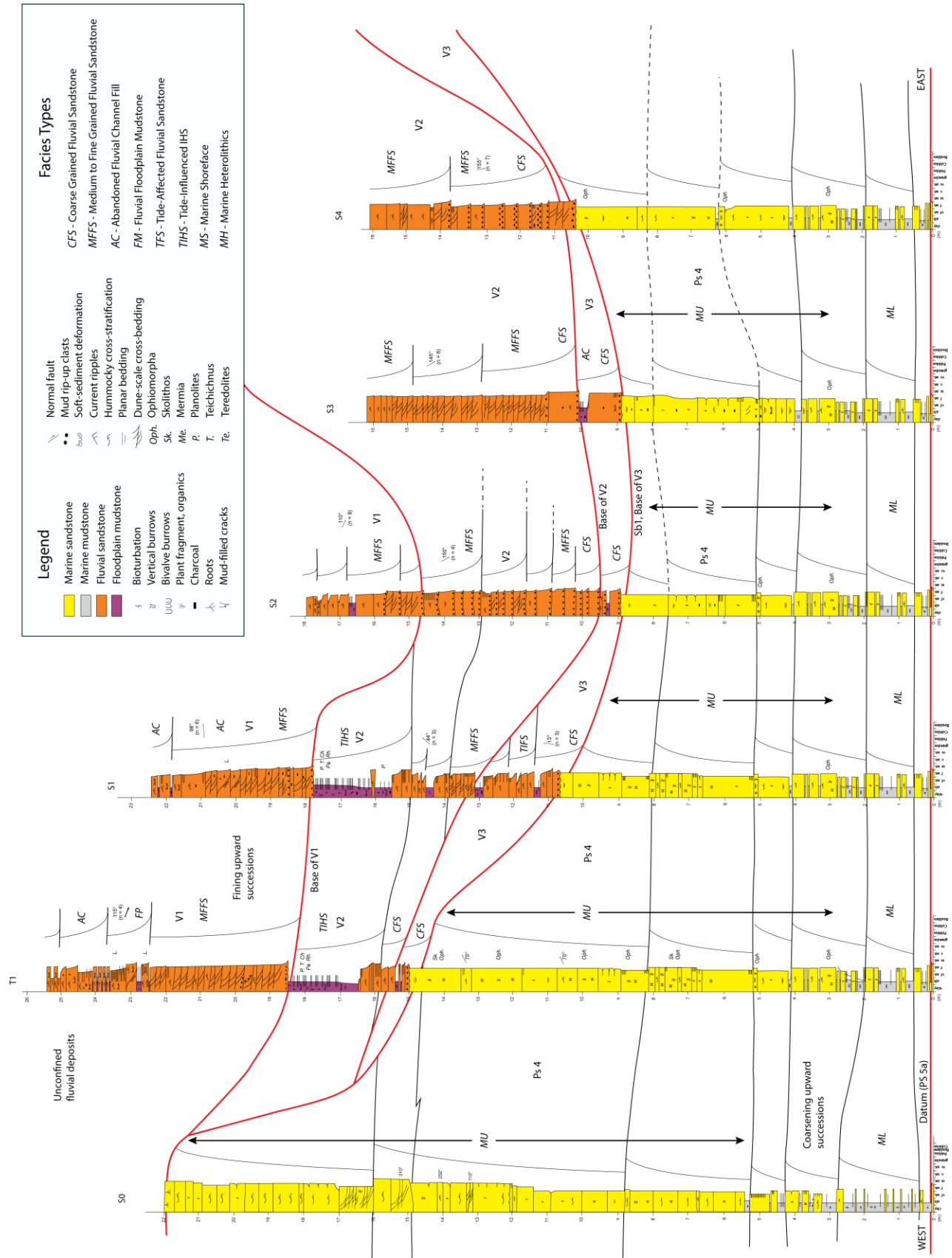


Figure 35. Measured sections T1, S0 – S4 taken along the North Cliff exposure. Note erosional truncation surfaces, sequence boundaries correlated across sections, seen by red lines.

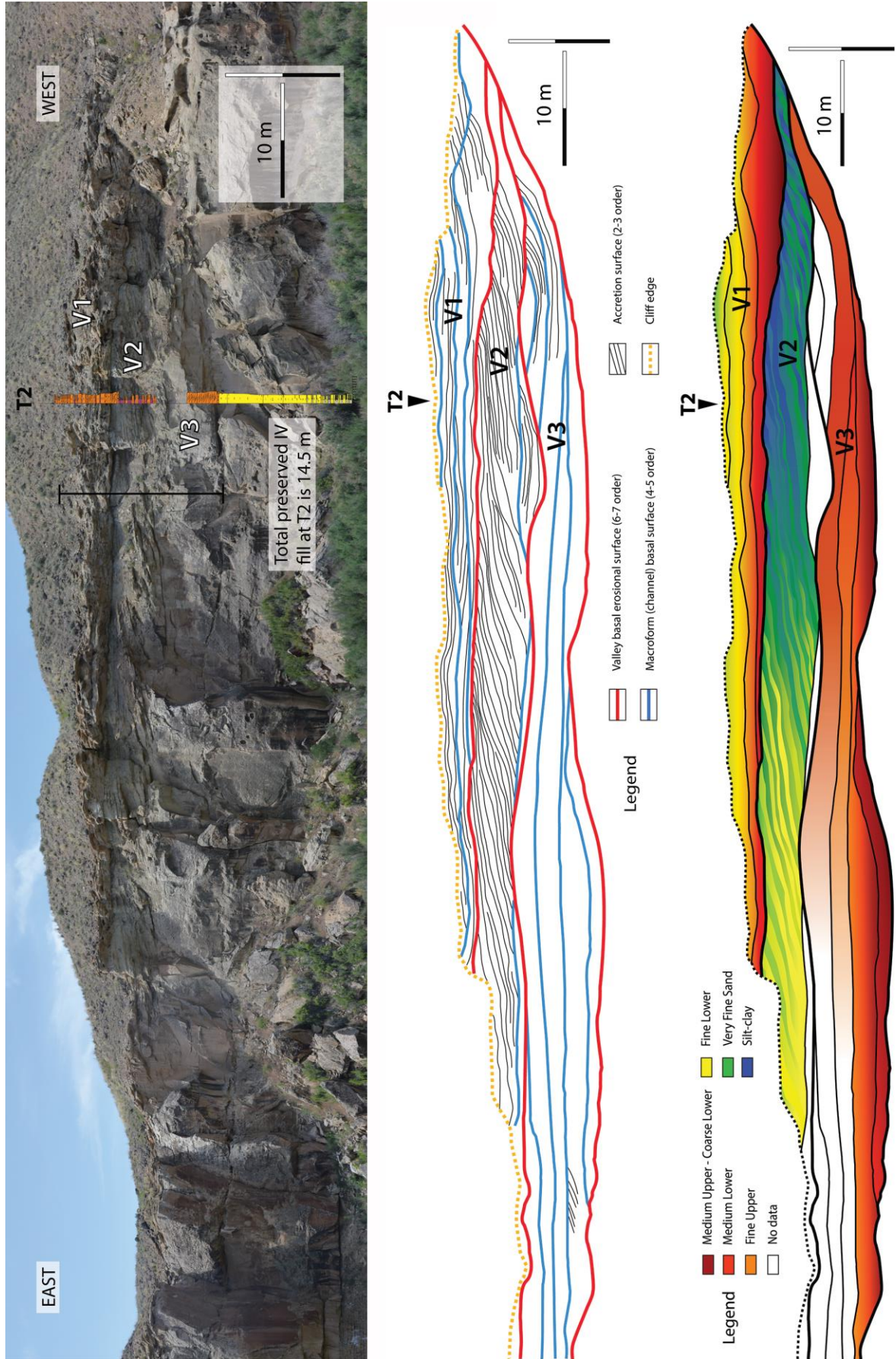


Figure 38. South Cliff exposure with gigapan photomosaic, bedding architecture diagram, and grain size distribution diagram.

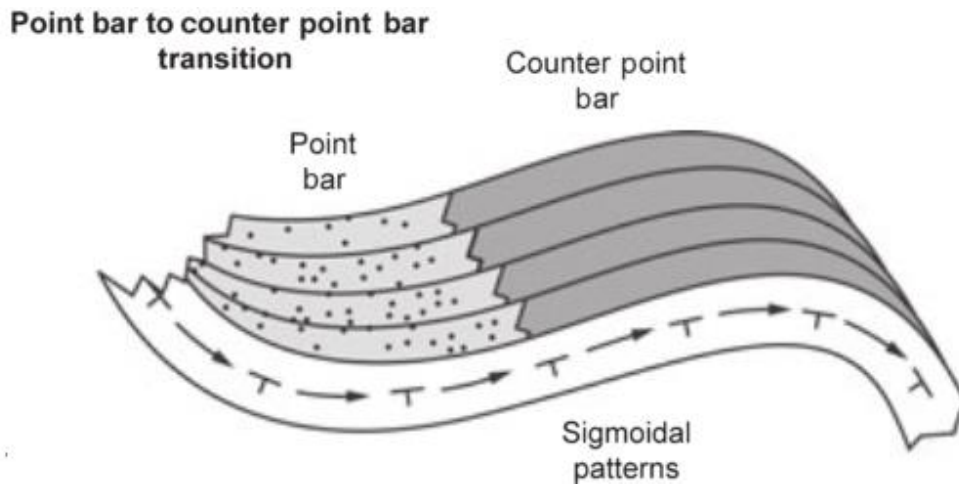


Figure 39. Schematic diagram of a single thread meandering fluvial channel transitioning in accretion style from lateral accretion to downstream accretion, from point bar to counter point bar (Smith et al., 2009).

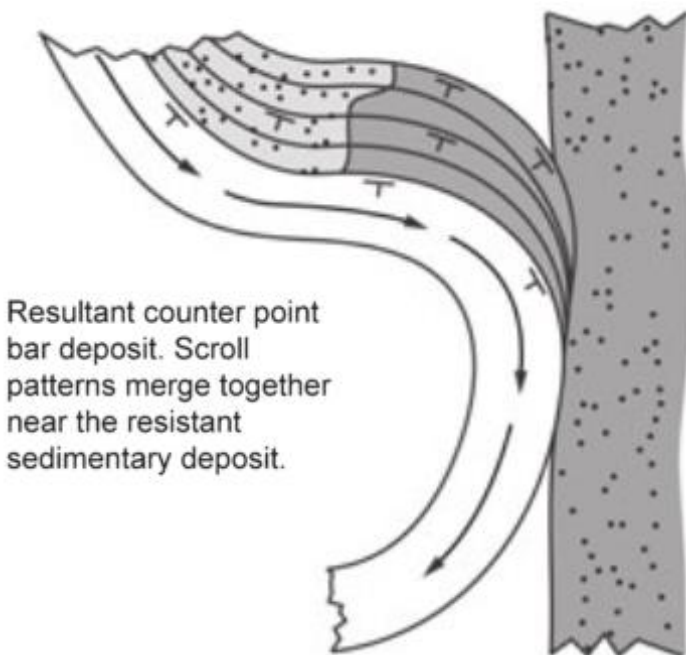


Figure 40. Meander inflection point within a counter point bar, which corresponds to the change in lithology from sand to mud deposition. The image below illustrates channel response to the valley margin and change from lateral to downstream migration (Smith et al., 2009).

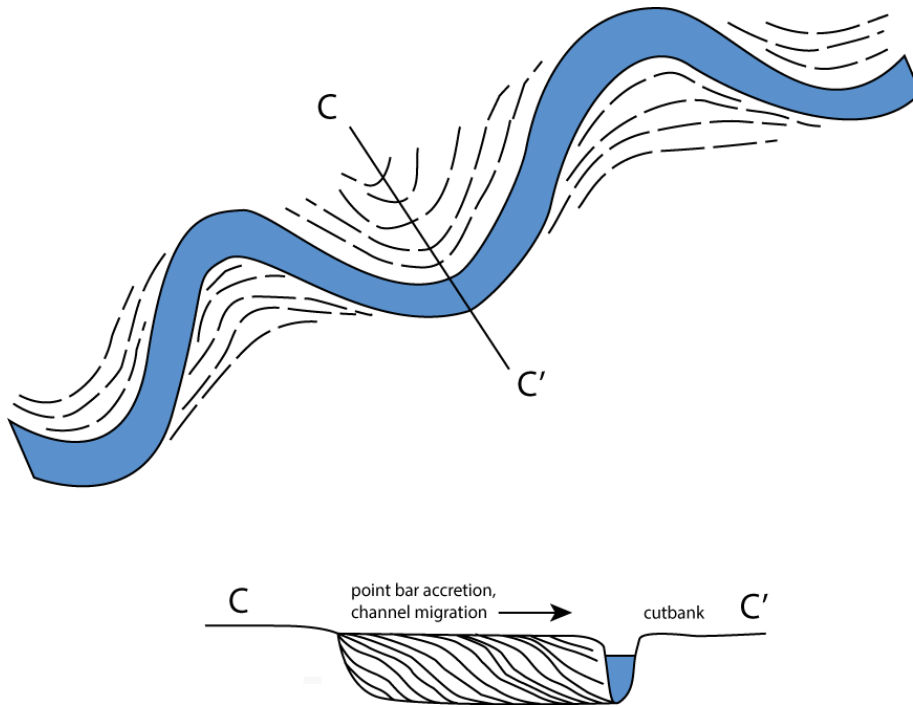


Figure 41. Schematic diagram of a single thread meandering fluvial channel and deposition of laterally accreting point bars within the inside of meander loops. Evidence for the channel becoming more sinuous over time.

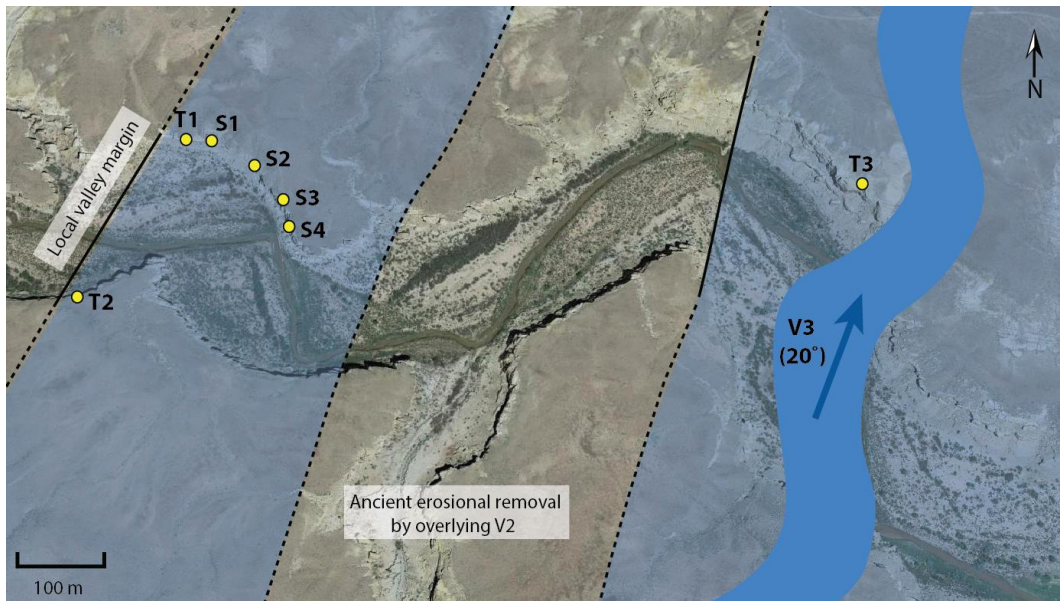


Figure 42. Paleogeographic reconstruction of V3 based on channel dimensions, bedding architecture, and paleocurrent flow data.

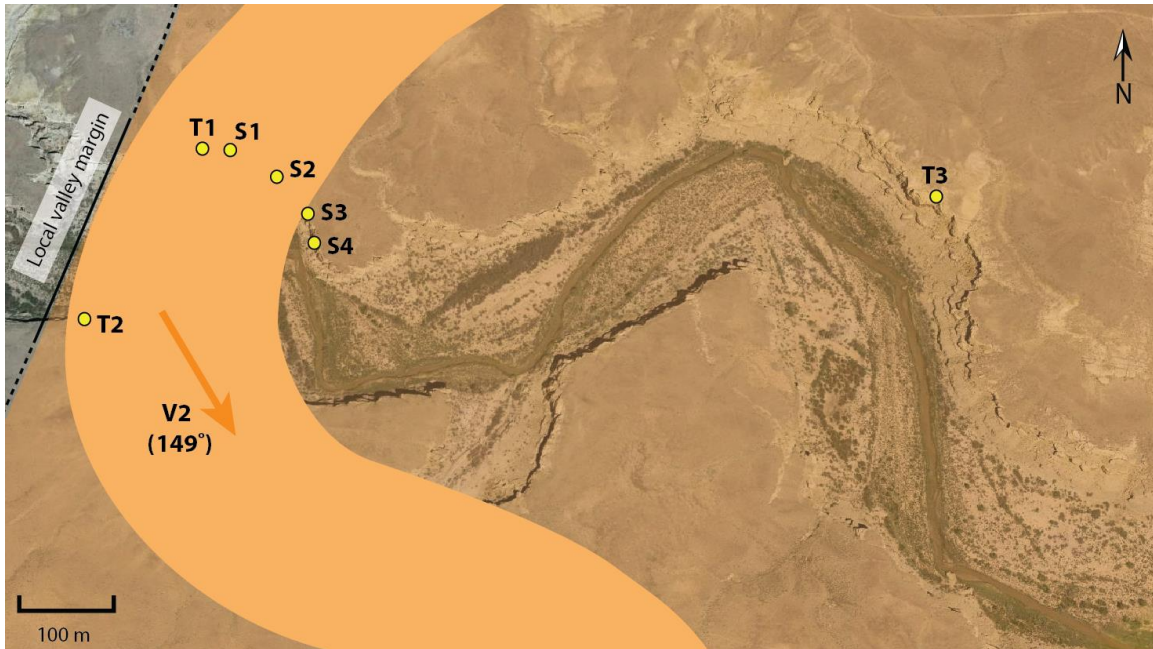


Figure 43. Paleogeographic reconstruction of V2 based on channel dimensions, bedding architecture, and paleocurrent flow data.



Figure 44. Paleogeographic reconstruction of V1 based on channel dimensions, bedding architecture, and paleocurrent flow data

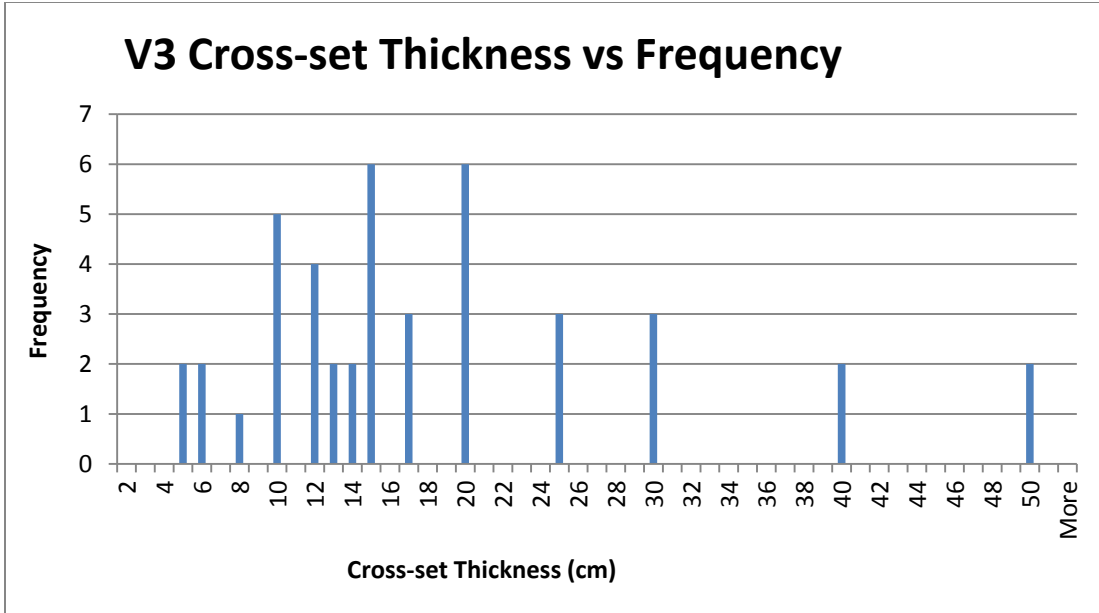


Figure 46. Histogram showing the cross-set thickness taken from V3 measured sections versus frequency.

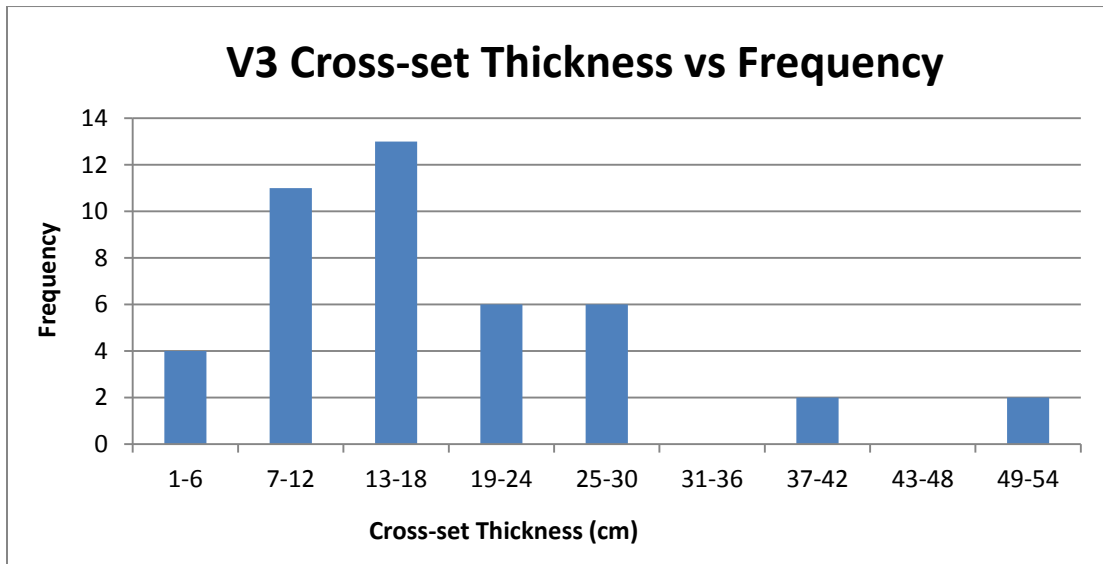


Figure 47. Histogram showing the cross-set thickness measurements from V3 which have been grouped by range to highlight the majority of cross-set thickness measurements which fall between 7 -18 cm.

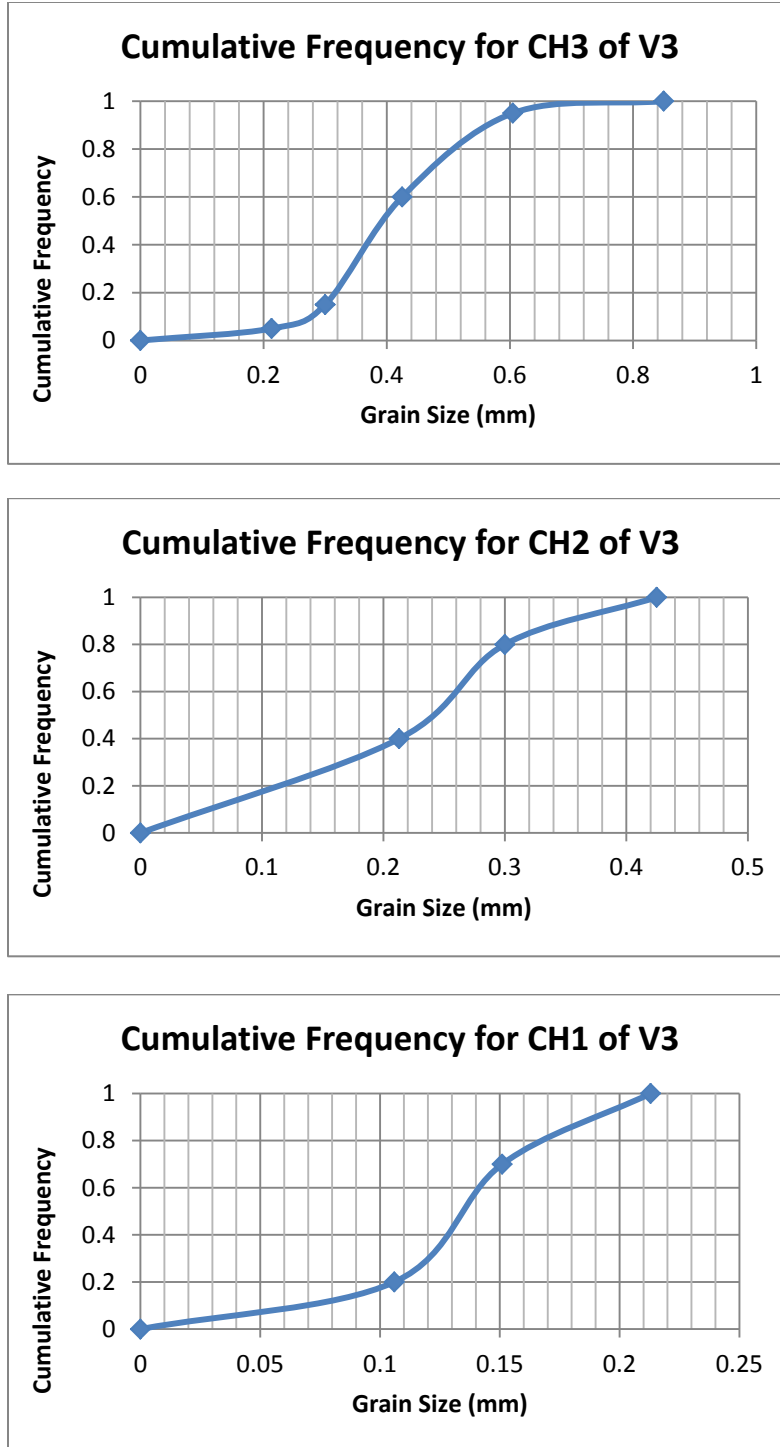


Figure 48. Grain size cumulative frequency curves for representative channels in V3; valley-basal channel is CH3, mid-valley channel is CH2, and upper-valley is CH1.

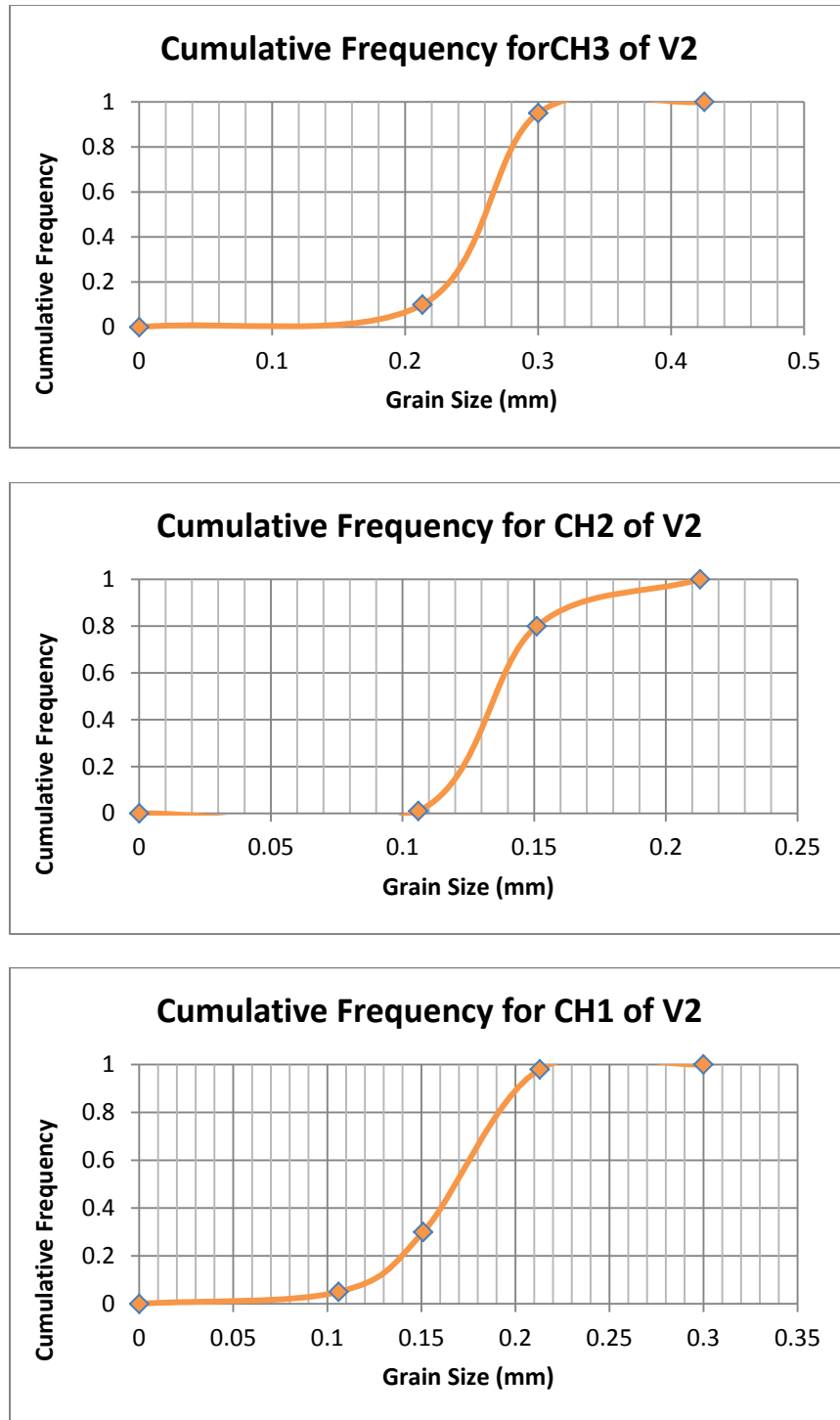


Figure 49. Grain size cumulative frequency curves for representative channels in V2; valley-basal channel is CH3, mid-valley channel is CH2, and upper-valley is CH1.

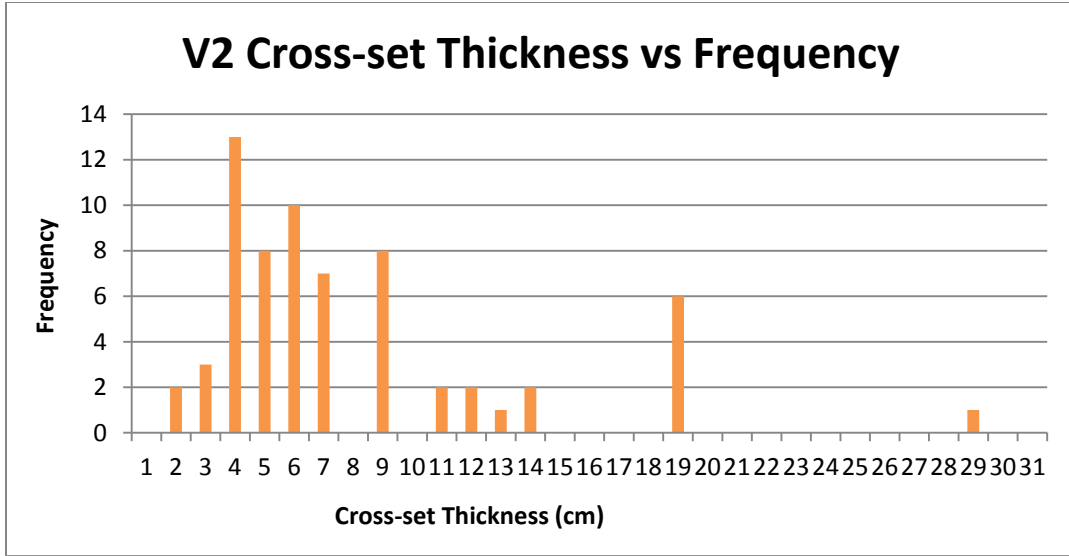


Figure 50. Histogram showing the cross-set thickness measurements from V2 taken from measured sections, versus frequency.

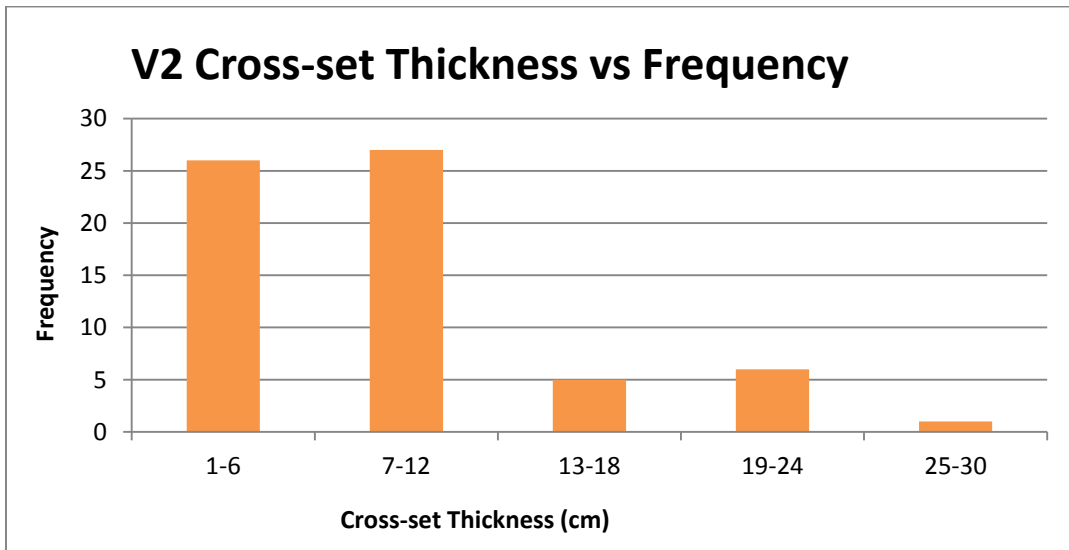


Figure 51. Histogram showing the cross-set thickness measurements from V2 which have been grouped by range to highlight the majority of cross-set thickness measurements which fall between 1-12 cm.

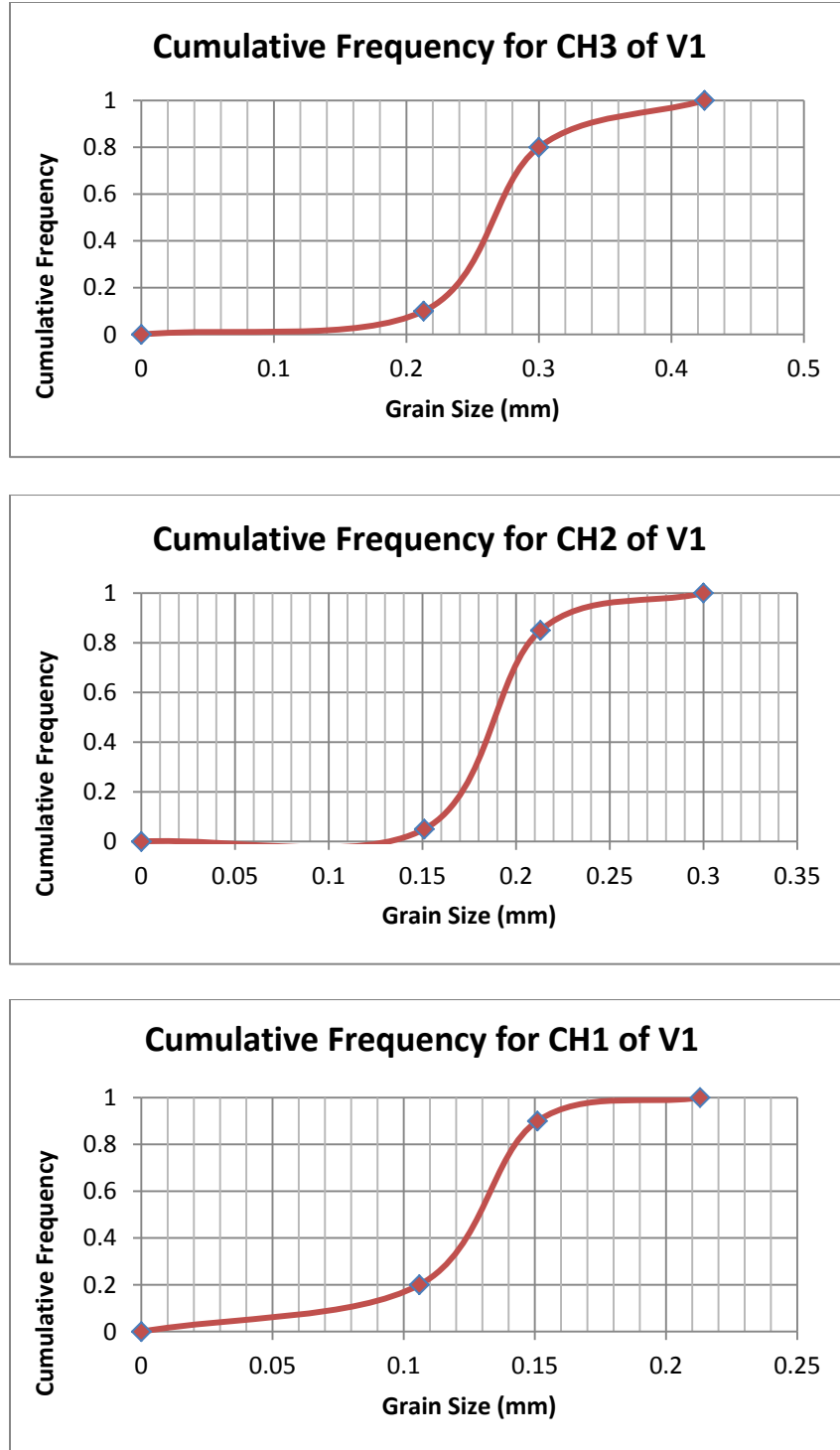


Figure 52. Grain size cumulative frequency curves for representative channels in V1; valley-basal channel is CH3, mid-valley channel is CH2, and upper-valley is CH1.

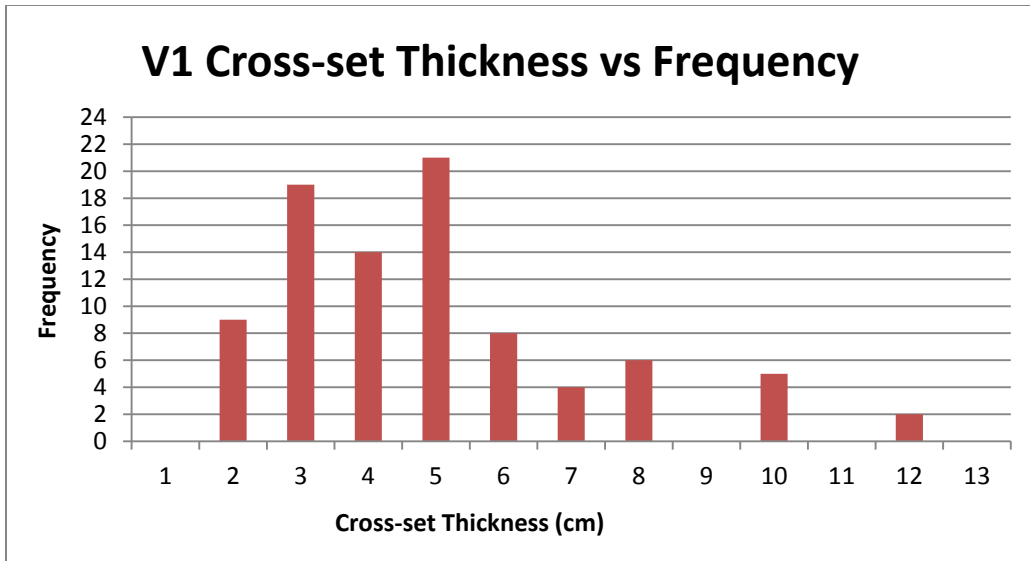


Figure 53. Histogram showing the distribution of cross-set thickness measurements from V1 taken from measured sections, versus frequency. The majority of cross-sets are between 2-6 cm in thickness.

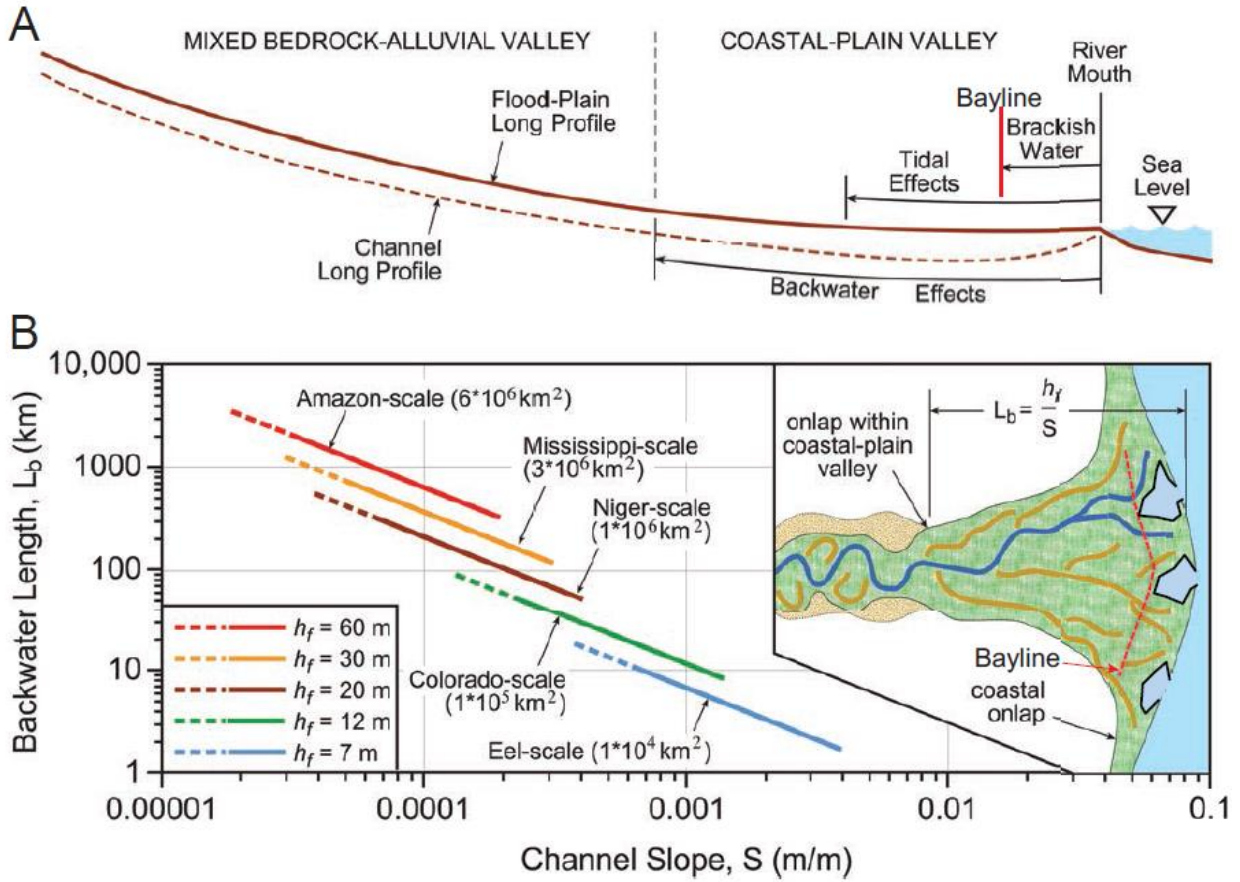


Figure 54. Conceptual model depicting the backwater model to express the limit of brackish water ingress along a river profile. **B.** The backwater concept (Blum et al., 2013) describes the landward most point where downstream effects can propagate upstream, known as backwater length.

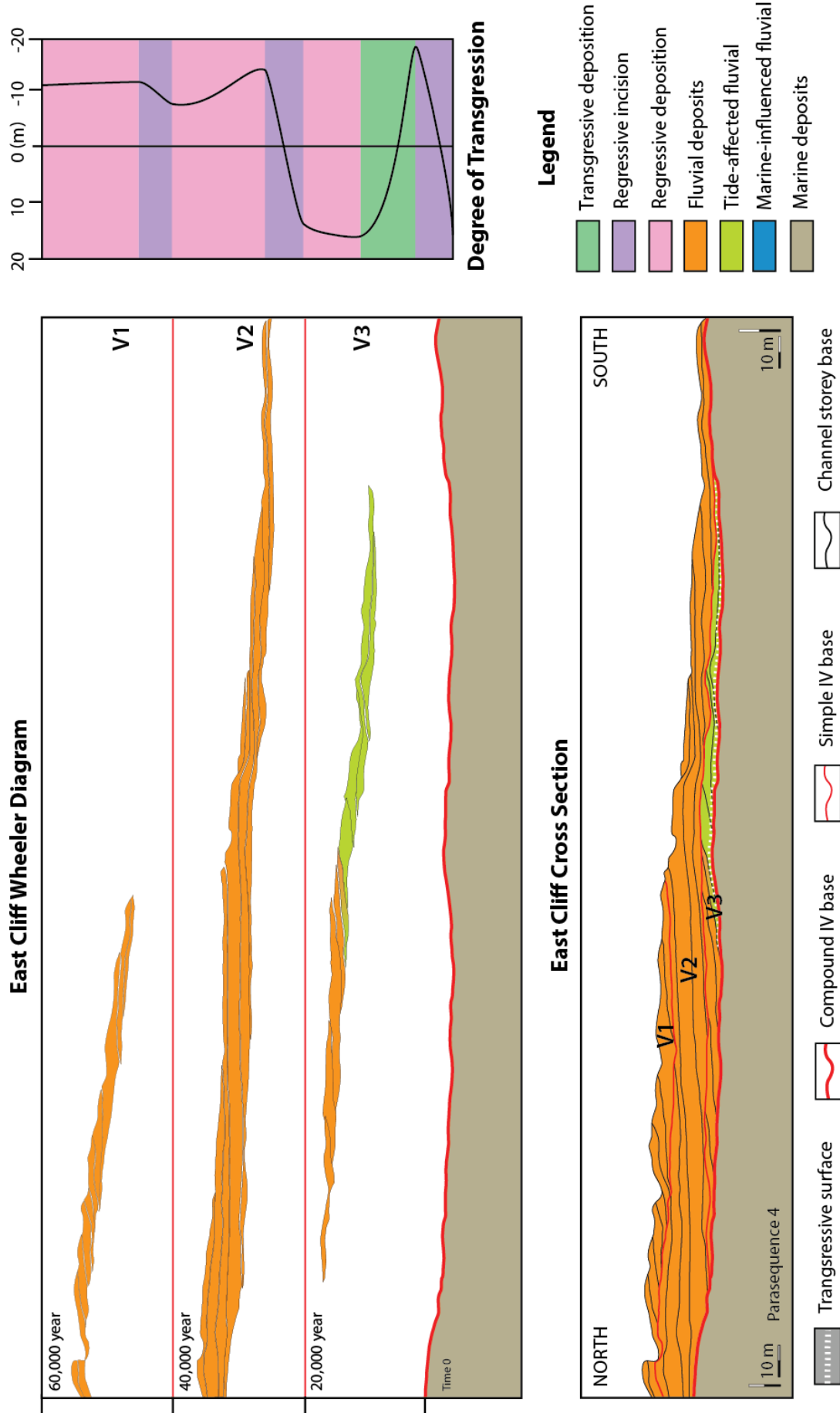


Figure 55. East Cliff Wheeler diagram showing timing of incision and fill, and facies distribution. Degree of transgression shows relative sea level during valley formation.

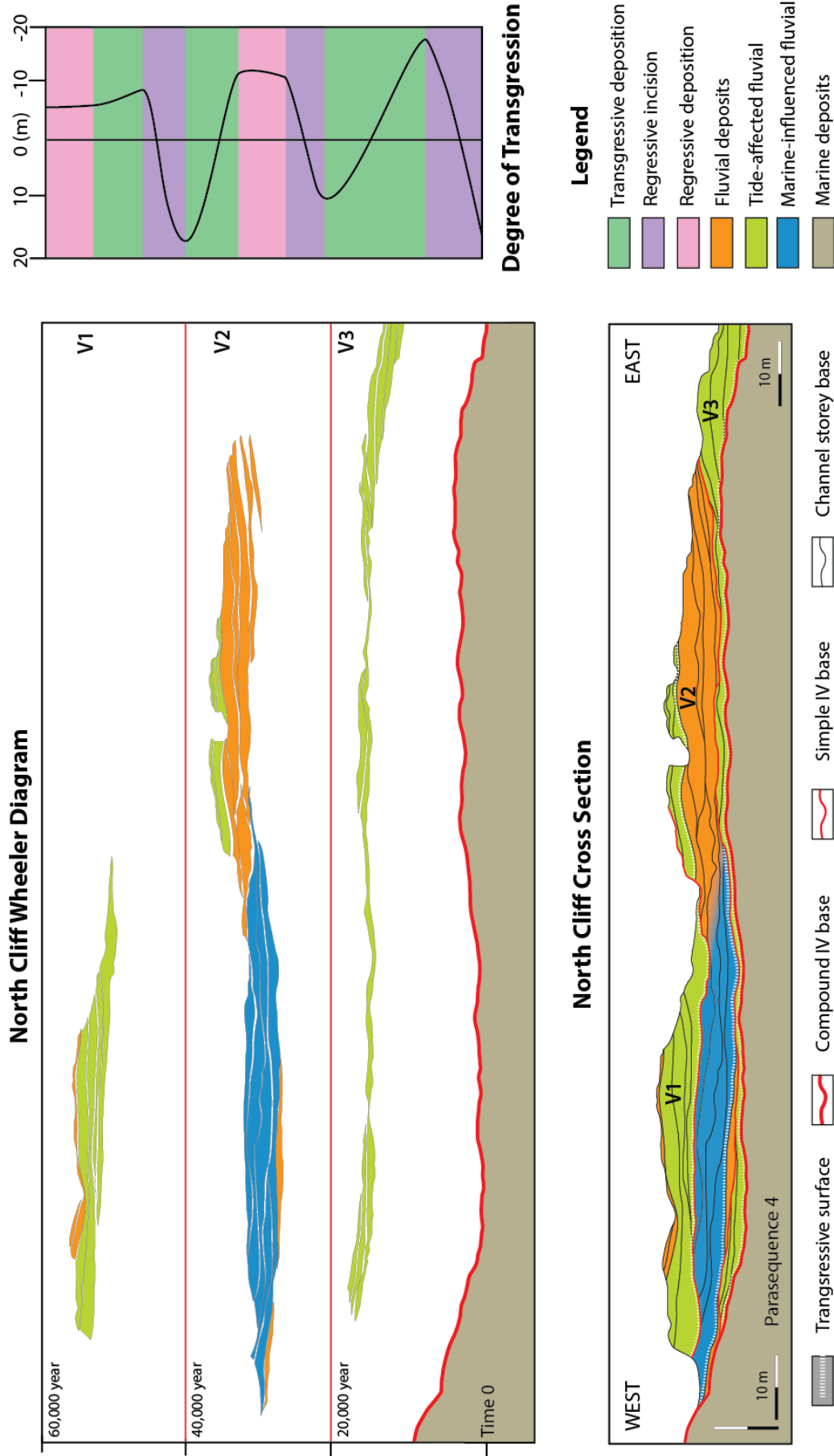


Figure 56. North Cliff Wheeler diagram showing timing of incision and fill, and facies distribution. Degree of transgression shows relative sea level during valley formation.

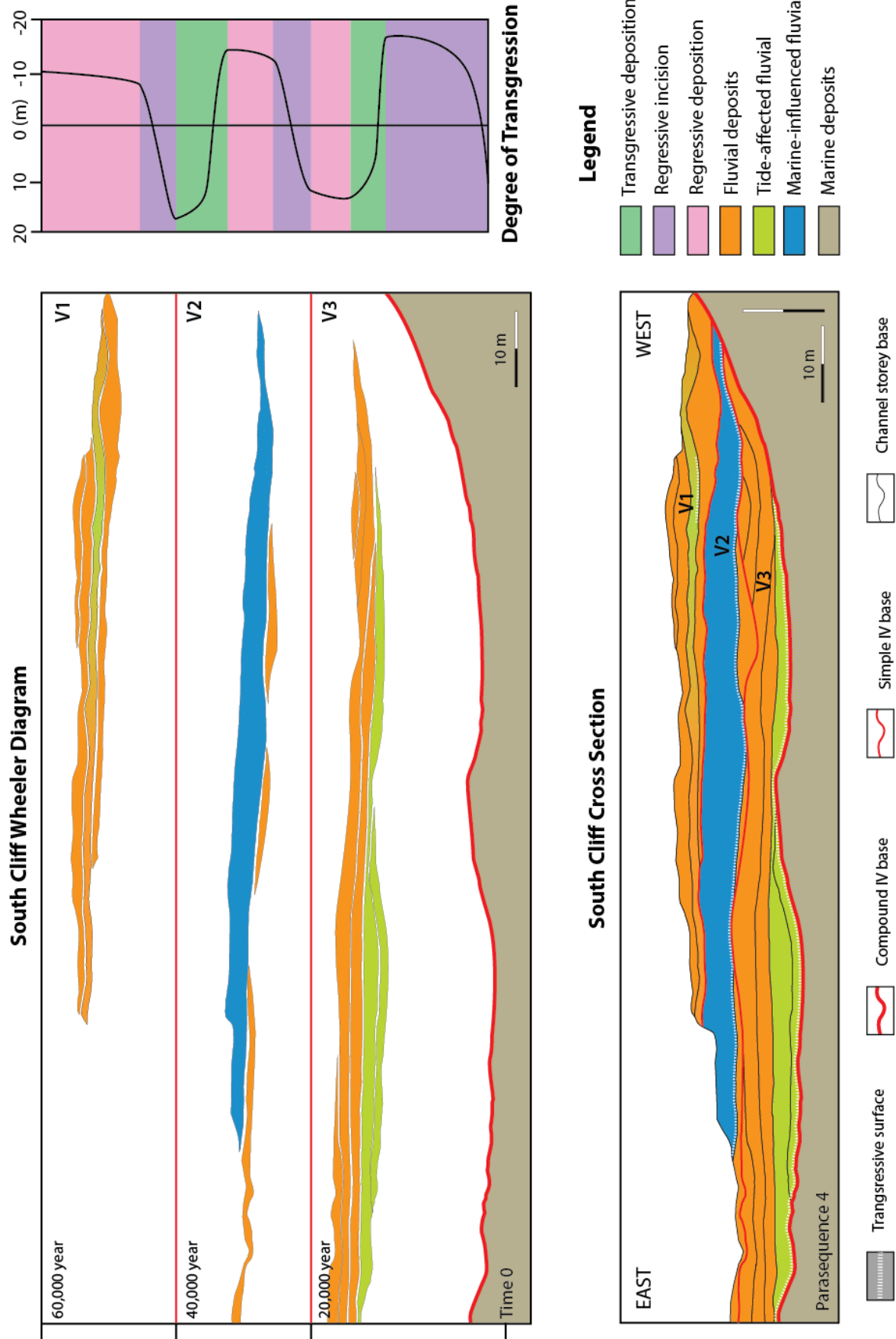


Figure 57. Wheeler diagram of the South Cliff exposure showing timing of incision and fill, and facies distribution. Degree of transgression shows relative sea level during valley formation.

Table 1. Order of bounding surfaces and depositional timescale and process for architectural elements and fluvial features, used in assigning surface hierarchy for architectural bedding diagrams (modified from Miall 1988; Miall 2010) (Fig. 36, 37, 38).

Order of Bounding Surface	Architectural element surface	Time scale (years), and depositional process
0 order – lamination surface	Lamina	10^6 , burst-sweep cycle
1 st order – set (microform) bounding surface	Ripples, crossbed set bounding surfaces	$10^5 - 10^4$, bedform migration
2 nd order – coset (mesoform) bounding surface	Dunes	10^3 , diurnal tidal cycle
3 rd order – avalanche surface, accretion surface	5-20° dipping accretion surface	$10^0 - 10^1$, seasonal, 10 year flood
4 th order – convex-up macroform top surface	Macroform i.e. Point bar, unit bar, crevasse splay	$10^2 - 10^3$, 100 year flood
5 th order – flat to concave-up channel basal surface	Fluvial channel	$10^3 - 10^4$, long term geomorphic process
6 th order – flat, regionally extensive surface, sequence boundary	Channel belt basal surface, simple incised valley base	$10^4 - 10^5$, 5 th order Milankovitch-scale cycles
7 th order – sequence boundary, flat, regionally extensive surface	Sequence, compound incised valley base	$10^5 - 10^6$, 4 th order Milankovitch-scale cycles
8 th order – regional disconformity	Basin-fill complex	$10^6 - 10^7$, 3 rd order cycles

Table 2. Facies descriptions based on the classification scheme by Miall (1996).

Facies	Lithology	Biota	Sedimentary Structures
Coarse Grained Fluvial Sandstone (CFS)	Pebbles to medium lower sandstone, mud rip-up clasts, organic and silt rich interbeds.	Log impressions with <i>Teredolites clavatus</i> . Also seen is <i>Teredolites longissimus</i> , <i>Paleophycus</i> , <i>Pelecypodichnus</i> , charcoal fragments, coal horizons, and plant material.	Often poorly stratified, thick mud rip-up clast rich zones, mud clast rich dune-scale cross beds, planar stratification, fining upward beds which show greater preservation of dune-scale cross beds.
Medium to Fine Grained Fluvial Sandstone (MFFS)	Fine lower to medium lower sandstone with minor coarse grains, and mudstone interbeds, abundant mud rip-up clast zones.	Minor plant material, charcoal, wood and log impressions, little to no estuarine biota.	Dune and bar-scale cross stratification. Planar and current ripple cross stratification, mud rip-up clasts concentrated along accretion surfaces and bases of bar and channel-scale bedforms, soft sediment deformation with large intraclasts, possible seismites.
Tide-Influenced Fluvial Sandstone (TFS)	Fine lower to medium lower sandstone, draped with coupled thin clay to siltstone laminations.	Bivalve burrows, <i>Planolites</i> and <i>Paleophycus</i> , <i>Teredolites clavatus</i> and <i>longissimus</i> . Minor plant material and coal.	Double mud drapes within dune-scale cross beds and quasi-planar stratification in fine sandstone. Alternating or rhythmic mud and fine sandstone beds indicate tidal cycles.
Tide-Influenced, Inclined Heterolithic Strata (TIHS)	Alternating silt-rich and very fine sand-rich 5-13 cm beds. Beds fine and thin upward.	Plant material and coal increases in abundance upward. Marine and estuarine ichnogenera are abundant in upper 1.5 m of point bar; <i>Chondrites</i> , <i>Planolites</i> , <i>Paleophycus</i> , <i>Rhizocorallium</i> , and <i>Teichichnus</i> .	Uniformly dipping beds range in thickness and dip 5-16° forming large-scale laterally accreting point bars which fine upward into muddy upper point bars. Heavy soft sediment deformation, including deformed current ripple cross lamination, dewatering, and normal small faults.
Abandoned Fluvial Channel Fill (AC)	Very fine lower to fine upper sandstone with frequent interbedded and interlaminated mudstones and coaly mudstones.	Bivalve burrows, <i>Lockeia</i> , along sand bed contacts. <i>Fugichnia</i> escape structures. Plant material and minor coal fragments.	Uniformly dipping beds (5-13°) which tend to fine or pinch out towards the valley margin. Low angle bar-scale accretion, ripple cross lamination, soft sediment deformation.
Fluvial	Finely laminated	No estuarine ichnogenera.	Mudstones are finely

Floodplain Mudstone (MF)	siltstones, mudstones and coaly mudstones with sparse fine sand interlamination.	Minor bivalve burrowing, <i>Lockeia</i> , along sand bed contacts. Abundant plant material, root casts, preserved wood impressions, slickensides, and cracks.	laminated, often fissile, and sand beds preserves current ripple cross lamination.
Marine Upper to Middle Shoreface (MU)	Fine lower to fine upper well sorted sandstone with minor mud and organic components.	Moderate to heavy bioturbation, increasing upward. Marine traces include <i>Skolithos</i> , <i>Ophiomorpha</i> , and <i>Rhizocorallium</i> .	Generally massive due to strong biotic colonization. Vague dune-scale cross bedding and planar stratification towards top, and hummocky and swaley cross stratification.
Marine Lower Shoreface (ML)	Interbedded siltstone and very fine upper to fine lower sandstone beds oriented at approximately horizontal. Sand beds thicken and coarsen upwards.	High bioturbation in mudstones and moderate bioturbation in sandstone beds. <i>Chondrites</i> , <i>Planolites</i> , and <i>Paleophycus</i> dominate mudstone ichnogenes, and <i>Skolithos</i> , <i>Ophiomorpha</i> , and <i>Thalassinoides</i> dominate sandstones. Minor plant and coal material is seen.	Hummocky and swaley cross stratification, oscillatory wave ripples, combined flow ripples and planar stratification in sand beds. Siltstone and mudstone interbeds are typically massive but can show normal grading, vague ripple cross lamination and planar stratification.

Table 3. Paleohydraulic calculations for valleys based on cross-set thickness and point bar height. Multiple slope estimates were used to calculate velocity and discharge, which accounts for the wide range in values. Minimum values correspond to slope for the lowermost channel within each valley (values given in Table 3, based on D₅₀), and maximum values were calculated based on incised valley relief across sequence 1, where slope is 0.0014.

Based on Cross-set Thickness	Valley	Bankfull Flow Depth (m)	Channel Width (m)	Channel Belt Width (m)	Velocity (m/s)	Discharge (m ³ /s)
	V3	6.1	237.2	1557 - 2292	1.2 - 3.1	1707 - 4506
	V2	2.7	56.2	375 - 775	0.8 - 1.8	127 - 279
	V1	1.4	16.4	111 - 307	0.8 - 1.3	19 - 30
Based on Point-bar Height	V3	3.33	78.7	523 - 999	1.1 - 2.0	285 - 536
	V2	5.89	221.8	1457 - 2179	0.7 - 2.2	880 - 2829
	V1	3.67	93.6	621 - 1139	0.9 - 2.2	1126 - 2851

Table 4. Grain size, D_{50} , and D_{90} as calculated from cumulative grain size frequency curves for V1, V2, and V3 for the present study area. Three representative channels have been sampled from each valley; the oldest channel from the lower valley (CH3), a mid-valley, and an upper valley channel, in order to estimate slope changes as each valley fills.

Valley	Channel Position	D_{50} Diameter (m)		D_{90} Diameter (m)		Channel Slope
V3	CH3 (oldest)	0.00040	mU	0.00048	mU	0.00040
	CH2	0.00024	fU	0.00036	mU	0.00024
	CH1 (youngest)	0.00014	fL	0.00019	fU	0.00013
V2	CH3	0.00026	mL	0.00029	mL	0.00030
	CH2	0.00014	fL	0.00017	fL	0.00015
	CH1	0.00017	fL	0.00020	fL	0.00019
V1	CH3	0.00026	mL	0.00034	mL	0.00057
	CH2	0.00019	fU	0.00022	fU	0.00042
	CH1	0.00013	fL	0.00015	fL	0.00028

Table 5. Channel widths based on point bar width. Method by Ethridge & Schumm (1977).

Measured Channel Width (m)			
	East Cliffs	North Cliffs	South Cliffs
V3	45	30	--
V2	90	45	53
V1	68	75	38

Table 6. Backwater and Bayline limits for V3, V2, and V1 based on bankfull channel depth and various slope estimates.

	Slope	Backwater Limit (km)	Bayline Limit (km)
V3	0.00040	9.5 – 15.2	5.0
V2	0.00030	9 – 22.	6.6
V1	0.00057	2.5 – 7.2	3.5
V3	0.0014	1.6 – 4.3	1.4
V2	0.0014	1.9 – 4.7	1.4
V1	0.0014	1.0 – 2.9	1.4